Developing a novel organ-on-a-chip model to study ovarian cancer

Matthew James Dibble

2015-2019

Submitted in partial fulfilment of the requirements of the Degree of Doctor of Philosophy

Statement of originality for inclusion in research degree theses

I, Matthew James Dibble, confirm that the research included within this thesis is my own work or that where it has been carried out in collaboration with, or supported by others, that this is duly acknowledged below and my contribution indicated. Previously published material is also acknowledged below.

I attest that I have exercised reasonable care to ensure that the work is original, and does not to the best of my knowledge break any UK law, infringe any third party's copyright or other Intellectual Property Right, or contain any confidential material.

I accept that the College has the right to use plagiarism detection software to check the electronic version of the thesis.

I confirm that this thesis has not been previously submitted for the award of a degree by this or any other university.

The copyright of this thesis rests with the author and no quotation from it or information derived from it may be published without the prior written consent of the author.

Signature:

Date:

Details of collaboration and publications:

I met a traveller from an antique land
Who said “Two vast and trunkless legs of stone
Stand in the desert. Near them, on the sand,
Half sunk, a shattered visage lies, whose frown,
And wrinkled lip, and sneer of cold command,
Tell that its sculptor well those passions read
Which yet survive, stamped on these lifeless things,
The hand that mocked them and the heart that fed;
And on the pedestal these words appear:
'My name is Ozymandias, King of Kings;
Look on my works, ye Mighty, and despair!'
Nothing beside remains. Round the decay
Of that colossal wreck, boundless and bare
The lone and level sands stretch far away.”

- *Percy Bysshe Shelley’s ‘Ozymandias’*

1. Acknowledgements

This work would not be possible without funding from The National Centre for the 3Rs. I am also eternally grateful for the guidance of both my supervisors, Julien Gautrot and Frances Balkwill, without them I would have been completely and utterly lost. I would also like to thank the CanBuild team for all their help.

Being a Gautrotter made my time in the lab so much more enjoyable as we have an amazing group, and I am hugely grateful to all the members of our lab, particularly Stef, Will, Ed, Yaqi, Piao, Dexu and Shoghik. But also thanks to the wider SEMS community who made this a much more fun and interesting experience, including Luis, Gaston and Miguel.

Some of my greatest thanks will go to my friends from undergraduate; Jamie, Ben, Nick and Chloe. In your own unique way, you guys have offered amazing support. I would like to thank my girlfriend Emilie Radley for her continued support, you have always pushed me to do my best and accept nothing less.

Finally, I would like to thank my family; Clive, Emma, Lucy, Kirsty, Becky and Kiki for their amazing support throughout my entire education. But most of all I would like to thank my mum, Tracy Mears. I don't believe anyone has offered more guidance, pride and love than you, and without your continuous and unconditional support this would not have been possible.

2. Abstract

Following the development of the lung-on-a-chip system there has been a rapid increase in interest in advanced tissue culture models embedded in microfluidic systems. Some models, and the focus of this thesis, utilise micro-structured compartments to control cell assembly and recapitulate tissue architecture. This thesis aims to develop a vascularised model of ovarian cancer within a microfluidic chip. Interactions between the vasculature and ovarian cancer have not been widely explored, though studies have demonstrated high micro-vessel density as an independent prognostic marker for worse progression-free survival in women with advanced epithelial ovarian cancer. In addition, the use of anti-angiogenics, such as bevacizumab, have been shown to be effective adjuvant and neoadjuvant therapies in high grade serous ovarian cancer (HGSOC) treatment. This thesis first examines the parameters enabling the formation of a reproducible stable microvascular system. Markers associated with the maturation of the microvasculture, including adheren and tight junction markers, are characterised, in addition to the quantification of the barrier properties of the endothelium. This system is then used to investigate the interactions between endothelial cells and various stromal cells potentially important for endothelium maturation. It is observed that pericytes inhibit vessel hyperplasia and reduce vessel permeability, in agreement with what is reported in literature, but also improve the stability of the vasculature in response to stress (low serum). The interaction between the vascular system and a HGSOC cell line (G33) is then presented. G33s are found to promote short-term vessel sprouting, whereas HUVECs were found to stimulate G33 proliferation and promote a change in morphology. Finally, our vascular model was used in developing a novel model for the assessment of efficacy of drug-therapy, via the embedding of G33 spheroids into a microvasculature.

Contents

3. Abbreviations

4′,6-diamidino-2-phenylindole	DAPI
A20 - binding inhibitor of NFκB-2	ABIN-2
Alpha-smooth muscle actin	α-SMA
Analysis of variance	ANOVA
Angiopoietin	Ang
Antigen ki67	Ki67
Basement membrane	BM
Basic fibroblast growth factor	bFGF
B-cell lymphoma 2	Bcl-2
Beta-catenin	β-cat
Bone mimicking microenvironments	BMi
Bovine serum albumin	BSA
Breast cancer type 1 susceptibility protein	BRCA1
Breast cancer type 2 susceptibility protein	BRCA2
Bromodeoxyuridine	BrdU
Cancer activated fibroblasts	CAFs
Cancer antigen 125	CA125
Cell counting kit-8 assay	CCK-8
Chemokine (C-X-C motif) receptor	CXCR
Chemokine (C-X-C motif) ligand	CXCL
Chondroitin sulfate proteoglycan 4	NG2
Control	CTRL
Delta-like ligand 4	Dll4
Dimethyl sulphoxide	DMSO
Dulbecco's modified eagle medium F-12	DMEM F12
Dulbecco's phosphate buffered saline	DPBS
Endothelial growth medium-2TM	EGM-2
Epidermal growth factor	EGF
Epidermal growth factor receptor	EGFR
Epithelial-to-mesenchymal	EMT

Extracellular matrix	ECM
Extracellular signal–regulated kinases	ERK
Fallopian tube secretory epithelial cells	FTSECs
Fluorescein isothiocyanate	FITC
Foetal bovine serum	FBS
Glycine-leucine-glycine-phenylalanine domain	PDZ domain
Green fluorescent protein	GFP
Heated Recovery	HR
Hepatocyte growth factor	HGF
High mobility group protein B1	HMGB1
High-grade serous ovarian cancer	HGSOC
Human bone marrow derived mesenchymal stem cells	hBM-MSC
Human dermal microvascular endothelial cells	HDMEC
Human omental microvascular endothelial cells	HOMECs
Human umbilical vein endothelial cells	HUVECs
Interleukin	IL
International Federation for Gynaecologists and Obstetricians	FIGO
Lung fibroblasts	LFs
Lymphoid enhancer factor 1	Lef1
Madin-Derby canine kidney cells	MDCK
Mammalian target of rapamycin	mTOR
Matrix-metalloproteinase	MMP
Michigan cancer foundation-7	MCF7
Micro-tumour	MCT
Mitogen-activated protein kinase	MAPK
Muscle mimicking microenvironments	MMi
No Recovery	NR
No Thermal Recovery	NTR
No Treatment	NT
Normal human lung fibroblasts	NHLFs
Notch-regulated ankyrin repeat protein	Nrarp
Nuclear factor kappa-light-chain-enhancer of activated B cell	NF-κB
Osteo-differentiated	OD

Overall survival	OS
Para-formaldehyde	PFA
Patient derived xenograft	PDX
Pericyte growth medium	PGM
Phosphatase and tensin homolog	PTEN
Phosphatidylinositol 3-kinase	PI3K
Phospholipase Cγ	PLCγ
Placenta growth factor	PIGF
Platelet-derived growth factor	PDGF-B
Platelet-derived growth factor receptor-beta	PDGFR-β
Poly-2-hydroxyethyl methacrylate	Poly-HEMA
Polydimethylsiloxane	PDMS
Progression-free survival	PFS
Protein kinase B	Akt
Region of interest	ROI
Retinoblastoma protein	pRB
Revolutions per minute	RPM
Room temperature	RT
Serous tubal intraepithelial carcinoma	STICs
Signal transducer and activator of transcription 3	STAT3
SRC Homology 3 domain	SH3 domain
Standard error of the mean	SEM
Three-dimensional	3D
Tissue plasminogen activator	tPA
Trans-diamine-dichloroplatinum (II)	*trans*-DDP
Transforming growth factor-beta	TGFβ
Tumour necrosis factor	TNF
Two-dimensional	2D
Type 1 collagen	T1C
Tyrosine kinase with immunoglobulin and EGF homology domains	Tie
Urokinase plasminogen activator	uPA
Vascular endothelial growth factor	VEGF
Vascular endothelial growth factor receptor	VEGFR

VE-cadherin	VE-cad
WST-8 [2-(2-methoxy-4-nitrophenyl)-3-(4-nitrophenyl)-5-(2,4-disulfophenyl)-2H-tetrazolium, monosodium salt]	WST-8
Zonula occludens-1	ZO-1

4. List of Figures and Tables

5. Introduction

5.1. Ovarian cancer characterisation

Ovarian cancer is the sixth most common female cancer in the UK, with 7,470 new cases diagnosed and 4,227 deaths in 2016, and is recognised as the most deadly female gynaecological malignancy [1, 2]. The term 'ovarian cancer' covers an array of separate diseases located in the pelvic region, including epithelial, sex cord-stromal and germ cell ovarian cancers. Epithelial ovarian cancer is the most common subtype, representing around 85-95% of all ovarian cancer (see Table 1) [2]. This thesis focuses on high-grade serous ovarian cancer (HGSOC), which represents around 65% of all epithelial ovarian cancers and disproportionately represents around 70-80% of all ovarian cancer fatalities. [2, 3].

Table 1: Ovarian cancer subtypes

Categories	**% of all ovarian cancers**
Epithelial	85-95
Sex-cord stromal	5-8
Germ cell	3-5
Metastatic	4-6
Other	1

This table was adapted from Auersperg et al [2].

Ovarian cancer is characterised according to the World Health Organizations classification, which examines the tissue of origin, phenotype and genotype. Epithelial ovarian cancers are categorised as either Type I or Type II, with Type I cancers being

recognised as being generally indolent and slow growing, examples include clear cell carcinoma and low-grade serous carcinoma [4]. Whereas, Type II, of which HGSOC is the most prevalent, are generally regarded as being more aggressive and typically diagnosed at a later stage, [4].

As well as sub-groups, epithelial ovarian cancer is defined according to its stage or grade, which is determined by disease progression. The most common system for grading epithelial ovarian cancer is the International Federation for Gynaecologists and Obstetricians (FIGO) system, which republished its clarifications in 2014 [5]. In this system, there are four stages, each which have separate sub-stages to define disease progression. The earlier stages, i.e. stage I, describes disease which is confined to the ovaries or fallopian tubes, whereas the later stages, i.e. stage IV, describes disease with distant metastases (excluding peritoneal metastases). In addition to the FIGO system, there are many different classification systems used to describe ovarian cancer disease progression, including the Silverberg system and a two-tier system proposed by Malpica *et al* [6, 7].

5.1.1. High-grade serous ovarian cancer morphology

HGSOC is the most prevalent Type II ovarian cancer, which are characterised by their rapid growth and aggression. It is therefore unsurprising that HGSOC is categorized as having a high mitotic index per high-power field [7]. In addition, HGSOC cells have high-grade nuclei with identifiable nuclei figures that are either moderately or poorly differentiated [8]. Furthermore, there is distinct disparity in HGSOC cell size, with giant mono- or multi-nucleated cells being relatively common. Other cellular characteristics associated with HGSOC include; enlarged round nuclei, irregular nuclear membranes,

irregular chromatin distribution and hyperchromasia [8]. HGSOC has a variety of different growth patterns, including: papillary, glandular, nested and diffuse/solid growth patterns, these patterns are specific to each individual tumour with patient-to-patient variation [8]. In addition to these morphological characteristics, HGSOC is also categorised by its genetic markers.

5.1.2. Genetic fingerprint of high-grade serous ovarian carcinoma

Understanding the genetic fingerprint of HGSOC is essential when developing novel disease models and therapies. HGSOC is characterised by mutations in a number of genes, with TP53 being the most prevalent - occurring in 96 % of all HGSOCs [9]. TP53 codes for p53 which is commonly regarded as 'the Guardian of the Genome' due to its role as a tumour suppressor. Wild-type p53 is a transcription factor, which when activated, broadly acts by inhibiting cell cycle progression, promoting senescence and inducing apoptosis [10]. Mutated p53 may have three different phenotypes: loss-of-function, dominant-negative or gain-of-function [11]. Typically, loss-of-function and dominant negative mutations makes cells more susceptible to transformation. Whereas gain-of-function mutations promote cell proliferation, metastasis, and resistance to chemotherapy [11, 12]. Gain-of-function mutations in p53 promoting cell proliferation may seem contradictory. However, these mutations are known to infer properties which are unrelated to wild-type p53 function, including, inhibition of wild-type p53 and upregulation of cyclin expression [13, 14]. Interestingly, as discussed further in the HGSOC origin section (5.1.3), TP53 is also regarded as a 'gateway mutation', with HGSOC progenitor cells commonly expressing a mutated TP53 signature [15].

Breast cancer type 1 susceptibility protein and 2 (BRCA1 and 2) are important regulators of the homologous recombination DNA repair pathway, which is essential for high-fidelity repair of DNA double-strand breaks [16]. When this pathway is not functional, cells repair DNA double-strand breaks via non-homologous end-joining, which is much more error prone and can lead to genetic instability [17]. BRCA1 and/or BRCA2 mutations predispose individuals to develop ovarian cancer, and is mutated in 13% of all HGSOCs [9]. BRCA1 has many roles in homologous recombination, and partners many proteins in response to DNA damage, including CtIP, whereby it promotes CtIP resection of DNA double-strand breaks [18, 19]. Whereas, BRCA2 is believed to act as an anchoring protein during homologous recombination, and is essential for nuclear localization of Rad51 and strand exchange following DNA damage [20, 21].

Retinoblastoma protein, or pRB, is coded by the RB1 gene and is an important tumour suppressor protein [22]. When active, pRB exists in a hypo-phosphorylated state, sequestering E2F transcription factors and inhibiting cell cycle progression from G1 into the S-phase [23]. pRB commonly undergoes hyper-phosphorylation by the cyclin-D/cyclin dependent kinase-4 complex, following this E2F is released and able to interact with DNA - promoting the transcription of various cell cycle proteins [24]. A 2001 study revealed that the pRB pathway was mutated in 61% of epithelial ovarian cancers [25]. The role of pRB and its pathway in epithelial ovarian cancer progression and therapy is contentious. Some studies report mutation of this pathway is associated with a worse prognosis, when compared with wild-type [26]. However, loss in RB1 expression has also been associated with long-term progression free survival and overall survival [27]. Whereas, another study demonstrated no association between the pRB pathway and patient's response to chemotherapy [28].

5.1.3. High-grade serous ovarian carcinoma origin

Recent evidence suggests that high-grade serous ovarian cancer could be a misnomer, with research indicating that HGSOC actually develops from fallopian tube secretory epithelial cells (FTSECs), and not the ovarian surface epithelium. This was first described in 1982 when light and transmission electron microscopy revealed that carcinoma cells found in the fallopian tube share a similar phenotype to HGSOC cells [29]. These progenitor cells are known as serous tubal intraepithelial carcinoma (STIC) cells. Further research details how cells from the distal fallopian tubes share a similar p53 'signature' as HGSOC – mutations in TP53 concomitantly with stabilisation of p53 [15, 30]. This is further supported by a genetic study which showed HGSOC cells share a more similar genetic profile with fallopian tube epithelial cells compared to the ovarian surface epithelium [31]. In addition, a particularly interesting study detailed how deletions of BRCA, TP53 and PTEN (phosphatase and tensin homolog), genes linked with HGSOC, led to the transformation of FTSECs into HGSOC cells in an *in vivo* model [32]. Shortened telomeres are recognised as an early hallmark of tumorigenesis, being shown to contribute to chromosomal instability [33]. However, overly-short telomeres are incapable of supporting extensive mitosis which typifies HGSOC. Telomerase, the enzyme responsible for the synthesis of telomeric DNA, is expressed in HGSOC cells, but not in ovarian surface epithelial cells [34]. Kuhn *et al* revealed that STIC cells had significantly shorter telomeres than normal fallopian tube epithelial cells and HGSOC cells [35]. Kuhn proposed that STIC cells underwent telomere shortening, before telomerase activity elongated telomeres, enabling continued cell division - supporting the hypothesis that STIC cells are HGSOC progenitors. It has been suggested that mutated FTSECs develop in the fimbrial region of the fallopian tube, before migrating to the ovaries, as shown in Figure 1 [36].

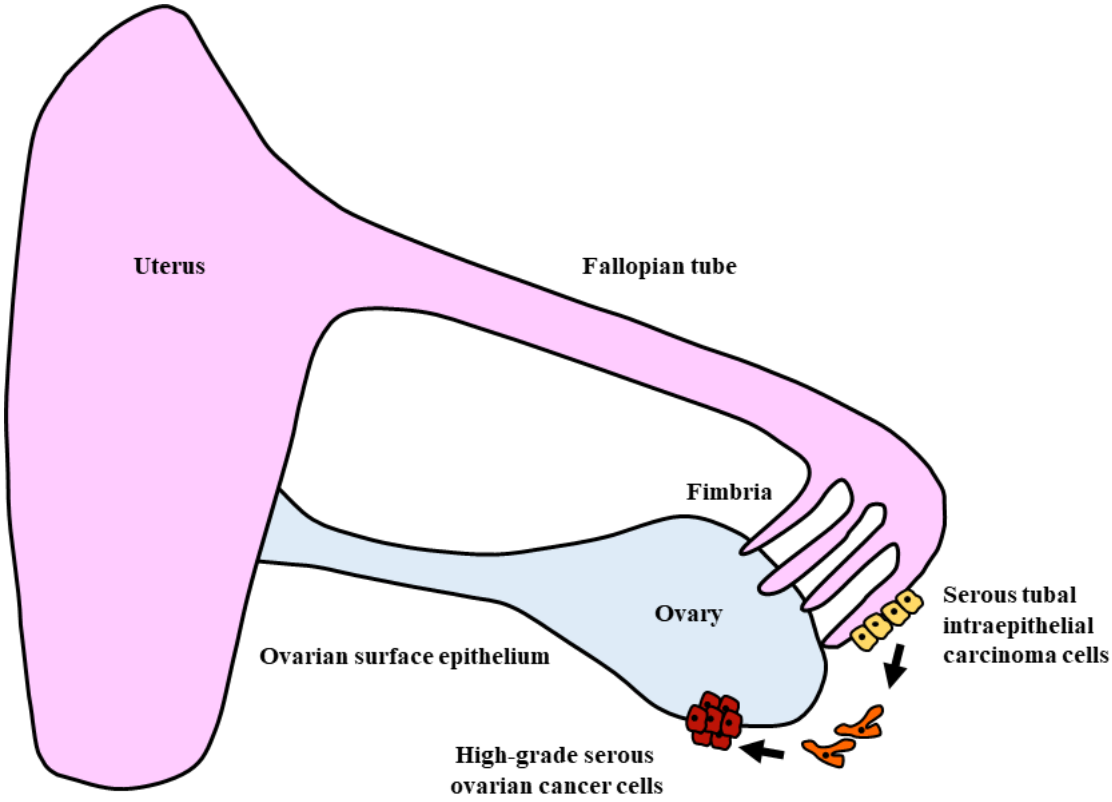

Figure 1. Origins of high-grade serous ovarian cancer. HGSOC develops within the fimbrial region of the fallopian tube (distal region). These cells further mutate and migrate to the ovaries before further invasion into the peritoneal cavity.

5.1.4. High-grade serous ovarian cancer metastasis and invasion

Following the establishment of the tumour in the ovaries, HGSOC cells are then able to spread according to the 'seed and soil' hypothesis proposed by Stephen Paget in 1889, which states cancer metastasis is not random, but depends on the specific crosstalk between cancer cells and the tissue microenvironment [37]. The peritoneum and omentum are recognised as being the primary secondary sites for HGSOC metastasis, and are primarily composed of adipocytes [38]. *In vitro* studies revealed that HGSOC cells promote primary omental adipocyte secretion of interleukin-6 and -8 (IL-6 and IL-8), which consequently promote HGSOC homing, migration and invasion [39]. This study

highlights how the primary tumour is able to manipulate secondary sites to encourage cancer cell seeding.

The main mechanism of HGSOC metastasis is not the classic hematogenous route, rather HGSOC cells are carried by the physiological movement of the peritoneal fluid to the peritoneum and omentum, in a process termed direct transcoelomic dissemination [38, 40]. Before undergoing metastasis, HGSOC cells undergo epithelial-to-mesenchymal transition (EMT), in which the cells gain a more invasive and mesenchymal phenotype. Loss in E-cadherin expression is commonly associated with the promotion of EMT, due to the role E-cadherin plays in cell-cell interactions [41]. Matrix-metalloproteinase (MMP)-9 dependent cleavage of the E-cadherin ectodomain promotes HGSOC cell or cluster shedding from the primary tumour into the ascites [42].

Though HGSOC is typically confined to the peritoneal cavity in 85% of patients, distant metastases have been recorded, with the brain, lungs and liver being recognised secondary sites [43, 44]. This demonstrates the clinical importance of non-orthodox HGSOC metastasis. Indeed, Pradeep *et al* demonstrated hematogenous metastasis to the omentum using a parabiosis mouse model [45]. In this system, the circulatory system of two mice were surgically joined and the host mouse injected intra-abdominally with HGSOC cells. After a period of up 3 months, omentum metastases can be observed in the guest mouse.

5.1.5. The high-grade serous ovarian cancer microenvironment and vasculature

There is a growing understanding of how tumours do not exist as an isolated collection of cancer cells, but rather a malignant organ featuring cancer cells, stroma, blood cells and the vasculature [46, 47]. Indeed, HGSOC cells drive a change in the local

microenvironment with an increased density of cancer-associated fibroblasts (CAFs), leukocytes and macrophages, and a reduced density of adipocytes [46].

CAFs are a major component of the tumour microenvironment, and are believed to be 're-programmed' native fibroblasts [48]. Gene expression analysis revealed that CAFs feature a significantly dysregulated cytokine, chemokine and growth factor expression when compared with normal fibroblasts. [49]. The role of CAFs in disease progression is extensive, including promoting tumour growth, invasion, EMT, angiogenesis, chemo-resistance and remodelling the microenvironment [48].

Tumour-associated macrophages (TAMs) constitute a major component of the tumour microenvironment and have a dual phenotype, being either anti-tumourigenic (M1) or pro-tumourigenic (M2) [50]. M2 macrophages promote ovarian cancer cell proliferation *in vitro* via the release of epidermal growth factor (EGF) [51]. In addition, TAMs accumulate at hypoxic sites, where they induce angiogenesis through the release of a number of growth factors and cytokines, including VEGF and IL-8 [52]. The infiltration of M2 TAMs in epithelial ovarian cancer is associated with a poor prognosis [53].

HGSOC is characterised by intra-peritoneal tumours and ascitic fluid build-up [54]. Both of these may be partly attributed to the formation of an extensive, immature vasculature [55]. The formation of an aberrant tumour microvasculature is recognised as an early event in epithelial ovarian cancer progression and coincides with the growth of intra-peritoneal solid tumours *in vivo* [56, 57]. Vessel formation is driven by a number of cells in the HGSOC tumour microenvironment, including cancer cells, CAFs and TAMs via the release of various angiogenic stimuli, including VEGF [54]. The intra-tumour levels of VEGF are inversely correlated with disease progression and patients survival [58, 59].

Angiogenesis is typically believed to promote tumour growth and disease progression via delivery of nutrients and oxygen, and removal of waste products [60]. In addition, endothelial cells promote HGSOC cell proliferation and chemo-resistance through angiocrine signalling [61]. Angiogenesis is driven by VEGF released by a number of cells, *in vivo* studies have also linked VEGF with the formation of an immature, hyper-permeable vasculature [62]. This 'leaky' vasculature is partly responsible for the extensive ascites accumulation observed in HGSOC, due to the movement of high protein fluid from the intravascular compartment to the peritoneal cavity [55]. These malignant ascites are responsible for anorexia, insomnia, fatigue, low capacity to walk, pain and lower limb discomfort in HGSOC patients [63].

As discussed further in section 5.2.5, pericytes are associated with endothelial cells and promote vascular stability [64]. Cancer-associated vasculature is characterised by sparse pericyte coverage, this is partly responsible for the observed vessel hyperplasia, hyper-permeability, and poor junction expression [65]. This phenotype is replicated *in vivo*, as IGROV-1 xenografts promote the formation of an immature vasculature, featuring poor pericyte coverage [66]. Interestingly, stroma associated pericyte expression is highly predictive for poor patient prognosis [67]. Indeed, *in vitro* ovarian cancer cell proliferation and invasion was promoted with the addition of pericytes. In addition, pericytes promoted ovarian cancer growth and metastases *in vivo*, with no effect on the vasculature. This suggests pericytes promote disease progression independently of their role in the vasculature.

5.1.6. High-grade serous ovarian cancer therapy

Regardless of the continued development of novel therapies, the 5-year survival rate of HGSOC has consistently stayed around 40 - 50% over the past 50 years [2], with a recent

study showing the median overall survival (OS) rate of patients with HGSOC being 40.7 months [68]. The lethality of HGSOC is related to its general late stage diagnosis, with the 5-year survival rate significantly decreasing from 90% to 15%, when diagnosed at an early stage (when the cancer is confined to the ovaries) compared with a late stage diagnosis [69]. The current standard first-line therapy involves cytoreductive surgical debulking, followed by adjuvant therapy with taxanes and platinum-based chemotherapeutics - often paclitaxel and carboplatin [70, 71].

Carboplatin is a second-generation cisplatin derivative commonly used in HGSOC therapy. Carboplatin and cisplatin share a similar mechanism-of-action, briefly, they crosslink with DNA, thereby inhibiting DNA replication and transcription, and leading to cell death [72, 73]. Carboplatin primarily binds to the N7 atoms of the imidazole rings of guanosine and adenosine, forming mono-adducts, intra-strand DNA crosslinks and inter-strand DNA crosslinks [74]. Studies have suggested that 1,2-d(GpG) intra-strand DNA crosslinks are the main cytotoxic DNA lesion formed by carboplatin [75]. The cisplatin trans isomer, *trans*-diamine-dichloroplatinum (II) (*trans*-DDP), is unable to form 1,2 intra-strand DNA crosslinks and is known to be biologically inactive. In addition, high mobility group protein B1 (HMGB1) recognises and binds the 1,2-d(GpG) intra-strand DNA crosslinks induced by platinum agents, whereby, through steric blocking inhibits translesion synthesis [76]. This DNA-platinum-HMGB1 complex is additionally stated to inhibit DNA transcription and replication, and initiate apoptosis [74].

Carboplatin is typically regarded as less efficacious than cisplatin, though treatment also displays fewer side-effects [73, 77]. This is related to the chemical structures of these compounds, which are displayed in Figure 2. Both compounds feature a doubly charged platinum ion surrounded by four ligands; two amine ligands, and either two chloride ions or a carboxylate compound (1,1-cyclobutanedicarboxylate), respectively. The amino

groups found in cisplatin and carboplatin are strongly bound to the central platinum ion, however chloride and 1,1-cyclobutnedicarboxylate act as leaving groups following hydrolysis [73]. The hydrolysis of carboplatin and cisplatin invokes the formation of a positively charged intermediate, which when transported to the nucleus is able to covalently and electrostatically bond with the N7 atoms of the imidazole rings of guanine and adenine - forming the aforementioned platinum-DNA mono-adducts and inter- and intra-strand di-adducts [78]. Carboplatin's 1,1-cyclobutnedicarboxylate ligand is a poor leaving group compared with chloride, hence reducing carboplatin's reactivity and DNA binding rate when compared with cisplatin. Kinetic studies revealed that the formation of carboplatin-DNA adducts is around 100-fold slower compared with cisplatin-DNA adducts [79].

As described in section 5.1.2, BRCA1 and BRCA2 mutations are commonly featured in HGSOC [9]. Indeed, the cumulative ovarian cancer risk to age 80 years was 44% and 17% for BRCA1 and BRCA2 mutation carriers, respectively [80]. The genetic makeup of HGSOC makes certain populations more susceptible, e.g. Ashkenazi Jewish women, who are well known to have mutations in BRCA1 and BRCA2 [3, 9]. This predisposition has led some groups to propose a personalized medicine approach to HGSOC treatment, and have suggested at-risk individuals take low-toxic drugs to limit HGSOC development [3]. Studies have shown oral contraception reduces the risk of developing ovarian cancer in both BRCA1 and BRCA2 populations [81]. Due to the lethality of HGSOC, reducing incidences is a particularly effective tactic in reducing mortality [82].

As described, HGSOC is significantly more lethal when diagnosed at a late stage than an early stage [69]. As such, improving early diagnosis of HGSOC is imperative in reducing the lethality. However, early detection of HGSOC is challenging, as until the tumour has metastasized from the pelvic region the disease is largely asymptomatic and only presents

symptoms at later stages of disease progression. To overcome this, a recent clinical trial, the Collaborative Trial of Ovarian Cancer Screening, determined that with annual multimodal screening with serum CA125 (cancer antigen 125) interpreted with use of the risk of ovarian cancer algorithm, there is a significant reduction in mortality [83].

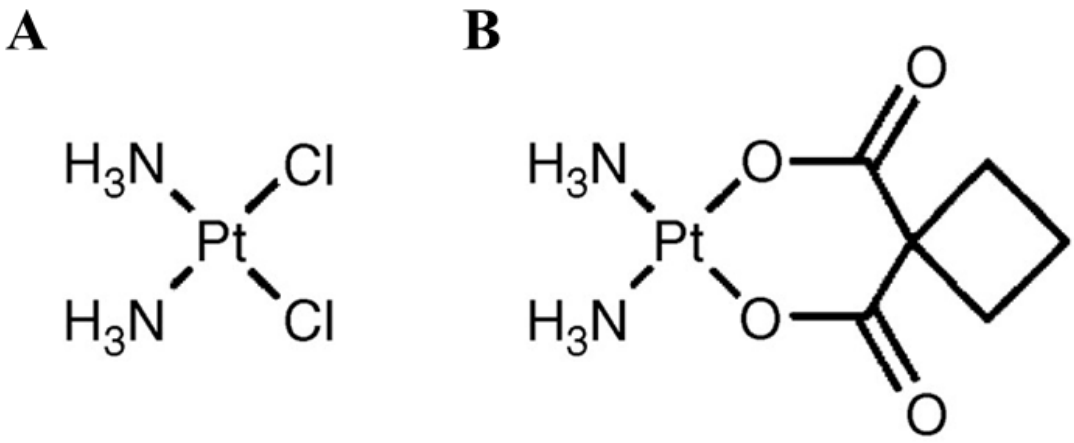

Figure 2. Cisplatin and carboplatin chemical structures. A) Cisplatin structure containing chloride leavings groups. **B)** Carboplatin structure containing a 1,1-cyclobutnedicarboxylate leaving group. Figure adapted from [84].

Poly(ADP-ribose) polymerase (PARP) inhibitors are a novel class of drug used in the treatment of BRCA1/2 positive breast and ovarian cancer [85]. PARP repairs single-strand breaks in DNA, via the recruitment of proteins into a repair complex at the site of DNA damage [86]. Inhibition of PARP results in the accumulation of single-strand breaks and the stalling of replication forks, which promotes double-strand DNA breaks [87]. In cells with BRCA mutations, these double-strand break are not repaired via homologous recombination, which results in genetic instability and cell death [85]. A recent clinical trial revealed that olaparib, a PARP inhibitor, increased the rate of freedom from disease progression and from death after 3 years from 27 to 60% [88]. This study highlights the effectiveness of PARP inhibitors in the treatment of BRCA-mutated ovarian cancer.

Angiogenesis is an important regulator of tumourigenesis, with tumours being limited to 1-2 mm diameter before requiring vessel formation [60]. Indeed, high micro-vessel density is recognised as an independent marker of poor prognosis in ovarian cancer [89]. Due to the importance of vessel formation many drugs have been developed which target this system, including the recombinant humanized monoclonal antibody, bevacizumab. Bevacizumab targets the angiogenic stimulant, vascular endothelial growth factor - A (VEGF-A), and inhibits its interaction with VEGF receptors - 1/2 (VEGFR-1/2) [90]. Two large phase III clinical trials, GOG218 and ICON7, assessed bevacizumab's suitability as a first-line treatment in ovarian cancer (administered with carboplatin and paclitaxel) [91, 92]. Both GOG218 and ICON7 concluded bevacizumab significantly improved the median progression-free survival (PFS) of women with 'newly diagnosed ovarian cancer who had undergone primary surgery', though no overall improvement in OS was observed. However, meta-analysis of the ICON7 study revealed that bevacizumab significantly improved the median OS for patients with sub-optimally debulked disease, stage IV ovarian cancer and inoperable stage III ovarian cancer [93]. Due to the success of bevacizumab in HGSOC therapy, further analysis of the interactions between the vasculature and ovarian cancer is shown in this thesis.

5.2. Angiogenesis and vasculogenesis

When referring to vessel formation, the nomenclature refers to processes with subtle differences. Angiogenesis refers to the formation of blood vessels from the pre-existing vasculature, whereas vasculogenesis is the *de novo* formation of vessels [94]. Vasculogenesis is typically believed to play an important role in the establishment of the vasculature from angioblasts during embryogenesis [95]. Due to this, the role of vasculogenesis in adults has been less extensively studied, though research has shown

there is some *de novo* vessel formation from bone marrow-derived cells [96]. Angiogenesis is typically regarded as the predominant mechanism to form new vessels in adults, with implications in wound healing, growth, and the action of female reproductive organs [97]. Both of these processes are essential for normal development, with aberrant vessel growth linked with a number of diseases, including cancer, psoriasis, arthritis, retinopathies, and atherosclerosis [97]. To better understand the role vessel formation plays in these diseases, it is important to understand the mechanism behind the physiological processes.

5.2.1. The role of VEGF in vessel formation

Vessel formation is controlled through a number of pro-angiogenic and anti-angiogenic factors. Principally amongst the pro-angiogenic compounds are the VEGF family of signalling proteins. This family of proteins contains many homologs, including VEGF-A, VEGF-B, VEGF-C, VEGF-D and placenta growth factor (PIGF), which each have different signalling specificities and mechanisms [98]. VEGF-A is primarily linked with the promotion of angiogenesis, whereas other members are typically linked with other processes, such as VEGF-C promoting lymphangiogenesis [99]. VEGF-A is expressed as various splice variants, with VEGF-A_{165} and VEGF-A_{121} being the most abundant isoforms [100].

VEGFs bind with a number of different receptors, including VEGFR-1, -2 and -3, neuropilins 1 and 2, and heparan sulfate proteoglycans [101]. However, VEGF-A's primary mechanism for inducing vessel formation is binding to, and signalling through, VEGFR-2, which are receptor tyrosine kinases extensively expressed by endothelial cells (see Figure 3) [102]. VEGF-A homodimers bind individual VEGFR-2 monomers,

inducing receptor dimerization and ligand-dependent tyrosine phosphorylation [103, 104]. VEGFR-2 activation promotes various downstream signalling cascades important in cell proliferation and survival [104]. *In vitro* experiments revealed VEGFR-2, but not VEGFR-1, was responsible for endothelial survival in serum-starved culture, through downstream activation of phosphatidylinositol 3-kinase (PI3K) and protein kinase B (Akt) [105]. In addition, VEGFR-2 dimerization and phosphorylation activates the Raf-1-MEK-MAPK pathway and mitogenesis, in a phospholipase Cγ (PLCγ) and protein kinase Cβ dependent manner [106].

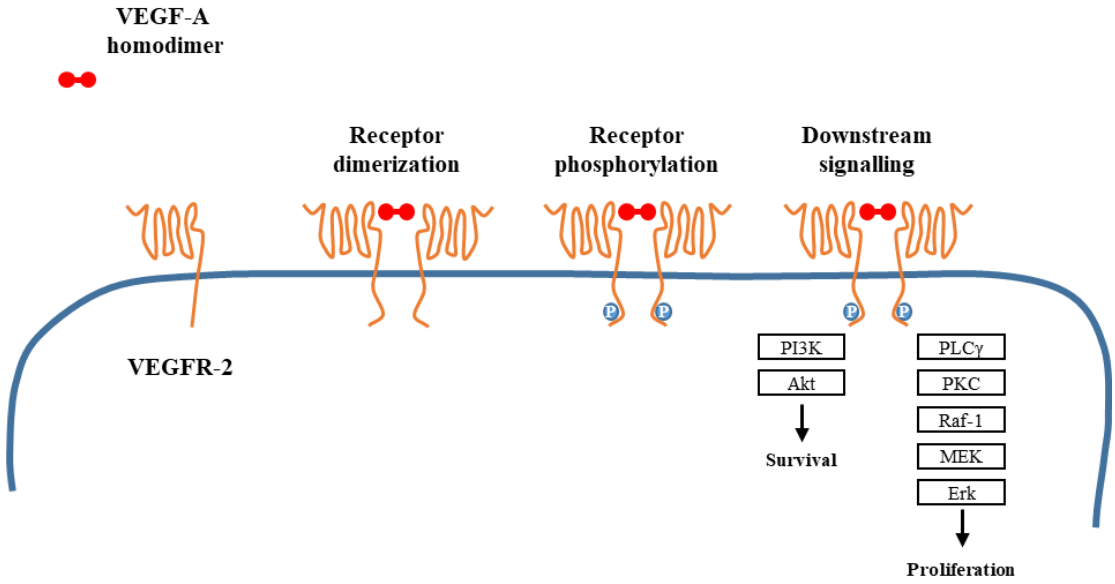

Figure 3. Vascular endothelial growth factor receptor 2 activation and downstream signalling. Following VEGF-A binding, VEGFR-2 dimerizes and intra intracellular tyrosine kinase domains are phosphorylated. This promotes activation of downstream signalling molecules leading to increased cell division and survival.

5.2.2. Mechanism of vasculogenesis

Vasculogenesis is largely considered to promote vessel formation during embryogenesis. However, it has also been shown to be a regulator in adult vessel formation. Drake clearly defined the steps in embryonic vasculogenesis as: 1) angioblast differentiation; 2) blood

island formation; 3) angioblast sprouting; 4) organization of isolated vasculature into an interconnected vascular plexus; 5) endothelialisation and lumenisation [107].

Vasculogenesis is highly regulated by a number of different molecular mechanisms, principally VEGF [107, 108]. Indeed, VEGFR-2 knockdown in mice is embryonic lethal, with embryos dying *in utero* between 8.5 - 9.5 days *post coitum* [109]. This is due to retardation of endothelial and haematopoietic development, with reductions in blood island formation, blood vessel growth and the number of haematopoietic progenitors. In addition, increased ectopic concentrations of VEGF have been shown to induce malformations in vessel structure in Japanese quail embryos, including abnormally large lumen formation [110]. Krah *et al* revealed that basic fibroblast growth factor (bFGF) plays an integral role in vasculogenesis, as addition of bFGF to quail blastodisc cells significantly promotes the formation of vascular structures [111].

As stated, vasculogenesis is also important in adult vessel formation. An interesting study by Shi *et al* demonstrated this using a prosthetic implanted in a canine, in a process they termed 'fallout endothelialization' [112]. It was hypothesised that following the implantation of the prosthetic, re-vascularisation of the graft would occur from the margins from elongating vessels, however Shi demonstrated that vascularisation also occurred from non-marginal areas of the prosthesis [112]. Further research has suggested that this neovascularisation occurs from circulating endothelial progenitor cells, which, following invasion into the prosthesis, were able to form an initially isolated vasculature [113]. In this study, Ashara *et al* demonstrated that circulating endothelial progenitor cells were found in ischaemia tissue and tumours, suggesting adult vessel formation is not entirely reliant on angiogenesis.

The molecular mechanisms behind vasculogenesis are less well-defined when compared with angiogenesis. In addition, the mechanisms which have been explored have focused on embryogenesis, which may rely upon different mechanisms than postnatal vasculogenesis.

5.2.3. Mechanism of angiogenesis

Angiogenesis mechanisms have been much further researched than adult vasculogenesis, with it being regarded as the predominant process promoting postnatal vascularisation. There are two different types of angiogenesis - sprouting and intussusceptive angiogenesis [114]. Sprouting angiogenesis has been studied in greater detail and, as the name would suggest, involves the sprouting of endothelial cells towards an angiogenic stimuli. Whereas, intussusceptive angiogenesis, also known as splitting angiogenesis, involves the dividing of a single vessel into two [114]. Both sprouting and intussusceptive angiogenesis are important in vessel formation within the ovaries [115].

5.2.4. Sprouting angiogenesis mechanism

The mechanism behind sprouting angiogenesis can be divided into different stages, there is the initial increase in vascular permeability coupled with basement membrane degradation, followed by endothelial cell proliferation and migration, and finally vessel stabilisation and lumen formation [114]. However, when discussing these individual mechanisms, it is important to consider them as complex dynamic processes, rather than linear relationships.

The basement membrane (BM) is similar to the extracellular matrix, however is denser and always in contact with cells [116]. It is an amorphous, dense, sheet-like structure

composed of around 50 different proteins, including type IV collagen, laminin and heparan-sulphate proteoglycans [116]. During angiogenesis, the BM is degraded by various matrix-degrading proteins, including MMPs, which are produced by endothelial, stromal and cancer cells [117]. Endothelial cells in contact with the intact BM are typically kept in a quiescent state through contact with collagen IV [118]. Following the degradation of the BM by matrix-degrading proteins, sequestered angiogenic growth factors are released, further promoting endothelial migration and proliferation, and detaching pericytes from endothelial cells [116]. In addition, endothelial migration and proliferation is promoted through the exposure of pro-angiogenic interstitial provisional matrix components, including laminin, the expression of which was found to correlate with newly formed vessels and tip cells [118].

Following BM degradation, endothelial cells undergo a process of migration and proliferation. Firstly, 'tip' cells are selected, these cells have long, thin filopodia which read guidance cues and migrate towards the source of angiogenic stimuli [119]. Tip cells are selected according to VEGF and Notch/Delta-like ligand 4 (Dll4) signalling, which is further illustrated in Figure 4 [120-123]. VEGF binds VEGFR-2 on the surface of endothelial cells, this promotes an upregulation of Dll4 in tip cells [121]. Consequently, Dll4 interacts with Notch receptors on stalk cells, promoting VEGFR-1 expression and inhibiting VEGFR-2 expression [124, 125]. Jagged-1 is expressed by stalk cells and inhibits Notch signalling in tip cells, attenuating VEGFR-1 and promoting VEGFR-2 expressions [120]. The actual selection of the tip cells depends upon small stochastic differences in VEGF concentration within the local environment and the relative expression of VEGFR-1 and -2, which may give an advantage in tip cell selection [126].

The direction of angiogenic sprouting is controlled by the filopodia on tip cells, which was shown by investigating VEGF signalling in postnatal murine retina [122]. It has been

proposed that the filopodia attach to the matrix, and following contraction of the actin filaments within, pull the cell along towards the angiogenic source [127]. Concurrently, stalk cells proliferate, projecting the nascent vessel to the angiogenic source [122, 128]. Endothelial expansion from the stalk cells, rather than tip cells, was shown using Ki67 staining and BrdU labelling [122]. Notch signalling has been extensively demonstrated to inhibit endothelial proliferation within *in vitro* and *in vivo* models [129, 130]. Harrington *et al* demonstrated that overexpression of the Notch ligand, Dll4, attenuated HUVEC proliferation via downregulation of VEGFR-2, impaired activation of the MAPK/ERK pathway, and upregulation of soluble VEGFR-1 [131]. Considering the upregulation of Notch in proliferative stalk cells and downregulation in non-proliferative tip cells, it seems counterintuitive that Notch inhibits endothelial expansion. Notch-regulated ankyrin repeat protein (nrarp) is a downstream signalling protein that expression is regulated by Notch [132]. Studies have shown that nrarp knockdown mice have significantly reduced endothelial cell proliferation and vessel coverage, due to nrarp's role as a negative regulator of Notch [133, 134]. In addition to attenuating Notch signalling, nrarp is an important mediator of Wnt induced angiogenesis [135]. Nrarp inhibits the ubiquitination of the downstream signalling protein lymphoid enhancer factor 1 (Lef1) [136], which through interactions with beta-catenin (β-cat) promote vessel formation [135]. This could be via promotion of cyclin D1 expression which drives cell cycle progression [137]. In addition to canonical Wnt signalling, non-canonical signalling, induced by Wnt5a, is also implicated in angiogenesis [138]. Masckauchán *et al* details how Wnt5a signalling induces endothelial cell proliferation through ERK 1/2 phosphorylation and upregulation of Tie-2 (tyrosine kinase with immunoglobulin and EGF homology domains - 2).

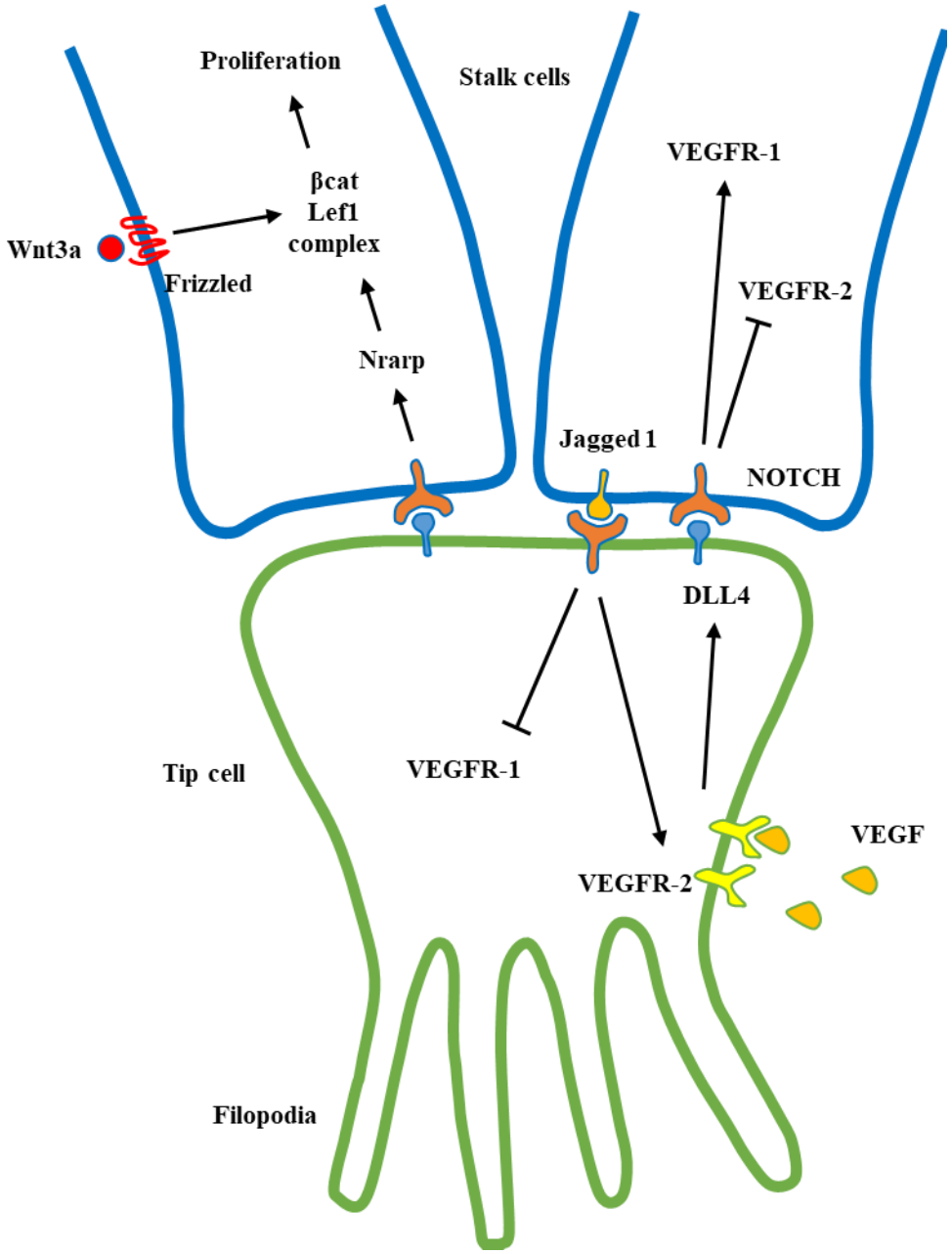

Figure 4. VEGF and Notch signalling within angiogenic sprouts. VEGF induced VEGFR-2 signalling promotes tip cell selection through increase Dll4 expression, which through Notch signalling in neighbouring stalk cells down-regulates VEGFR-2 expression. Jagged-1 in turn inhibits Notch signalling in tip cells. Nrarp coordinates Notch and Wnt signalling via a β-catenin Lef1 complex which drives cyclin D expression and cell cycle progression.

Following sprouting towards the angiogenic source, the vessel is stabilised and lumen formed to ensure correct function - though in cancer these vessels are more aberrant. Lumen formation in the endothelium is believed to occur through three main processes;

cell hollowing, cord hollowing and budding [139]. During cell hollowing, intracellular vacuoles form throughout the endothelial cells and alight with vacuoles in adjacent cells, before fusing and forming a continuous network [140]. Whereas cord hollowing refers to the process of extracellular vacuole fusion and cell rearrangement. Zovein *et al* details an interesting mechanism whereby β1 integrin ablation in nascent endothelium, disrupts cell polarity and adhesion marker localization, concomitantly promoting the accumulation of intracellular vacuoles and occlusion of vessels - identifying β1 integrin as an important mediator of lumen formation [141].

The angiopoietin (Ang) and Tie axis is an important mediator of vessel stabilisation and maturation [142]. Tie receptors include Tie-1 and Tie-2, and are extensively expressed by endothelial cells [142]. Tie-1 is an orphan receptor with no known ligand. Regardless, murine null mutants of Tie-1 developed severe oedema and died between days 13.5 and 14.5 of gestation - suggesting Tie-1 plays an integral role in vessel stabilisation [143]. Angiopoietins are a family of glycoproteins and are known ligands of Tie-2 receptors, family members include Ang-1, -2, -3 and -4. Interactions between Ang-1 and Tie-2 have been extensively linked with vessel maturity, cell-cell adhesion, cell survival and reduced vessel permeability [144-146], this is through various downstream signalling pathways including the activation of Akt and MAPK, and inhibition of NFκB via activation of ABIN-2 [147-149]. Ang-1 has been proposed to promote vessel stability through the recruitment of pericytes, or perivascular cells [147, 150]. The mechanisms behind this are unknown, but ultrastructural examination has shown Ang-1 knockout mice have an aberrant endothelium lacking perivascular coverage [151]. Interestingly, Uemura *et al* details how following the abolition of perivascular coverage, via the addition of a platelet-derived growth factor receptor-beta (PDGFR-β) antagonist, the addition of Ang-1

restored the hierarchical vascular architecture and protected against retina oedema and haemorrhaging [152].

5.2.5. Pericytes and the vasculature

Pericytes or perivascular cells are essential components of a stable and mature vasculature, and are located within the basement membrane surrounding the endothelium [153]. Pericytes were first described in the 19th Century, since then their role has been slowly elucidated, and are now recognised to play an important role in maintaining vascular hierarchical architecture, reducing vascular permeability and promoting vessel stability [152, 154-156]. The ratio of pericytes-to-endothelial cells changes depending on location, with a positive correlation being linked with endothelium function. It is therefore unsurprising that the blood-brain-barrier contains the highest ratio, with 1:1 pericytes-to-endothelial cells [64, 157]. Further estimates have predicted that the ratio of pericytes-to-endothelial cells ranges from 1:1 - 1:10, with abluminal endothelial coverage ranging between 70 - 10% [64]. This range was suggested according to experimental observations, but in addition, if much lower ratios were observed, significant proportions of the endothelium would not be in contact with pericytes - a typical pathophysiological observation [64].

Pericytes are notoriously difficult to identify, as such, many studies refer to perivascular or stromal cells when referring to pericyte-like cells [158, 159]. This difficulty is due to there being no universally accepted marker which is specific and stable in expression. Some commonly used pericyte markers include, chondroitin sulfate proteoglycan 4 (NG2), PDGFR-β and alpha-smooth muscle actin (α-SMA) [160]. However, each of these markers are additionally expressed by other cells types, i.e. α-SMA being expressed by

smooth muscle cells and myofibroblasts [161], and as such, are not entirely reliable. But though difficult to identify, the role pericytes play in vessel formation and stability has been extensively studied.

5.2.6. The PDGF-B - PDGFR-β axis

The PDGF-B - PDGFR-β axis plays an essential role in the recruitment of pericytes to nascent vessels, and is perhaps the greatest studied system when considering pericyte - endothelial interactions [155]. PDGFR-β is a receptor tyrosine kinase, which upon PDGF-B binding, undergoes receptor dimerization that activates downstream signalling cascades, including the PLCγ and PI3K pathways [162]. Loss of PLCγ and PI3K interactions with PDGFR-β in mesangial cells and mouse embryonic fibroblasts causes a reduction in cell proliferation and migration [162]. However, this same effect was not observed in an *in vivo* mouse model, suggesting some compensatory mechanism. Indeed, activation of PDGFR-β has also been linked with downstream activation of the ERK/MAPK pathway, which is known to drive PDGF-B induced cell proliferation in NIH3T3 cells, a commonly used PDGF-B sensitive fibroblast cell line [163]. This could suggest that following the abolition of downstream PLCγ and PI3K signalling, PDGFR-β could alternatively promote cell proliferation through the ERK/MAPK pathway.

PDGF-B may function as either a hetero- or homo-dimer (PDGF-BB or PDGF-AB) but is more commonly considered as the homodimer when interacting with PDGFR-β. PDGF-B is commonly expressed by endothelial cells [164]. Indeed, Hellström *et al* revealed that it is immature and sprouting endothelial cells that express PDGF-B, promoting pericyte recruitment to nascent vessels [165]. They went on to show that

pericytes proliferate at sites of PDGF-B expression, highlighting the role of PDGF-B as a pericyte mitogen.

The importance of pericytes in normal endothelium development is highlighted by a number of PDGFR-β or PDGF-B knockout mouse models [155, 165, 166]. One model revealed how the abrogation of pericyte interactions with endothelial cells promoted endothelial hyperplasia, increased capillary diameter, and reduced vessel permeability [166]. Hellström suggests that this increase in vascular permeability may be a result of tight junction disruption observed in PDGF-B and PDGFR-β knockout embryos.

5.2.7. Vascular junction proteins

The barrier properties of the endothelium rely upon a number of junction protein complexes, most notably tight junctions, but also adheren junctions [167]. Tight junctions are the most apical located intercellular junction complex in the polarized endothelium, and function by inhibiting the diffusion of polar substances from the blood into the basolateral compartments [168]. In addition, tight junctions act as fences to transmembrane proteins and lipids, ensuring they remain in their distinctive apical or basolateral domains. Claudins are a family of proteins that have been linked with playing an integral role in barrier formation in tight junction, and may function as either barrier- or pore-forming structures [169]. This is thoroughly described by Günzel *et al*¸ who extensively details the properties of a number of individual claudin proteins [169].

Zonula occludens-1 (ZO-1) is a junctional adaptor protein, essential for the stabilisation and function of tight junctions [170, 171]. *In vitro* knockdown of ZO-1 in epithelial cells results in increased solute permeability, which may be recovered with the expression of an N-terminal construct containing the PDZ, SH3, and GUK domains of ZO-1 [170]. This

was repeated in endothelial cells by Tornavaca *et al*, who demonstrated ZO-1 knockdown increased transendothelial permeability, due to loss in claudin-5 expression [172]. Highlighting the importance of ZO-1 in development, ZO-1 homozygous knockout mouse models are embryonic lethal, with defective angiogenesis and extensive apoptosis observed [173]. Interestingly, Katsuno *et al* reported that ZO-1 knockout led to the development of no identifiably mature or remodelled endothelial vessels after 9 days compared with wild-type mice. Similarly, ZO-1 siRNA inhibited vessel formation in a 3D microcarrier based fibrin gel angiogenesis assay [172]. Though ZO-1 is primarily considered to interact with tight junction proteins, it is also an important regulator of adheren junctions [174]

Adheren junctions are located more basally than tight junctions and are important mediators of cell-cell adhesion, intracellular signalling, and actin cytoskeleton remodelling [174]. VE-cadherin (VE-cad) is an essential component of adheren junctions and is anchored to the actin cytoskeleton by a number of intracellular adheren junction proteins, including the catenin family members; α-, β-, δ-, and γ-catenin (cat) [175]. Similar to what is reported in ZO-1 knockout mice, VE-cad-deficient mice are embryonic lethal due to vascular defects [176]. Interestingly, a nascent vascular plexus forms, but fails to mature and remodel, leading to extensive vessel regression and endothelial apoptosis. This was due to preventing the formation of a VE-cad, β-cat, PI3K and VEGFR-2 complex, which is responsible for VEGF-A induced activation of downstream Akt and Bcl-2, and prevention of endothelial apoptosis. The role of VE-cad in vascular integrity was further clarified by Corada *et al*, who revealed that upon the treatment of a VE-cad blocking monoclonal antibody an increase in vascular permeability was observed in the heart and lungs of an *in vivo* mouse model [177].

5.3. High-grade serous ovarian cancer models

The development of novel models of HGSOC, either *in vitro* or *in vivo*, offers an opportunity to further understand disease pathogenesis. There are currently many different models of HGSOC, each with their own distinct advantages and disadvantages.

5.3.1. *In vivo* models of high-grade serous ovarian cancer

Patient derived xenograft (PDX) models are commonly used *in vivo* representations of HGSOC. In PDX models malignant cells are extracted from the patient tumour and injected directly into immune-deficient mice, however, more commonly, mice are injected with *in vitro* grown ovarian cancer cells lines (xenograft mouse models). Cells are typically injected either intra-peritoneally, intra-bursally or subcutaneously, where they then spread throughout the abdomen and peritoneum - resembling the metastatic human disease. The advantage of transferring cells directly from the tumour to mice, is culturing cells *in vitro* prior to transfer enables the development of mutations affecting morphology, motility, invasion and proliferation [178]. Human tissue hetero-transplantation is an advanced xenograft model, where the native stroma and extracellular matrix are also transferred to the host mouse. Using this system, Xu *et al* demonstrated a high growth rate of tumours following implantation of tumour specimens in the intra-abdominal gonadal fat pads of severe combined immune-deficient (SCID) mice [179]. This success was suggested to be as a result of cancer cells being integrated within a native microenvironment, enabling them to more efficiently assimilate within the host environment. In addition, this technique lessens the reduction in cell heterogeneity which inevitably occurs when implanting ovarian cancer cell lines. Due to this, and the added native stroma and matrix, surgical hetero-transplantation allows the PDX model to more closely mimic HGSOC [179]. A proposed model by Elkas *et al* details the creation of an

ovarian carcinoma PDX model through the intraperitoneal injection of tumorigenic 'slurry' [180]. This model replicated tumour progression through the development of metastatic spread and bloody ascites. In addition, when administered with an adenoviral-mediated p53 gene therapy, tumour weight significantly decreased, suggesting these to be suitable models to investigating novel therapies. This study highlights the effectiveness of PDX models as systems to study novel therapeutics.

Genetically engineered mouse models (GEMM) are another commonly used *in vitro* model of HGSOC. An earlier mentioned study by Perets *et al* details the creation of GEMMs expressing a Tet on-off system to knockdown BRCA, TP53 and PTEN expression via a (paired box 8) PAX8 promoter – specifically targeting the fallopian tube cells [32]. This study demonstrated with the knockdown of HGSOC marker genes, Dox-activated fallopian tubes undergo increased secretory cell proliferation, loss of cell polarity, cellular atypia and serous histology – mimicking the STIC histology. Interestingly, this progresses into a 'pseudo-HGSOC' involving tumour metastasis to the ovaries and peritoneal cavity. This study demonstrates the importance of understanding disease biology when developing a model for cancer.

5.3.2. *In vitro* models of high-grade serous ovarian cancer

Traditional *in vitro* models cultures cells on tissue culture plastic in two-dimensional (2D) monolayers. A recent investigation into the genomic profiles of 47 commonly used HGSOC cell-lines has demonstrated that many are unrepresentative of the disease [181], this includes some of the most popular cell lines such as SKOV3 and IGROV1. This is highlighted by the twelve most suitable candidates to represent HGSOC accounting for only 1% of PubMed citations describing HGSOC models in 2013, out of the 47

investigated [181]. According to this study, cell lines which most represent HGSOC genetically are often misclassified, i.e. KURAMOCHI cells are classified as undifferentiated carcinoma. The failure of popular cell lines to not accurately represent HGSOC is undoubtedly varied, with miscommunication in the scientific community undoubtedly playing a role [182]. In addition, the cell lines investigated have been cultured for many years which may impact on their genetic makeup [183]. These studies highlight the importance of selecting a representative cell line for studies, particularly when evaluating drug response.

Traditional two-dimensional (2D) models of disease are critiqued for their validity in representing observed pathophysiology. Three-dimensional (3D) models are being explored as more accurate representations of the tumour microenvironment, which better mimic the *in vivo* response during drug development [184]. Typically, 3D models involve the embedding of cells within a natural, or artificial 3D hydrogel. Natural hydrogels, such as Matrigel^{TM} and fibrinogen, are currently the gold-standard 3D matrix due to their inherent extracellular matrix (ECM)-like biological properties, with cells displaying high viabilities within these system [185]. However, manipulation of biological and mechanical properties of natural hydrogels is challenging, though fibrinogen concentration is known to have a positive correlation with structural modulus [186]. The manipulation of hydrogel properties when mimicking disease pathophysiology is extraordinarily important, particularly as stiffness was recently shown to be positively correlated with disease score in HGSOC [46].

Peptide-functionalised multiarm polyethylene glycol gels are commonly used artificial hydrogels, and are frequently formed via the factor XIII-catalysed cross-linking mechanism [180, 187]. Gel stiffness can be controlled through changing the polymer dry mass of the hydrogel. Biological functions can be added to these matrices through the

incorporation of peptides (Arg-Gly-Asp) and other components during the gel formation stage. Gel degradation can be regulated through the incorporation of specific degradation motifs throughout the matrix, allowing cells to remodel their microenvironment, an important process in angiogenesis. A study by Loessner *et al* used PEG gels to investigate HGSOC and the effect of cell-ECM interactions on sphere formation, using OV-MZ-6 and SKOV-3 cells [187]. It was demonstrated that more compact and smaller cell spheroids grow in stiffer gels. In addition, integrin engagement significantly increased cell proliferation. Furthermore, the inhibition of cell-mediated matrix remodelling significantly inhibited proliferation. OV-MZ-6 cells cultured in 3D are more chemo-resistant to paclitaxel than when cultured in 2D, cell viability being reduced by 40% and 80%, respectively [187]. This chemo-resistance has been attributed to decreased penetrance of the anti-cancer drug and increased survival signalling. The differences observed between 2D and 3D cultures can be credited to forcing cells to grow in unnatural condition, which is known to alter cell behaviour [188, 189].

HGSOC is believed to originate from transformed FTSECs. Lawrenson *et al* developed a 3D model to mimic these early stages of HGSOC [190]. This model features FTSECs which have been isolated from fallopian tubes immediately following surgery, before seeding on poly-2-hydroxyethyl methacrylate (poly-HEMA)-coated tissue culture dishes, inducing spheroid formation. The FTSECS formed mono- or multi-layer epithelial sheets around a central hyaline matrix core. Gene expression analysis identified >1000 genes which were differentially expressed between spheroid FTSECS and those grown in 2D.

5.4. Microfluidics

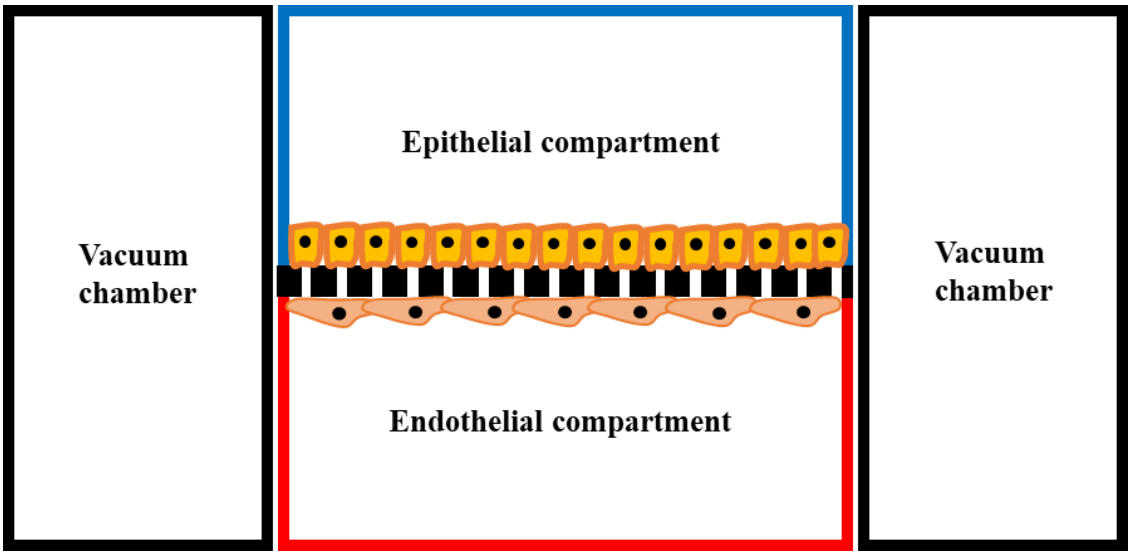

Figure 5. Schematic of the lung-on-a-chip. Representation of the lung-on-a-chip device developed by Huh *et al* [191]. Human alveolar epithelial cells and microvascular endothelial cells are seeded in separate channels. The epithelium channel is perfused with air, whereas the endothelium layer is perfused with blood. The vacuum applied to the hollow side channels induces physiological stretching of the adhered cells mimicking breathing

Microfluidics and micropatterning offer an interesting new avenue to develop novel HGSOC models. Organ-on-a-chip devices were pioneered by Ingber *et al*, who developed the lung-on-a-chip device, which was shown to accurately mimic organ function [192]. This model can be seen in Figure 5 and constitutes two central channels that are separated by a porous polydimethylsiloxane (PDMS) membrane coated with ECM proteins. Human alveolar epithelial cells and microvascular endothelial cells are introduced to opposite surfaces of the PDMS porous membrane, forming cellular monolayers. Intrapleural pressure is replicated by two hollow lateral microchannels, which when a vacuum is applied, causes elastic deformation of the cell-containing microchannels and stretching of the PDMS membrane and adherent cell layers. When the vacuum is released the PDMS membrane and adherent cells relax, this process replicates breathing. In addition, air is

flown through the alveolar epithelial layer and blood through the microvascular endothelial layer. This system was successful in demonstrating the effectiveness of on-a-chip models. Since the creation of the lung-on-a-chip, magnitudes of similar devices have been developed for different organs, including brain, liver, kidney, bone marrow and gut [193-197]. .

5.4.1. Current microfluidic platforms

Organ-on-a-chip is a colloquial term used to describe devices which are typically created using photo- and soft-lithography, which is further described in the Materials and Methods section (p. 59). This technology is easy to use and replicate, with the ability to innovate your own designs dependent on your objectives.

One of the most commonly used designs, as shown in Figure 6, features a central gel channel and two lateral medium channels. The gel channel is separated from the media channels by vertical posts. During hydrogel injection into the central channel, the posts ensure laminar gel flow - preventing gel leakage into side compartments. Upon curing of the hydrogel, medium is added to the lateral side channels, which is then able to diffuse through the gaps between posts into the central channel and supply any embedded cells with nutrient etc.

Jeon *et al* used a three-channel microfluidic chip to investigate organ-specific human breast cancer cell extravasation into bone- (BMi) and muscle- (MMi) mimicking microenvironments through a microvasculature [198]. Depending on the microenvironment being mimicked, the central channel was injected with one of two cell tri-cultures. When mimicking bone, human bone marrow derived mesenchymal stem cells (hBM-MSC), osteo-differentiated (OD) hBM-MSCs and primary GFP-tagged human

umbilical vein endothelial cells (HUVECs) were embedded in fibrin gel. Whereas, hBM-MSC, GFP-tagged HUVECs and C2C12 (myoblast cell line) were embedded in fibrin gel to mimic muscle. This study demonstrated that extravasation rates of MDA-MB-231 metastatic breast cancer cells in the BMi microenvironment were significantly higher compared to MMi microenvironment and control (no stromal cells). They concluded that C2C12 derived adenosine inhibited cancer extravasation in the MMi, which was inhibited with the introduction of an adenosine receptor antagonist.

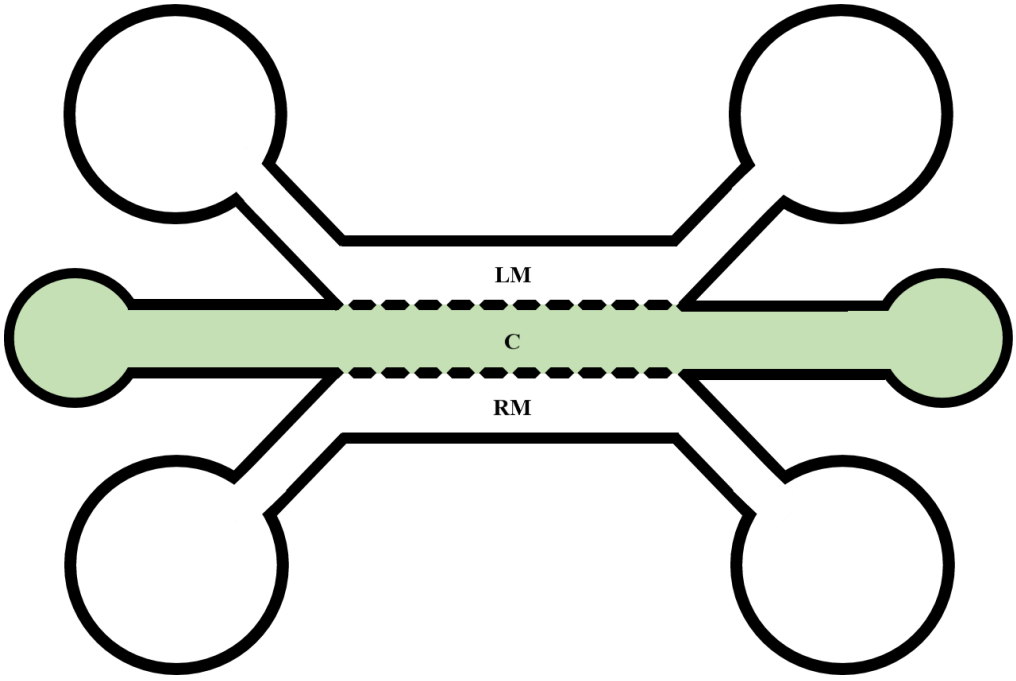

Figure 6. Schematic of three-channel device. Representation of device used by Jeon *et al* to investigate cancer cell extravasation [198]. The device incorporates a central gel channel (C) and two lateral medium channels (LM and RM). Schematic is not to scale.

Another commonly used microfluidic device incorporates five parallel channels; a central gel channel, two stromal cell culture channels and two medium channels – as shown in Figure 7. Kim *et al* investigated vasculogenesis and angiogenesis using this platform [199]. To investigate vasculogenesis, HUVECs were seeded in the central channel embedded within a fibrin gel, whereas normal lung fibroblasts (LFs) were seeded in the

flanking stromal cell channels (LS, RS). Remarkably, HUVECs were able to form perfusable network when co-cultured with the LFs without additional VEGF. This was due to exogenous factors being released by the LFs. To investigate angiogenesis, HUVECs were cultured on the left side-wall of the acellular fibrin matrix of the C channel, LFs were then seeded in the opposite RS channel – this exposed HUVECs to a pro-angiogenic gradient. It was observed that HUVECs sprouted in a directional response to LF pro-angiogenic secretions. The co-culture of HUVECs with highly malignant multiforme cells (U87MG) was also explored, in the angiogenesis paradigm. In this model HUVECs were again cultured in the central channel, but with U87MG cells replacing LFs in the stromal channel (RS). It was demonstrated that in comparison to LF induced sprouting, U87MG sports had an aberrant morphology, including the presence of immature branching and poorly lumenised vessels.

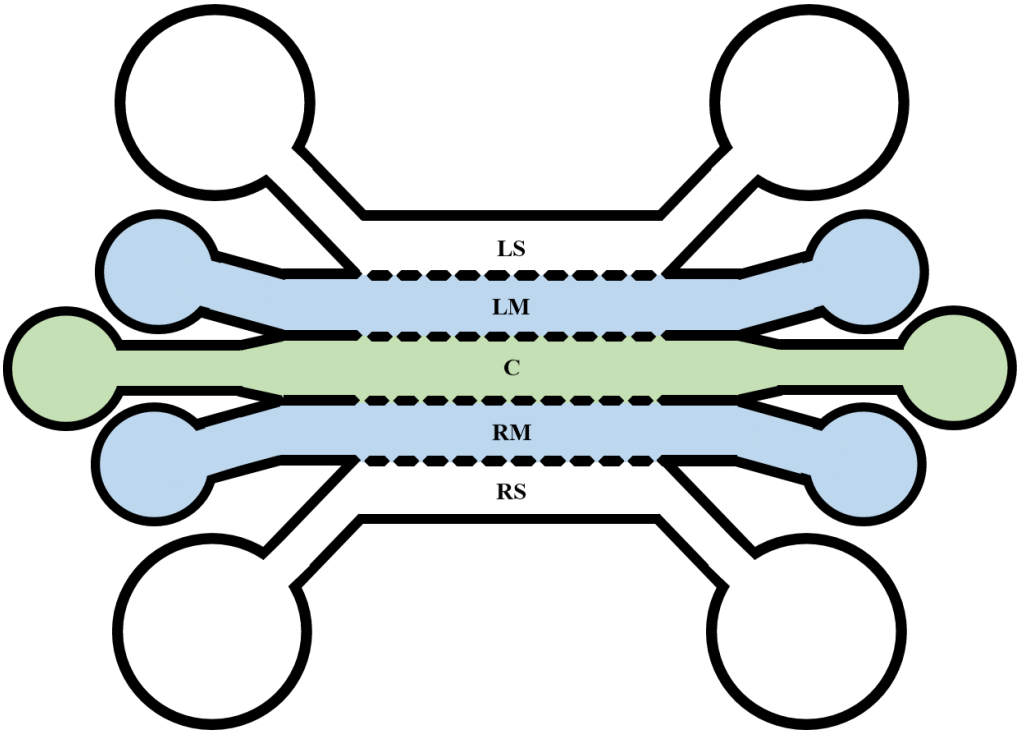

Figure 7. Schematic of a five-channel PDMS device. Representation of device used by Kim *et al* to investigate vasculogenesis and angiogenesis [199]. The device incorporates central gel channel (C), separated from two stromal compartments (LS and RS), by lateral medium channels (LM and RM). Schematic is not to scale.

Shin *et al* proposed a novel microfluidic platform incorporating four separate hydrogel compartments separated by three channels (see Figure 8) [200]. This system was designed to allow the investigation of a number of different mechanisms within one system, as cells may be seeded in four different gel compartments, or three 2D channels. This allows a number of different mechanisms of cell-cell communication, be it autocrine, juxtacrine or paracrine. The authors propose this design could be used to investigate cancer-dependent angiogenesis. In this system HUVECs would be seeded in the central channel and cancer cells in an opposing channel (with normal medium in the other). This would allow cancer-vasculature paracrine signalling and the analysis of angiogenesis, vessel structure and function, and the impact of angiocrine signalling on cancer cells. The authors have used this platform to study processes such as angiogenesis, cancer metastasis and hepatocyte morphogenesis [201, 202].

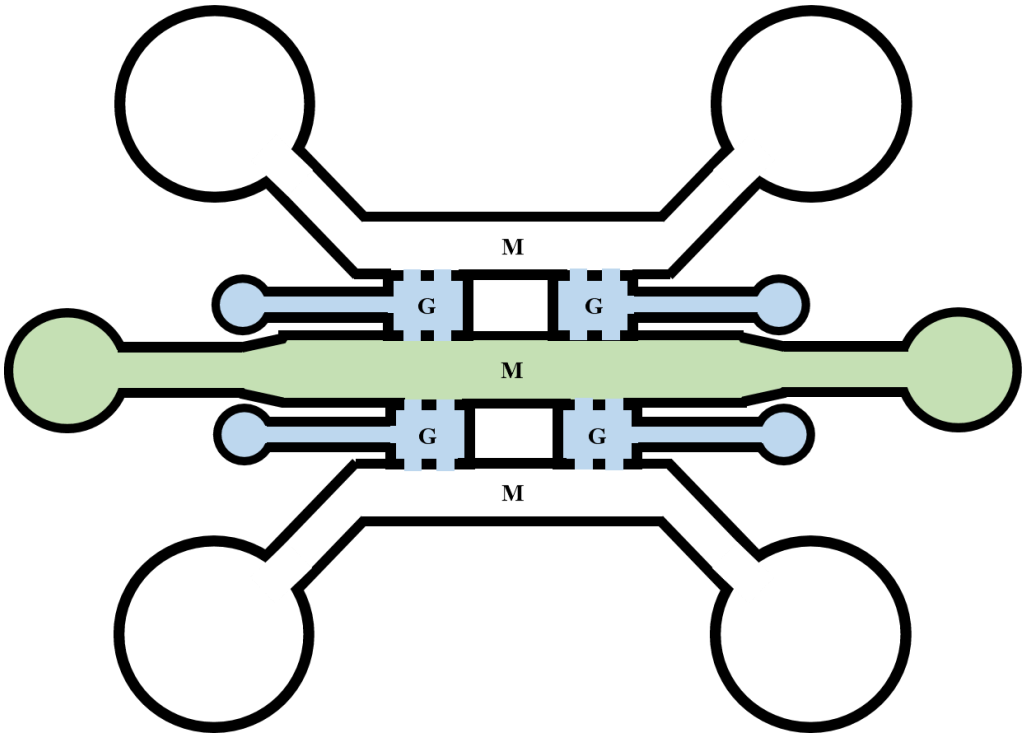

Figure 8. Schematic of seven-compartment PDMS device. Representation of device proposed by Shin *et al* to investigate multiple paradigms [200]. The device incorporates four gel compartments (G) which are separated by three parallel channels (M). Schematic is not to scale.

5.4.2. Advantages and limitations of microfluidic devices

It was announced in 2014 by the Tufts Center for the Study of Drug Development that the average cost of bringing a new drug to market is $2.6 billion - significantly more than the $802 million reported in 2003 [203]. A large part of this cost was due to difficulties and delays regarding safety, and efficacy (or both), with compounds in the early stage of development. Microfluidics and organ-on-a-chip devices can act as effective links between traditional *in vitro* and *in vivo* models, and potentially reduce this cost burden by acting as more representative models of pathophysiology.

Organ-on-a-chip devices have a number of advantages when compared with traditional *in vitro* and *in vivo* models, further described in Table 2. Compared with 2D *in vitro* models, microfluidic systems cultures cells in a 3D microenvironment which offers phenotypic and genotypic advantages [184]. Indeed, culturing A549 lung adenocarcinoma in vascularised 3D microfluidic devices allowed the more accurate prediction of the efficacious concentrations of 12 compounds which inhibited EMT, compared with 2D culture [204]. In addition, Aref *et al* highlighted that the design of the device allows the researcher to determine how different cell populations communicate. As well as determining how cells communicate, microfluidics allows control of how the physical microenvironment communicates with the cell, this could be through the manipulation of the substrate to which cells are adhered, or through the induction of flow [192, 205]. Furthermore, microfluidics, as the name implies, requires little material and cells for culture - this is especially beneficial when dealing with particularly expensive reagents and/or cells.

Compared with *in vivo* experiments, microfluidic models have less ethical constraints regarding animal experiments (though many reagents used are derived from animals). In addition, *in vivo* models are expensive, requiring more reagent and many repeats.

Whereas, microfluidic culture is much cheaper, using less reagents and requiring a standard cell culture laboratory. Microfluidic systems also allow live-imaging, requiring simple protocols and relatively standard equipment. Whereas, *in vivo* live-imaging can involve invasive, technical procedures, such as cranial windows within rodents [206]. This is perhaps best demonstrated by the lung-on-a-chip system, which clearly demonstrated with the use of real-time, high resolution microscopy that mechanical stress from breathing motions promotes interleukin-2 (IL-2) induced pulmonary oedema during cancer therapy [192].

Though microfluidics offers some key advantages over more traditional models, it also, like all techniques, has limitations. Organ-on-a-chip systems allows researchers to further the understanding of organ function and molecular interactions. But some physiology is impossible to mimic using these systems, for example behavioural experiments which are extensively used in anti-depressant/-anxiety studies. However, organ-on-a-chip models can be used to further understand brain function, on a cell and molecular level [193, 207, 208]. PDMS is extensively used in organ-on-a-chip studies due to its inherent properties of flexibility, optical clarity, biocompatibility, cost, and easy bonding with glass. However, PDMS is also known to absorb low concentrations of small hydrophobic compounds - suggested to reduce pharmacological concentrations [209]. This can make PDMS devices unsuitable to test many small molecule compounds, though by evaluating drug absorbance, it is possible to adjust drug concentrations suitably. Organ-on-a-chip studies have attracted great interest due to their ability to recapitulate the human physiology. However, the techniques and understanding required to create these devices are alien to many researchers, particularly those from biology backgrounds. Thus, researchers need to be more transparent when describing the techniques used to enable uptake and further research. Perhaps the panacea of this is 3D printing of devices, which

would allow the rapid uptake of organ-on-a-chip techniques across institutes and groups - though this is an area with its own difficulties. In addition, certain microfluidic device designs make extensive molecular biological experiments difficult (e.g. Western blot and PCR). This is due to the covalent bonding between the PDMS and underlying glass substrate, making it extraordinarily difficult to extract the hydrogel/cells from the device to conduct further analysis. However, Lee *et al* revealed that by replacing the glass substrate with a PSA film, this allows non-covalent bonding of PDMS to the underlying substrate and easy detachment [207]. This allowed Lee to detach the PDMS and remove the cells embedded with the hydrogel and conduct Western blot analysis. This highlights that with innovation, microfluidic device design allows you to overcome different issues.

Microfluidics offers a reliable bridge between traditional *in vitro* and *in vivo* models. Perhaps not best suited to broad, high-throughput screening like traditional 2D culture, but following the identification of lead compounds, could allow the accurate analysis of toxicology and efficacy, before progressing to further *in vivo* studies. This could enable the identification of efficacious and safety issues described previously, and reduce the cost and time for novel drug development.

Table 2. Advantages and limitations of microfluidic models

Compared with in vitro		**Compared with *in vivo***	
Advantages	*Limitations*	*Advantages*	*Limitations*
Control cell interactions	Limited molecular biology analysis	Less time-consuming	Behavioural experiments
More complex	Less throughput	Less ethical issues	More complex
Fluid flow	Cheaper	Human cells	
Use less cells and material	Requires expertise and equipment	Live-imaging	
Mechanical cues	Not standardised		

6. Aims and objectives

Microfluidics offers a robust and affordable approach towards developing novel models for human disease. These platforms are simple in design, yet mimic the human physiology, while enabling us to carefully manipulate the microenvironment to investigate disease progression. Cancer-on-a-chip models for various diseases currently exist, with breast, liver and bone marrow cancer all being successfully mimicked [197, 198, 210, 211]. However, to the best of our knowledge, no such model currently exists for HGSOC. The proposed model aims to integrate HGSOC cells with a perfusable endothelium, which will allow the perfusion of drugs and perhaps cells throughout this system.

Research will initially focus upon the development of a reproducible vascularised network, based upon similar reported systems. However, the literature is inconclusive regarding the exact parameters to use, with little explanation regarding final published concentrations. This thesis therefore aims to explain the relationship between the final developed vasculature-on-a-chip, and the reagents used to create it.

Following the development of this vascular system, interactions between the vasculature and stromal cells will be investigated. As mentioned, many system use stromal support cells to promote the formation of the vasculature, such as lung fibroblasts and pericytes [156, 199]. This thesis aims to investigate the impact of these cells, particularly pericytes, on the developed vasculature, to see if they support vessel stability, improve barrier function and inhibit vessel hyperplasia.

Using the developed vascular system, interactions between endothelial cells and HGSOC will be investigated. These studies will aim to investigate the impact of HGSOC on the

vasculature, and vice versa. In addition, the impact of chemotherapeutics, namely carboplatin, on the developed system will be investigated.

7. Materials and Methods

7.1. Cell culture

7.1.1. HUVEC and G33 culture

HUVECs were obtained from Lonza and cultured in Endothelial Growth Medium-2™ (EGM-2, Lonza) or EGM-2™ BulletKit™ (Lonza), with passages 2-6 used in experiments. G33 cells were isolated from patient biopsies and cultured in Dulbecco's Modified Eagle Medium F-12 GlutaMax™ (DMEM F12, Thermo Fisher Scientific) supplemented with 10% foetal bovine serum (FBS) and 1% penicillin/streptomycin, with passages <30 used for experiments. G33 cancer cells were kindly gifted from the Balkwill lab. Pericytes were obtained from Promocell and cultured in Pericyte Growth Medium™ (PGM, Promocell), with passages 2-6 used in experiments. Normal Human Lung Fibroblasts (NHLFs) were obtained from Lonza and cultured in the Fibroblast Growth Medium-2 Bulletkit™ (Lonza), with passages 2-10 used in experiments. Cells were cultured in T75 flasks until achieving 80-90% confluency and then either passaged or used in experiments. Cells were maintained in a humidified incubator at 37 °C and 5% CO_2. Except pericytes, when passaging cultures, cells were initially washed with Dulbecco's Phosphate Buffered Saline (DPBS, Sigma-Aldrich) before detachment using a 9:1 ratio of Versene (Thermo Fisher Scientific) and Trypsin (Life Technologies Ltd) respectively, before centrifugation (5 min, 1,200 revolutions per min (RPM)) and resuspension in their respective medium. Pericytes were detached using the Detach-30 kit™, as according to manufacturer's protocol, before centrifuging (3 min), 1,200 RPM) and resuspension in PGM. Cells were then quantified using a haemocytometer before resuspension in a new flask.

7.1.2. Cryopreservation and resuscitation of samples

Samples were prepared in a 70% medium, 20% FBS and 10% dimethyl sulphoxide v/v solution (DMSO, Sigma-Aldrich), with 1×10^6 cells/mL. 5×10^5 cells were added per cryovial (Nalgene), before temporary storage overnight in a Mr. Frosty at -80 °C, following by long-term storage in a liquid nitrogen cryobank.

Samples were removed from the cryobank and thawed in a 37 °C water bath before diluting samples in 20 mL of medium and centrifugation. Following centrifugation, samples were re-suspended in 10 mL of their respective medium and seeded in a T75 flask, with medium replaced after 24 h.

7.1.3. Vasculogenesis cell seeding

This protocol was developed throughout this thesis and is the final reported iteration. Reported concentrations and conditions may therefore differ to what is discussed throughout this thesis. In addition, given concentrations are final, but when creating fibrin gels fibrinogen and thrombin solutions are mixed 1:1, thus initial concentrations of starting solutions will be higher. Fibrinogen solutions were prepared by mixing bovine fibrinogen (Sigma-Aldrich) in DPBS, and dissolving in a 37 °C water bath for 2 h, with the final concentration being 10 mg/mL. Concomitantly, a thrombin solution was prepared by mixing thrombin and DPBS, achieving a final concentration of 2 U/mL. Following HUVEC detachment, cells are counted, re-centrifuged and re-suspended achieving a final concentration of 6×10^6 HUVECs/mL in the thrombin solution. During pericyte single-channel co-culture pericytes are also added to the same thrombin solution, achieving a final density of 6×10^5 pericytes/mL. 10 µL of cell suspension is mixed with an equal amount of the fibrinogen solution before injecting into the gel channel. Devices are then incubated for 5 min in a humidified incubator at 37 °C and 5% CO_2. The inlet

reservoirs are loaded with EGM-2, and using suction, the hydrophobic side-channels are filled, with a total of 400 µL medium per chip. When seeding PDMS wells, a total of 40 µL gel was injected before adding 100 µL EGM-2. To promote vessel formation, EGM-2 is further supplemented with 50 ng/mL VEGF (Peprotech), with medium replaced every 24 h.

7.1.4. Cancer cell seeding

Fibrin gels were created similarly as reported in 7.1.3. G33s were re-suspended in the thrombin solution achieving a final cell density of 6×10^5 G33s/mL. The cell suspension was mixed 1:1 with fibrinogen solution before injecting into the PDMS wells and adding 80 µL EGM-2. PDMS wells were incubated at 37 °C and 5% CO_2. Culture medium was replaced every 24 h.

7.1.5. Cancer spheroid seeding

G33 cancer spheroids were cultured in Corning™ 96-well clear ultra-low attachment well plates (Fisher Scientific). G33 and HUVEC cells were detached, re-suspended and counted (as previously described), before seeding 2×10^4 and 5×10^3 cell respectively per well, with a total of 300 µL suspension per well. Spheroids were cultured for 72 h before use.

7.1.6. LIVE/DEAD assay

The LIVE/DEAD™ viability/cytotoxicity kit (Thermo Fisher Scientific) was used according to manufacturer's protocol. Briefly, samples were washed twice with DPBS followed by 1 h incubation, at 37 °C, with 5 µM ethidium homodimer and 4 µM calcein

AM dissolved in DMEM F12. Samples were then washed thrice with PBS before imaging.

7.1.7. Immunostaining

Devices were washed three times with phosphate buffered saline (PBS, Sigma-Aldrich) before fixation in 4% para-formaldehyde (PFA) for 20 min at room temperature (RT). Samples were then washed thrice with PBS and incubated with 0.4% Triton X-100 solution for 10 min at RT, before washing twice with PBS. Next, samples were blocked >4 h in 3% bovine serum albumin (BSA, Sigma-Aldrich) blocking buffer solution at RT, before overnight incubation (4 °C) with primary antibodies. Mouse monoclonal alpha-human smooth muscle actin (α-SMA) Alexa Fluor 488-conjugated antibody (R&D Systems) 1/100, mouse monoclonal human CD31 Alexa Fluor 488-, 594- and 647-conjugated antibodies (BioLegend) 1/100, mouse monoclonal zona occludens-1 Alexa Fluor 594-conjugated antibody (Thermo Fisher Scientific) 1/200, mouse monoclonal beta-catenin Alexa Fluor 647-conjugated antibody (Thermo Fisher Scientific) 1/100, mouse monoclonal VE-cadherin Alexa Fluor 488-conjugated antibody (Fisher Scientific) 1/100, and rabbit monoclonal Ki67 Alexa Fluor 488-conjugated antibody (Abcam) 1/200 were used for staining. Following antibody staining, cell nuclei are stained using 4′,6-diamidino-2-phenylindole (DAPI, Sigma-Aldrich) 1/1000 and F-actin filaments were stained using Phalloidin-Tetramethylrhodamine B isothiocyanate (Merck) and Phalloidin Alexa Fluor 555 (Thermo Fisher Scientific) at 1/500 and 1/40, respectively, for 1 h at RT. Following staining, samples were washed with PBS and stored at 4 °C before imaging.

7.1.8. Cell counting kit-8 assay

Cell counting kit-8 assay (CCK-8, tebu-bio) was used to evaluate carboplatin treatment of G33 and G164 cancer cells. IC50 values were obtained for cells cultured on 2D tissue culture plastic, re-suspended within a 3D fibrin gel or as a spheroid embedded within fibrin gel, with 2×10^4 cells always being tested. Cells were cultured for 24 h before adding carboplatin EGM-2 solutions (0-5000 µM). Following carboplatin addition, cell metabolism was evaluated after 24, 48 and 72 h using the CCK-8 assay kit. Briefly, 30 µL of reagent was added per 500 µL medium and incubated for 4 h with the sample. Following incubation, colour change was evaluated using the SPECTROstar Nano plate reader (BMG Labtech), measuring absorbance at 450 nm.

7.2. Microfabrication and material characterisation

7.2.1. PDMS well fabrication

A PDMS polymer was cast in a petri dish, at a 10:1 ratio between the PDMS base and curing agent, before being cured for 24 h in a dry oven at 60 °C. Following thermal curing, PDMS was cut into shape and gel reservoirs punched using 4 mm or 6 mm biopsy punches. PDMS devices and glass coverslips were cleaned with deionised water, ethanol, acetone and nitrogen gas, followed by attachment via treatment with oxygen plasma for 60 seconds to form covalent bonding between them. Hydrophobicity was restored to the PDMS after plasma treatment by dry oven baking at 80 °C for 2 hours and sterilized by UV irradiation before each experiment. 4 mm and 6 mm wells were used in G33 and HUVEC experiments respectively.

7.2.2. Microfluidic chip fabrication

Microfluidic devices were fabricated using a process of photo- and soft lithography. A master with positive relief patterns of SU-8 2050 photoresist (A-Gas Electronic Materials) on a silicon wafer (PI-KEM) was prepared by photolithography. A PDMS (Ellsworth Adhesives) polymer was cast against this master and thermally cured to obtain a negative replica piece. After separation from the master, hydrogel ports and medium reservoirs were punched from the PDMS using a sharpened needle and a 4 mm biopsy punch. The PDMS device and glass coverslip are cleaned using tape and nitrogen gas followed by attachment via treatment with oxygen plasma for 60 seconds to form covalent bonding between them. Devices were then sterilized via autoclaving at 126 °C for 30 min. To dry, and restore devices hydrophobicity post-plasma treatment, devices were dry oven baked at >60 °C for 3 days.

7.2.3. Contact angle

Contact angle was used to investigate PDMS hydrophobic recovery post-plasma treatment. Four conditions were investigated; pristine PDMS, plasma treated PDMS with no recovery, plasma treated PDMS with 3 days RT recovery and plasma treated PDMS with 3 days 60 °C recovery. Upon completion of plasma treatment for the plasma treated PDMS with no recovery, samples were exposed to a 5 µL deionised water droplet. The contact angle between the PDMS and water droplet was extrapolated using the 'Default Method' of the DSA 100 (Kruss Scientific) software. Three replicates per repeat were quantified.

7.3. Analysis

7.3.1. Quantification of vascular formation and morphology

Vessels were fluorescently labelled with either phalloidin or CD31 conjugated primary antibodies. Following staining, vessels were imaged using the Leica TCS SP2 confocal and multiphoton microscope (Leica). Due to the 75 µm height of devices, Z-projections of the microvasculature were obtained and combined using Trans function. Following imaging, vessel formation was quantified using CellProfiler™ [212]. Firstly, vessel visualisation was optimised using various functions, including 'close' and 'clean', followed by skeletonization, which gave a 1-pixel diameter skeleton overlay. This allowed the quantification of the overall skeleton length, termed 'Area Occupied by Tubes' by the software or 'Total Tube Length' in this thesis. Branching could also be investigated to describe vessel formation, however this was highly positively correlated with total tube length, thus the latter was more commonly used to determine vasculogenesis. In addition, vessel Feret's diameter may be determined using CellProfiler. Firstly, the total vessel length is quantified, followed by determining the total pixelated area. Dividing the total pixelated area by the total tube length gives the absolute vessel diameter. Knowing the calibration number of the image allows you to convert this into actual length or area (µm, mm, cm).

7.3.2. Investigating vascular permeability

To investigate the impact of pericytes on vascular permeability and endothelial barrier function, an assay was established based on previous reports in literature [207, 213]. In this assay the vascular system was initially cultured according to previously described protocol, the medium reservoirs were then aspirated and 30 µL EGM-2 containing 25 µg/mL 70 kDa FITC-dextran dye (Thermo Fisher Scientific) added to a single reservoir.

This FITC-dextran dye perfused throughout the vascular network and allowed the visualisation of barrier function by recording dye diffusion across the endothelium into the extravascular compartment over a 30-minute period, using a Lumascope LS720 (Etaluma) live-imaging platform. Using ImageJ, vascular permeability was quantified using a parameter termed 'net-fold intensity change'. Briefly, the intravascular and extravascular dye intensity were recorded at three regions of interest (ROI) per device (image). Following this, the change in net-fold intensity between intravascular and extravascular zone was investigated at T=0 and T=30 min - with a greater fold change indicative of more permeable vessels. T=0 was determined as when the dye intensity was deemed stable within the vessel, therefore some devices were analysed for shorter time periods (shortest time period being 28 min).

7.3.3. Quantification of G33 morphology and number

ImageJ was used in image processing and quantification. Cell density was quantified via manual counting of DAPI stained cell nuclei per ROI, with two ROI per repeat. Cluster morphology was carried out by converting the image into a binary mask, before cleaning the image using 'Remove Outlier' function, the 'Watershed' function was then used to separate clusters. If Watershed did not separate clearly defined clusters this was done manually. Following separation of clusters, each cluster size (area) and circularity was recorded.

7.3.4. Statistical analysis

Multiple statistical analysis tests were carried out dependent on the experimental condition, with all tests being performed with Prism (GraphPad). This includes; unpaired

one-tailed student t-tests, one-way analysis of variance (ANOVA), and two-way ANOVAs. Results are shown as mean ± standard error of the mean (SEM). Statistical significance was assumed for $p < 0.05$. * represents $p < 0.05$, ** represents $p < 0.01$, *** represents $p < 0.001$.

8. Developing a vasculature-on-a-chip

8.1. Introduction to vascularised fibrinogen gels

Vascularised fibrinogen gels have been used in organ-on-a-chip studies to investigate and mimic a range of physiologies and diseases, including the vasculature itself, and colorectal and breast cancers [156, 159, 207, 214, 215]. Using these systems, groups have been able to develop mature lumenised vessel network which express various junction markers and basement membrane proteins indicative of a mature vasculature, including VE-cad, β-cat, ZO-1, laminin and collagen IV [198, 199, 216]. These systems have been shown to have functional properties, as evidenced by the vessels having functional barrier properties [199]. In addition, researchers have been able to study the integration of spheroids within a vessel network, observe cancer cell extravasation through a similar system and observe the change in barrier function with the addition of pericytes [156, 198, 216]. However, little has been published regarding the standardisation of this technique, with different concentrations of fibrinogen, thrombin solutions, HUVEC densities, stromal cells, exogenous factors and compounds being reported without clear justification [159, 198, 199, 213-215]. Such variation in technical details can lead to variability of results and poor reproducibility, potentially limiting the adoption of these platforms by a wider community.

8.2. Development of vascularised fibrinogen gels in PDMS wells

To understand how the different components of vascularised fibrin gels influence the final vessel network, they were investigated to ensure conditions guaranteeing proper vasculogenesis were optimised. This would allow us to later investigate the interactions

between the vasculature and HGSOC. These conditions were initially investigated using a PDMS well system, with conditions commonly described in the literature shown in Table 3. PDMS wells were used, as we believed they were better adapted for more 'high-throughput' experimentation of conditions enabling vascularisation than the subsequently used microfluidic devices.

Table 3. Standard fibrinogen gel components (final concentrations)

Components	**Concentration/time**
HUVECs (Million/mL)	6
Fibrinogen (mg/mL)	2.5
Thrombin (U/mL)	2
Type 1 Collagen (mg/mL)	0.2
Aprotinin (U/mL)	0.15
VEGF (ng/mL)	50
Duration (Days)	4

The process of PDMS well fabrication is further described in the Materials and Methods section of this thesis (p. 58). 100 µL fibrinogen gel was added to 6 mm diameter PDMS wells. Following gelation, 200 µL EGM-2 supplemented with 50 ng/mL VEGF was added. To determine if this system was suitable for further use, an initial experiment investigating the impact of fibronectin on vessel formation following 4/5-days culture was conducted. Fibronectin was selected to be investigated due to its important role in blood vessel morphogenesis and prevalence in HGSOC [46, 217]. As shown in Figure 9, no significant differences were observed between any of the groups investigated, with

neither time or fibronectin impacting the vascular networks formed, as quantified through the total tube length (pixels).

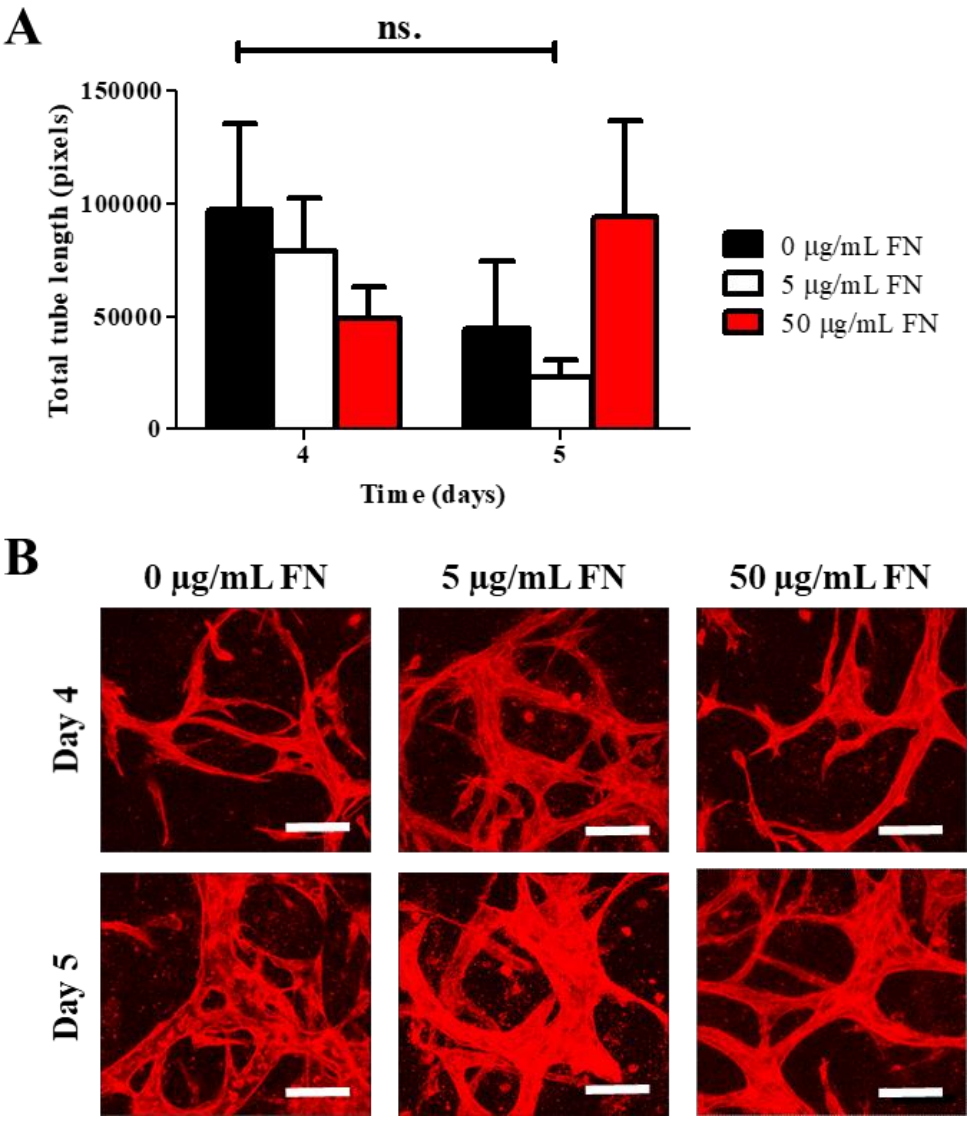

Figure 9. Impact of fibronectin on vessel formation. Using a PDMS well system, the impact of fibronectin on vasculogenesis was studied **A)** Fibronectin and time did not have a significant impact on total tube length. **B)** Representative images. Time points: Day 4 and 5. Supplemented with 50 ng/mL VEGF. Red, phalloidin. Scale bar: 75 µm. FN = fibronectin. Statistics correspond to N=3.

Though no significant differences were observed, the large errors associated with the measurements indicated that this assay may not be suitable to quantify precisely the

contribution of multiple factors on vascular network formation. The injection of 100 µL of gel into an open well results in the formation of several layers of vasculature, this makes imaging and quantification of the vascular layers challenging. To address this, we imaged small ROI using a 40X objective, as we believed this would allow us to avoid imaging such a broad depth of gel, however, as shown in Figure 9, this technique was unsuccessful. We therefore decided that PDMS wells were not suitable to investigate the impact of multiple parameters on vascular network formation. Instead microfluidic chips were seen as a more viable solution. This is due to chips having a defined, enclosed, narrow chamber, allowing a 3D HUVEC network to form within a relatively thin layer of gel and allowing the rapid imaging of large area whilst reducing user bias.

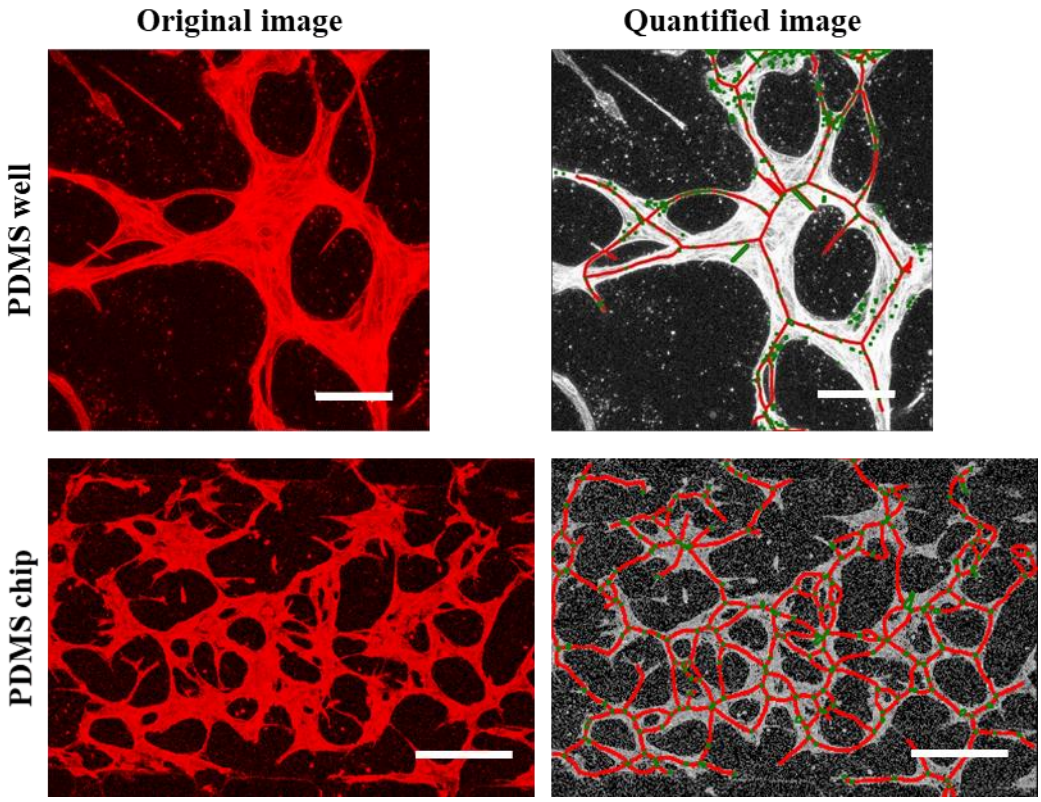

Figure 10. HUVEC vascularisation in PDMS wells and PDMS chips. PDMS chips have a defined area, allowing the imaging of vascularised 3D monolayers. Whereas, PDMS wells feature vascular overlay making imaging more challenging. Red, phalloidin. Scale bars: PDMS wells 75 µm, PDMS chips 300 µm. Time point: Day 4. Supplemented with 50 ng/mL VEGF.

8.3. Design of three-channel microfluidic device

The PDMS chip used to optimise vasculogenesis in this thesis is based upon a design commonly reported in the literature [198, 213]. This design features a central gel channel which is flanked by two lateral medium channels, with posts separating the individual channels - see Figure 11. This design enables the injection of a cell-laden fibrinogen gel into the central channel, and following gelation, the addition of medium into the lateral channels that is able to diffuse through the gaps between the posts into the central gel channel - promoting vessel formation.

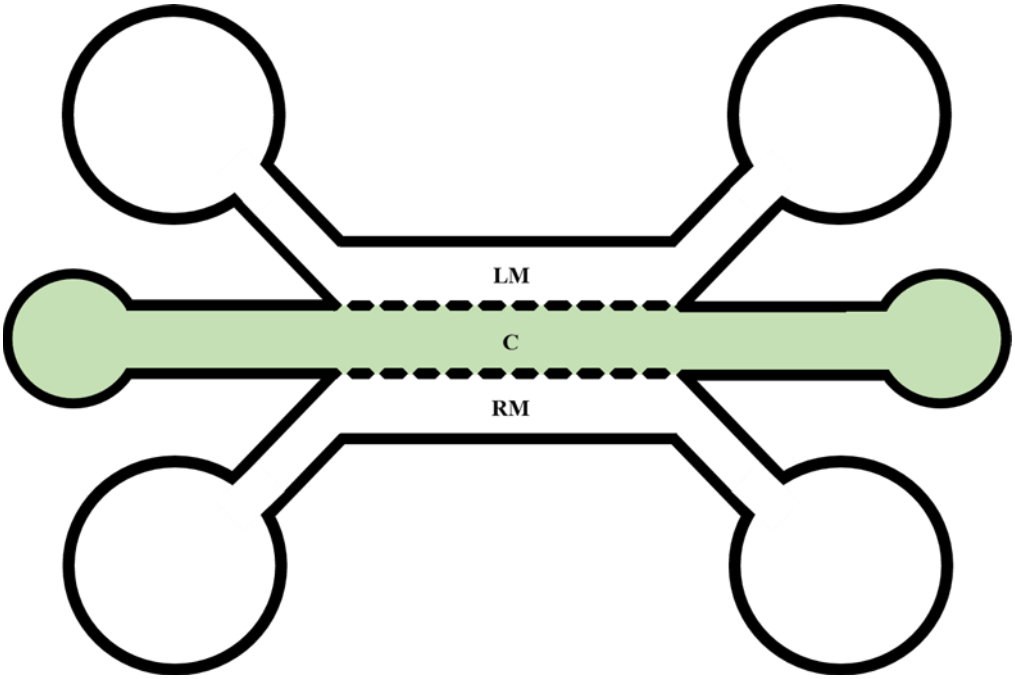

Figure 11. Schematic of three-channel device. Schematic representation of the three-channel device. This system has two lateral medium channels (LM and RM) and a central gel channel (C). Each channel is 75 µm in height and 1000 µm in width. Posts are 300 µm in length with 75 µm gaps between each post. Schematics are not to scale. Same schematic as Figure 6.

8.4. Development of a vascularised microfluidic system

Organ-on-a-chip devices were developed based on microfabrication techniques used in the microelectronics industry, hence their name of "chips". It is through this combination of photo- and soft-lithography, that cell based microfluidics has been able to expand. PDMS, used in the process of soft-lithography, is viewed by many as an almost ideal material for rapid prototyping of microfluidic devices, due to properties such as low-cost, optical clarity, reproducibility, bio-compatibility, gas permeability and ease of use [209]. The process of soft-lithography is described in greater detail in the Materials and Methods section (p. 59). Briefly, PDMS is poured onto a negative photomask, degassed, cured, and attached to a glass coverslip following plasma oxidation treatment. Cured PDMS is hydrophobic, however plasma oxidation leads to a significant reduction in hydrophobicity, due to the formation of silanol groups on the material surface and change in the surface nano-structure [218, 219]. This change is temporary, with research demonstrating hydrophobic recovery with storage time. This recovery has been attributed to low molecular weight chains diffusing to the thermodynamically unstable hydrophilic surface and the reorientation (and possible diffusion) of silanol groups into the bulk polymer [219, 220].

The impact of plasma oxidation on PDMS hydrophobicity was investigated by contact angle (Figure 12). Untreated cured PDMS has a contact angle of 107.9 ± 1.1 °, however this decreases to 29.0 ± 0.3 ° following plasma treatment. PDMS hydrophobicity can be recovered with storage time, this process is enhanced when the substrate is heated. This is observed in Figure 12, as following plasma treatment, storing the PDMS at RT for 72 h significantly increases the contact angle to 81.7 ± 2.2 °, however, this is further increased to 88.8 ± 1.9 ° when the sample is stored at 60 °C. These values are comparable with what is observed in the literature, with Bodas *et al* showing 'pristine PDMS' having

a contact angle of 120 °, whereas oxygen plasma treated PDMS after 72 h storage recovery having a contact angle of ~75 ° [218]. A similar phenomenon was described by Kaneda *et al* who demonstrated PDMS hydrophobicity can be recovered following oxygen plasma treatment [221].

Many organ-on-a-chip studies include the recovery of PDMS hydrophobicity in the methods, with PDMS hydrophobicity desirable due to its reduced wettability - limiting leakage into side-compartments following gel injection [199, 214]. The importance of PDMS hydrophobic recovery on 'successful injections' was further investigated and shown in Figure 12, with successful injections defined when a device was injected with a fibrinogen gel and did not leak into either side compartments. As shown in Figure 12, chips that underwent 60 °C thermal recovery compared with chips that underwent RT recovery showed a significant increase in observed successful injections (100 vs 50 (range 60-42) % respectively, across all post lengths). The improved recovery of hydrophobicity observed by water contact goniometry resulted in significantly improved success rates of injection of hydrogels. Interestingly, the range of post length tested did not have an impact on injection success rate. Following this, future devices underwent 72 h hydrophobic recovery at 60^{o} prior to gel injection.

Although frequently cited, the impact of hydrophobic recovery of PDMS on gel injection is rarely reported in the literature. An extensive paper published by Shin *et* al [200] details the protocol for developing similar microfluidic systems and describes the importance of restoring hydrophobicity to prevent the 'unintended breakage of optimal surface tension when gel filling'. The method proposed in this thesis differs to the Shin protocol - they propose heating devices at 80 °C for 24 h (they do state this step can be increased up to, but not exceeding 72 h), whereas the protocol developed in this thesis heats the devices at 60 °C for 72 h. We have investigated the impact of 24 h 60 °C recovery (plus an

additional 48 h RT recovery) on PDMS hydrophobicity, however no significant difference was observed between that and PDMS which had not undergone thermal recovery (72 h RT recovery, data not shown), and was therefore not further investigated. Thus, a shorter thermal recovery time would be expected to cause a decrease in the rate of successful injections - this is potentially negated by Shin *et al* due to the higher temperature they use.

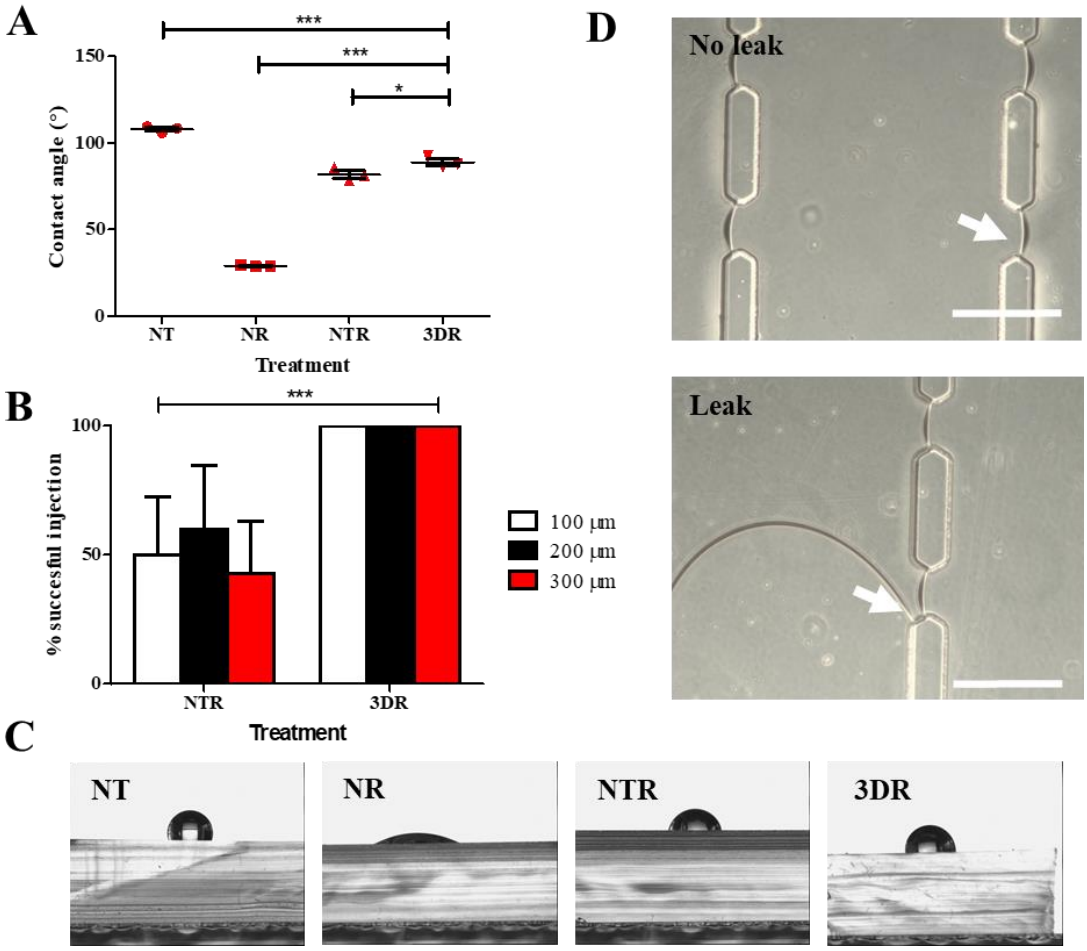

Figure 12. Impact of PDMS hydrophobicity on gel injection. A) Using water contact angle goniometry it was revealed that plasma oxidation significantly reduced PDMS hydrophobicity. This was restored following storage time (3 days), but could be significantly enhanced with heating (storage in 60 °C oven). Acronyms: NT - No Treatment, NR - No Recovery, NTR - No Thermal Recovery, HR - Heated Recovery (60 °C). Statistics correspond to N=3. **B)** Restoring hydrophobicity through thermal recovery led to a significant increase in successful injections across all posts lengths tested, when compared with NTR samples. Statistics correspond with 36 tested samples. **C)** Representative images of water droplets at PDMS interfaces tested in A. **D)** Representative images of gel injection, with and without gel leakage. The corresponding interfaces are indicated by white arrows. Scale bar: 300 µm.

8.5. Determination of the optimum VEGF concentration to promote vessel formation

VEGF is a well-established angiogenic factor, encountered as a range of splice variants, which are further discussed in the introduction of this thesis (p. 28). $VEGF_{121}$ is extensively used in vascular and organ-on-chip studies, perhaps due to its lower concentration biological range when compared with other VEGF isoforms.

The concentration of VEGF used in organ-on-chip studies is quite consistent, with most groups reportedly using 50 ng/mL $VEGF_{121}$, though certain groups report using lower concentrations (20 ng/mL) [199, 213, 216, 222]. To determine the optimal concentration for inducing vessel formation in microfluidic devices five concentrations of $VEGF_{121}$ were investigated (0, 25, 50, 100, 150 ng/mL), using total tube length to describe network formation. The EGM-2 used in this experiment was purchased from Lonza, which contains as additional indiscriminate concentration of VEGF. However, all experiments reported hereafter in this thesis used EGM-2 purchased from Promocell. This is due to delivery issues concerning the former, and Promocell EGM-2 containing a known concentration of basal $VEGF_{165}$ (0.5 ng/mL).

All concentrations (except 100 ng/mL) of VEGF significantly promoted vessel formation when compared with basal EGM-2 (Figure 13). The mean total tube length ± SEM were 5.1 ± 0.9, 8.3 ± 0.1, 8.7 ± 0.6, 8.3 ± 0.8 and 9.0 ± 0.6 mm for 0, 25, 50, 100 and 150 ng/mL, respectively. All results represent the mean of 3 repeats, except 100 ng/mL, which is 2 repeats, hence no significant difference is observed. In addition, VEGF concentration had no impact on vessel diameter (mean diameters between 36.7 - 51.4 μm).

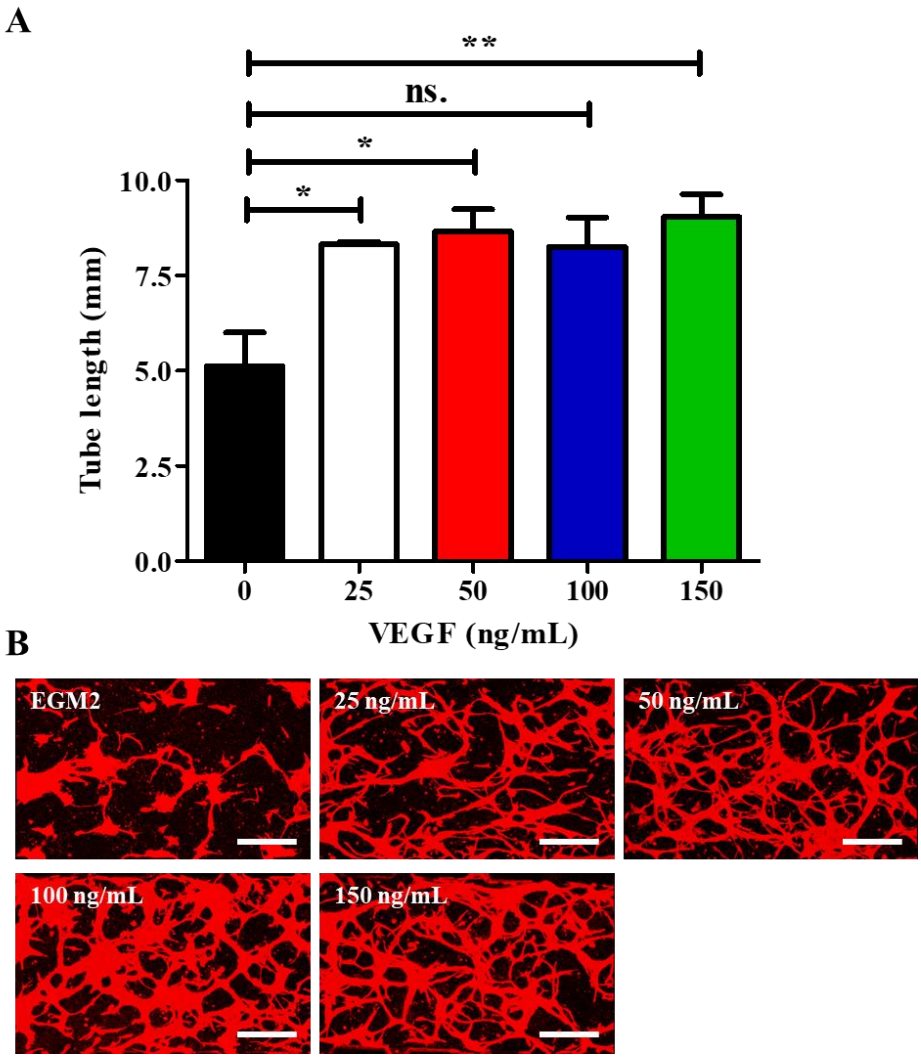

Figure 13. Optimum VEGF concentration to promote vessel formation. A) Impact of VEGF concentration on tube length. All concentrations of VEGF tested promoted a significant increase in total tube length compared with basal EGM-2, except 100 ng/mL. However, no significant difference is observed between VEGF containing groups. **B)** Representative images. Time point: Day 4. Red, phalloidin. Scale bar: 300 µm. Statistics correspond to N=3, apart from 100 ng/mL (N=2).

Our results are largely in agreement with what is reported in the literature, as 50 ng/mL VEGF significantly promoted vessel formation when added to basal EGM-2 [198, 213]. However, according to our results, medium is often supplemented with VEGF at higher concentrations than the level at which a plateau in tube formation has been achieved (25 ng/mL). Above this concentration, no significant difference in total tube formation is

observed. VEGF is also regarded to regulate blood vessel diameter, with a positive correlation reported between concentration and diameter [223]. However, we do not observe a similar relationship between VEGF and vessel diameter. Increasing VEGF concentrations may have had an effect that was not quantified in this experiment. Considering VEGF was first identified as vascular permeability factor, and is known to promote vessel permeability, via nitrogen oxide and prostacyclin interactions, increased VEGF may enhance vessel permeability, though this was not further investigated in this thesis [224]. Due to vascular networks being morphologically similar within the range of 25-150 ng/mL VEGF, the standard concentration of 50 ng/mL used in the literature was satisfactory for the continuation of this study.

8.6. Impact of HUVEC density on vessel formation

Endothelial cells form the endothelium, which is the inner-monolayer of all blood and lymphatic vessels. In this thesis, HUVECs are the endothelial cells used to replicate the vasculature. Though other types of endothelial cells are available, HUVECs are the predominantly used endothelial cell type in organ-on-a-chip devices that incorporate a vascular component. Human dermal microvascular endothelial cells (HDMECs) are also commonly used - though HUVECs are still seen as the gold standard. This is due to HUVECs ease of isolation (and commercial availability), ubiquity and reliability in many studies [225, 226]. However, there is a growing understanding of the heterogeneity within endothelial subtypes and how this impacts physiology and function [227, 228]. This is highlighted by the endothelium in different organs having vastly different phenotypes, with continuous, tightly-regulated endothelium located in the brain, fenestrated endothelium in the kidneys, and discontinuous endothelium in the liver [228]. This heterogeneity highlights the flaw in that much of our understanding of vascular biology

is structured around the use of HUVECs. To address this, much research has been conducted on developing alternative endothelial sources, including isolated induced pluripotent stem cells, the aforementioned HDMECs and an array of other venous and arterial endothelial cells which are commonly available [229]. Interestingly, and unsurprisingly, the microenvironment has been shown to play an integral role in endothelial cell heterogeneity, as when cultured *in vitro* endothelial cells have been shown to 'lose' their tissue-specific genotype within 48 h of culture [230]. Due to their extensive current use in microfluidic systems, HUVECs were further used in this study, allowing comparisons with other research.

The density of HUVECs used to achieve a perfusable network varies greatly in literature, with some studies reporting concentrations as low as 2×10^6 HUVECs/mL and others as high as 20×10^6 HUVEC/mL [199, 214, 231]. Perhaps the most detailed study regarding the impact of HUVEC density on vessel formation was conducted by Whisler *et al*, who investigated the impact endothelial cell number on the number of branches formed, branch length, vessel diameter and % area coverage of a vessel network [222]. They reported that increasing HUVEC density had little impact on the number of branches and branch length of the networks formed, but led to an increase in % area coverage and vessel diameter. In this thesis, total tube length was used to describe overall vessel formation as it highly correlated with number of branches, thus preventing repeating results.

Four cell densities (2, 4, 6 and 8×10^6 HUVECs/mL) were cultured over a 4-day period, after which samples were fixed, stained and imaged. As shown in Figure 14, increasing HUVEC densities led to a significant increase in total tube length (mm), 5.4 ± 0.8, 8.4 ± 0.7, 12.7 ± 0.9 and 13.2 ± 0.4 mm for 2, 4, 6 and 8×10^6 HUVECs/mL, respectively. In addition, a significant increase in % area coverage is observed with increased HUVEC density, 15.1 ± 1.5, 24.8 ± 3.2, 47.9 ± 2.4 and 56.1 ± 6.9 for 2, 4, 6 and 8×10^6

HUVECs/mL, respectively. These results are in agreement with previous reports by Whisler [222]. In contrast, there was no significant impact on vessel diameter, results ranging from 39.8 to 58.5 μm. No significant differences were observed between 6 and 8 × 10^6 HUVECs/mL in any quantified parameters, suggesting that 6 × 10^6 HUVECs/mL would be most suitable to achieve optimum tube formation, whilst reducing the number of cells required for each experiment (a limiting factor for routine vascular network experiments).

We report similar results to what is published by Whisler *et al* concerning the impact of cell density on network formation and % area coverage, however, they also observe an increase in vessel diameter that we do not. This difference may be a result of the duration of the experiment and the formation of a mature vasculature. They report the formation of a lumenised vasculature after day 4, whereas we report complete lumination at day 10 (reported later in Figure 18). This suggests the Whisler microvasculature reaches maturity sooner than what we report. This could be due to a different source of HUVECs or general differences with handling cultures. If we extended the duration of these experiments to allow the formation of a more mature microvasculature, perhaps a difference in vessel diameter would be observed, however, this was not further examined.

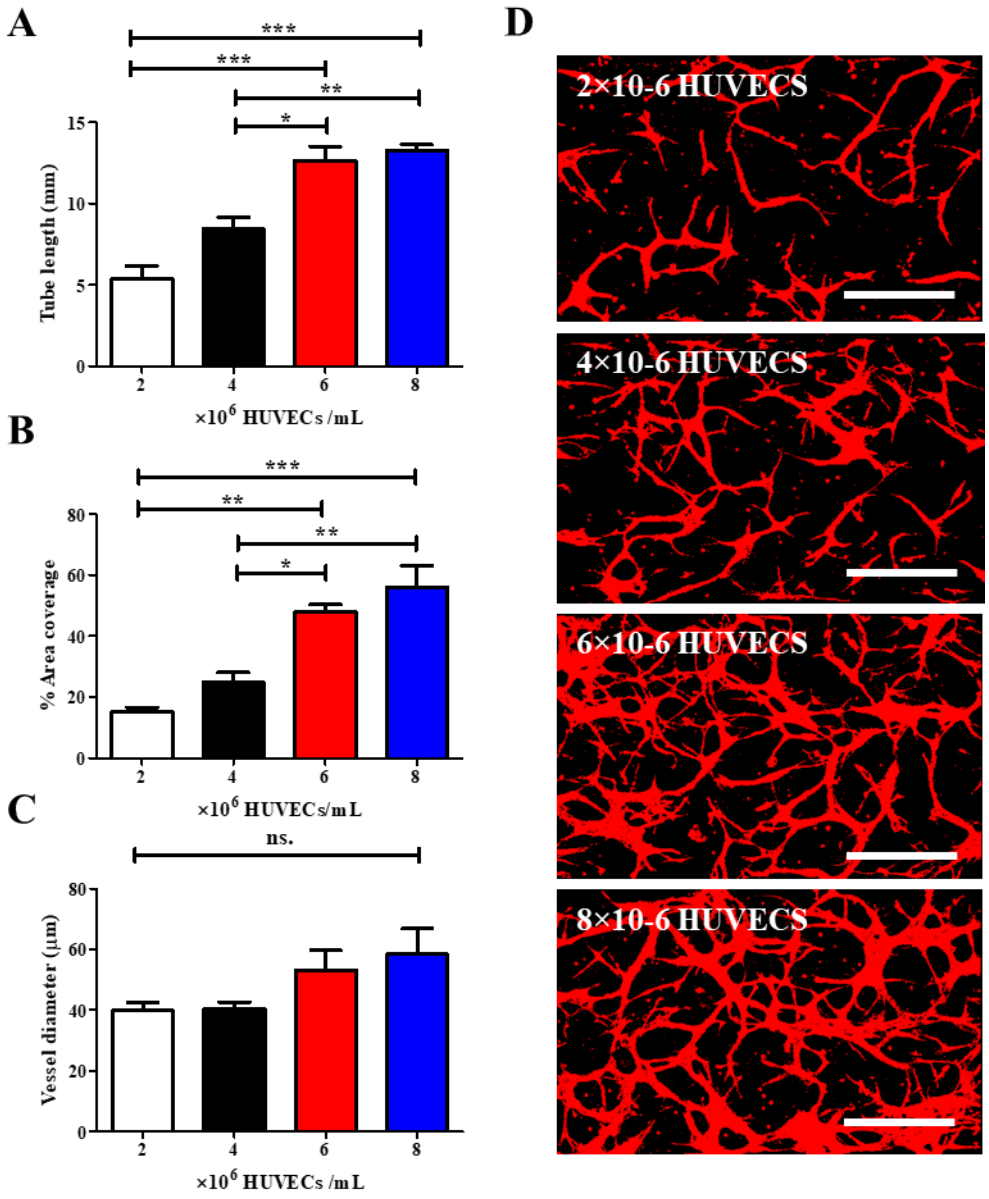

Figure 14. Impact of cell density on vessel formation. Varying HUVEC densities (2, 4, 6, 8 × 10^6 HUVECs/mL) were injected into microfluidic device and the impact of density on vessel formation was investigated. **A)** Changes in total tube length (mm), with increasing HUVEC density. **B)** Changes in % area coverage with increasing HUVEC density. **C)** Changes in vessel diameter with increasing HUVEC density. **D)** Representative images. Time point: Day 4. Supplemented with 50 ng/mL VEGF. Red, phalloidin. Scale bar: 300 µm. Statistics correspond to N=3.

8.7. Impact of aprotinin on vessel formation

Aprotinin is a small protein bovine pancreatic trypsin inhibitor which was previously administered during complex surgery to limit bleeding, due to its mechanism as an anti-

fibrinolytic. Bayer later withdrew Aprotinin due to increased risk of death following administration compared with alternative treatment [232]. However, aprotinin is still a useful tool to investigate and limit *in vitro* fibrinolysis, which is the process of fibrin breakdown. This is a complex and tightly controlled process with abnormalities leading to a range of disorders including bleeding and thrombosis [233]. Plasmin is the most common fibrinolsyin and is formed from plasminogen by either tissue plasminogen activator (tPA) or urokinase plasminogen activator (uPA) - with uPA being produced by monocytes, macrophages and the urinary epithelium, and tPA by endothelial cells [233]. Interestingly, though tPA is released from endothelial cells, its role in vasculogenesis is not well documented, rather it has been more thoroughly studied in the context of fibrin clot breakdown. Instead the role of uPA in vessel formation has been more extensively investigated, and as well as converting plasminogen to plasmin, promotes the release and/or expression of transforming growth factor (TGF)-β, bFGF, VEGF and various MMPs, which are known to promote vessel formation [234]. However, due to the presence of HUVECs within our system, plasminogen would be expected to be predominantly activated by tPA. The main mechanism of action for aprotinin mediated fibrinolysis inhibition is the direct inhibition of plasmin [235, 236].

Aprotinin is commonly used in organ-on-a-chip studies to limit fibrinolysis, and reduce gel degradation and vessel hyperplasia. It is typically added as a gel component during gel formation, at a concentration of 0.15 U/mL [199, 215, 237]. However, these cultures are not further supplemented with aprotinin for the duration of the experiment. We hypothesised that, long-term, this would not limit gel breakdown and vessel hyperplasia, as other studies would suggest. To test the impact of aprotinin on vessel formation, cell-loaded gels were formed in the presence of 0.15 U/mL aprotinin alone or supplemented at a concentration of 0.15 U/mL throughout the experiment, or in the complete absence

of aprotinin during the gel formation stage and during culture. The end-point of this experiment was after 4 days, and analysis of total tube length and vessel diameter.

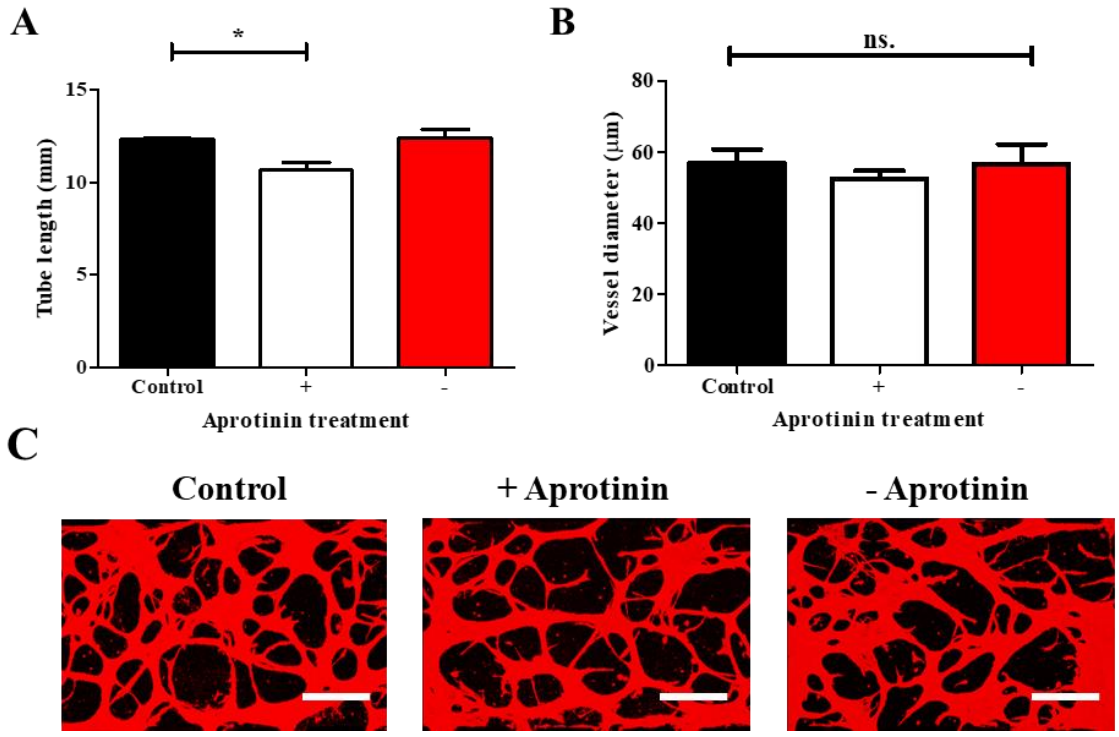

Figure 15. Impact of aprotinin on vessel formation. Three different conditions were investigated: control, 0.15 U/mL aprotinin supplemented during fibrin gel formation alone; + aprotinin, 0.15 U/mL aprotinin supplemented throughout; - aprotinin, no aprotinin supplemented at any point. **A)** Aprotinin supplemented medium significant reduces total tube length compared with control. **B)** Aprotinin has no significant impact on vessel diameter. Vessel diameters: 57.0 ± 3.8, 52.4 ± 2.3 and 56.6 ± 5.5 µm for control, + and - aprotinin, respectively. **C)** Representative images. Time points: Day 4. Supplemented with 50 ng/mL VEGF. Red, phalloidin. Scale bar: 300 µm. Statistics correspond to N=4.

No significant difference in total tube length between the control (aprotinin introduced during gel formation alone) and the aprotinin-free culture (no aprotinin introduced at any point, see Figure 15) was observed. However, compared with the control, a significant decrease in total tube length in the cultures fully supplemented with aprotinin (during the gel formation and throughout the culture) was observed, 12.3 ± 0.0 vs 10.65 ± 0.4 mm

respectively. This suggests that aprotinin supplemented fibrin gels does not impact gel breakdown, and that aprotinin should be supplemented in the medium throughout the experiment in order to inhibit fibrinolysis significantly. In addition, though total tube length was inhibited, aprotinin had no impact on vessel diameter, further suggesting that the effect of aprotinin at commonly used concentrations is limited.

These results suggest that the addition of aprotinin during fibrin gel formation alone, at the concentration stated, does not impact vessel formation or stabilisation. This has not been well described in the literature, and aprotinin is often simply used without further experimental justification [199, 215, 237]. In addition, a number of studies do not supplement cultures with aprotinin, further supporting that its addition during gel formation is superfluous [213, 222]. If intending to use aprotinin to inhibit fibrinolysis, it should be supplemented in the medium throughout the culture and potentially at higher concentrations than what is commonly reported in the literature. Future experiments described in this thesis did not use aprotinin to limit fibrinolysis as no marked improvement to the vasculature was observed.

8.8. Impact of thrombin solution on vessel formation

In vivo fibrin is most commonly associated with the formation of haemostatic clots in conjunction with platelets. This process is adopted *in vitro* for the creation of fibrin gels using fibrinogen and thrombin. This is through the conversion of fibrinogen into fibrin, following the thrombin dependent cleavage of fibrinopeptides A and B, exposing a binding site in the central domain of fibrin, which is then able to interact with a complementary site at the end domain of other fibrin molecules [238]. The growth of these fibrin polymers leads to the formation of protofibrils, which upon aggregation form the thick fibres which are seen in 3D fibrin networks. As reported in the Material and

Methods section (p. 55), fibrin gels are formed by mixing a fibrinogen solution with a thrombin-HUVEC solution, in a 1:1 ratio, before injecting the mix into a microfluidic device, which is then stored in an incubator at 37 °C for 5 min before adding medium to the device reservoirs. In the literature, the makeup of these solutions is varied, with fibrinogen and thrombin being dissolved in either DPBS or EGM-2 before mixing [199, 222, 231, 237, 239]. The impact of these differing conditions is largely unreported and was thus further examined. It was hypothesised that EGM-2 would be the preferred medium as HUVECs would not become deprived of nutrients during gel cross-linking.

Fibrinogen solutions are first allowed to dissolve for 2 h, at 37 °C, before filtering and use, to ensure adequate and consistent dissolution. When dissolved in EGM-2, fibrinogen prematurely cross-linked, becoming difficult to handle and suggesting a previously undescribed catalytic activity of EGM-2 (data not shown). This effect has not been previously described in the literature by studies using a similar protocol [237, 239]. In these studies, the length of time required for complete dissolution of fibrinogen was not stated. If they used a shorter time than 2 h (what we report) this may explain why they did not observe the catalytic effect of EGM-2. Due to this effect, future fibrinogen solutions were always prepared in DPBS.

Prior to cell resuspension, 4 U/mL thrombin solutions are produced (final thrombin concentration 2 U/mL). As stated, the main component of these solutions is either DPBS or EGM-2. The impact of dissolving thrombin in different solutions (EGM-2 or DPBS) was investigated. As shown in Figure 16, no significant difference in vessel formation was observed between groups, with mean total tube length ± SEM being 18.1 ± 2.6 vs 19.5 ± 2.6 mm for DPBS and EGM-2, respectively.

Following fibrinogen gelation and short-term nutrient deprivation, the ability of HUVECs to undergo vasculogenesis is not impaired. This relative robustness would explain the varied methods observed in literature regarding this gelation step. The impact of this step may have been more pronounced if the cells were nutrient deprived for longer, however, studies report incubating samples for up to 10 min following gel injection with no observed detrimental effects [215, 222]. To improve reproducibility, future experiments were conducted with thrombin mixed with EGM-2 prior to cell resuspension. Interestingly, thrombin concentration is believed to have a significant impact on vessel formation, credited with the changes in the observed fibrin ultrastructure (an increased gel permeability at low thrombin concentration) [240]. However, the impact of thrombin concentration on vasculogenesis was not investigated in this thesis, as 2 U/mL thrombin (final concentration) produced a hydrogel which was easy to handle and required only 5 min incubation to cross-link.

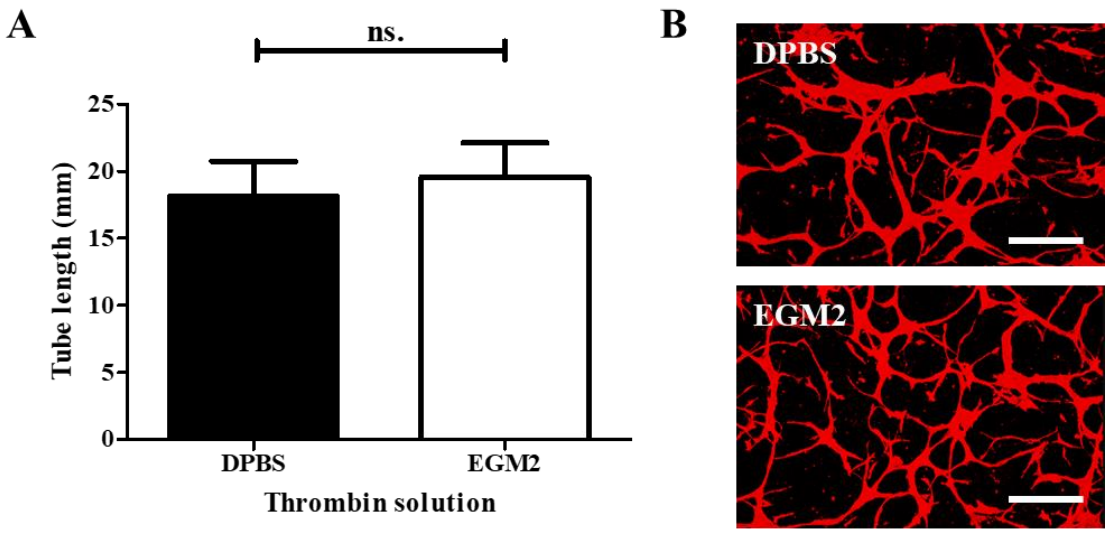

Figure 16. Impact of thrombin solution on vessel formation. A) No significant impact on tube formation was discovered, whether thrombin was dissolved in DPBS or EGM-2. **B)** Representative images. Time points: Day 4. Supplemented with 50 ng/mL VEGF. Time points: Day 4. Supplemented with 50 ng/mL VEGF. Red, phalloidin. Scale bar: 300 µm. Statistics correspond to N=3.

8.9. Role of type 1 collagen on vessel formation

Type 1 collagen (T1C) is the most abundant collagen found in the body and is an important structural support for cells. A report by Newman *et al* describe how *in vitro* endothelial lumenogenesis can be inhibited with the knockdown of various fibroblastic genes, including T1C [241]. They went on to demonstrate that this abrogation in lumen formation may be reversed with the addition of a cocktail of exogenous ECM components, including T1C. Due to T1C's ubiquity and reports of enabling angiogenesis, it is commonly used as an ECM component in microvascular systems [199, 200, 241].

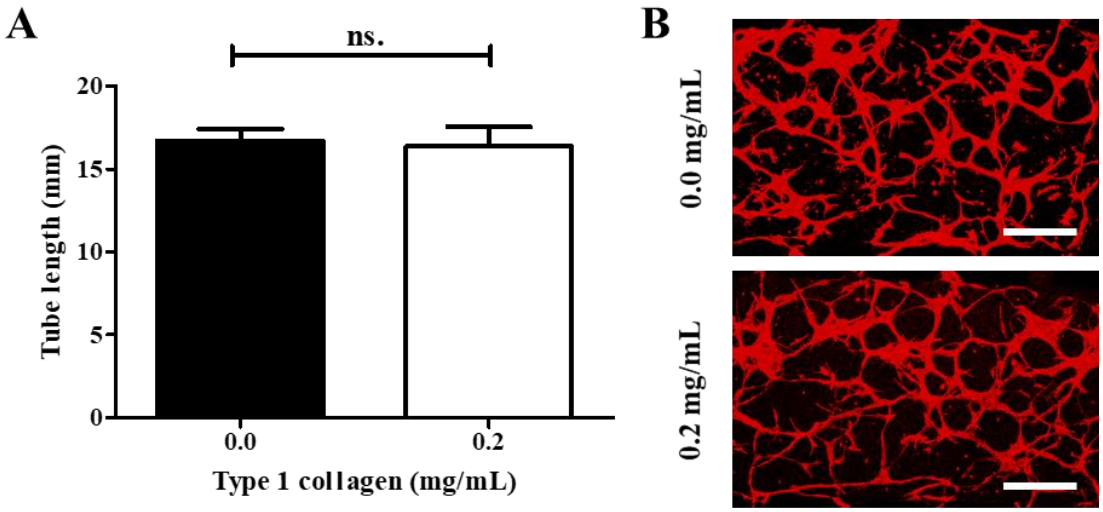

Figure 17. Impact of type 1 collagen on vessel sprouting. A) The addition of T1C to fibrinogen gel has no significant impact on vessel sprouting compared with no T1C, 16.7 ± 0.7 and 16.4 ± 1.2 mm for 0.0 and 0.2 mg/mL, respectively **B)** Representative images. Time points: Day 4. Supplemented with 50 ng/mL VEGF. Red, phalloidin. Scale bar: 300 µm. Statistics correspond to N=3.

The impact of T1C on vessel formation was further investigated in this thesis. Total tube formation was examined with and without 0.2 mg/mL exogenous T1C following 4-days culture. We selected to investigate 0.2 mg/mL T1C as this concentration is reported in similar micro-physiological systems [199]. The addition of T1C led to no significant difference in total tube length (see Figure 17). This is in agreement with reports indicating

that the knockdown of collagen 1 significantly inhibits lumen formation, but has no impact on endothelial sprouting [241]. However, due to the short length of our experiment neither conditions clearly promoted lumenogenesis (although this was not specifically characterised and is only based on the examination of bright field images). To investigate further, future experiments could determine by which time-point lumination is observed, as a result of T1C concentration. However, this was not further investigated in this study and subsequent devices were not supplemented with exogenous T1C. This is further beneficial as when T1C is added to fibrinogen solutions it rapidly cross-links, which can lead to variation in results, especially if carrying out multiple experiment in parallel.

8.10. Impact of fibrinogen concentration on vessel formation

Fibrin gels are one of the most commonly used hydrogels when developing vascular networks in microfluidic devices, with concentrations of fibrinogen ranging from around 2.5-10.0 mg/mL. However, across this concentration range, gel stiffness differs considerably, with the Young's Modulus increasing with fibrinogen concentrations associated with considerable changes in the gel structure [186, 242]. Increasing fibrin concentration (between 1.5-10.0 mg/mL) and stiffness has been reported to attenuate vessel formation *in vitro* [222, 243]. As such, it was hypothesised that increasing fibrinogen concentration would alter HUVEC vascularisation.

Four different concentrations of fibrinogen were investigated (1.25, 2.5, 5.0 and 10.0 mg/mL). As shown in Figure 18, following 4-days vasculogenesis, no significant difference in total tube length is observed (mean total tube lengths ranging from 15.1-16.5 mm). In addition, there is no significant difference in vessel diameters between groups (mean vessel diameter ranging between 34.7 to 39.6 µm). HUVECs cultured in

1.25 mg/mL fibrin degraded the matrix and adhered to the underlying glass substrate, so images were not quantified.

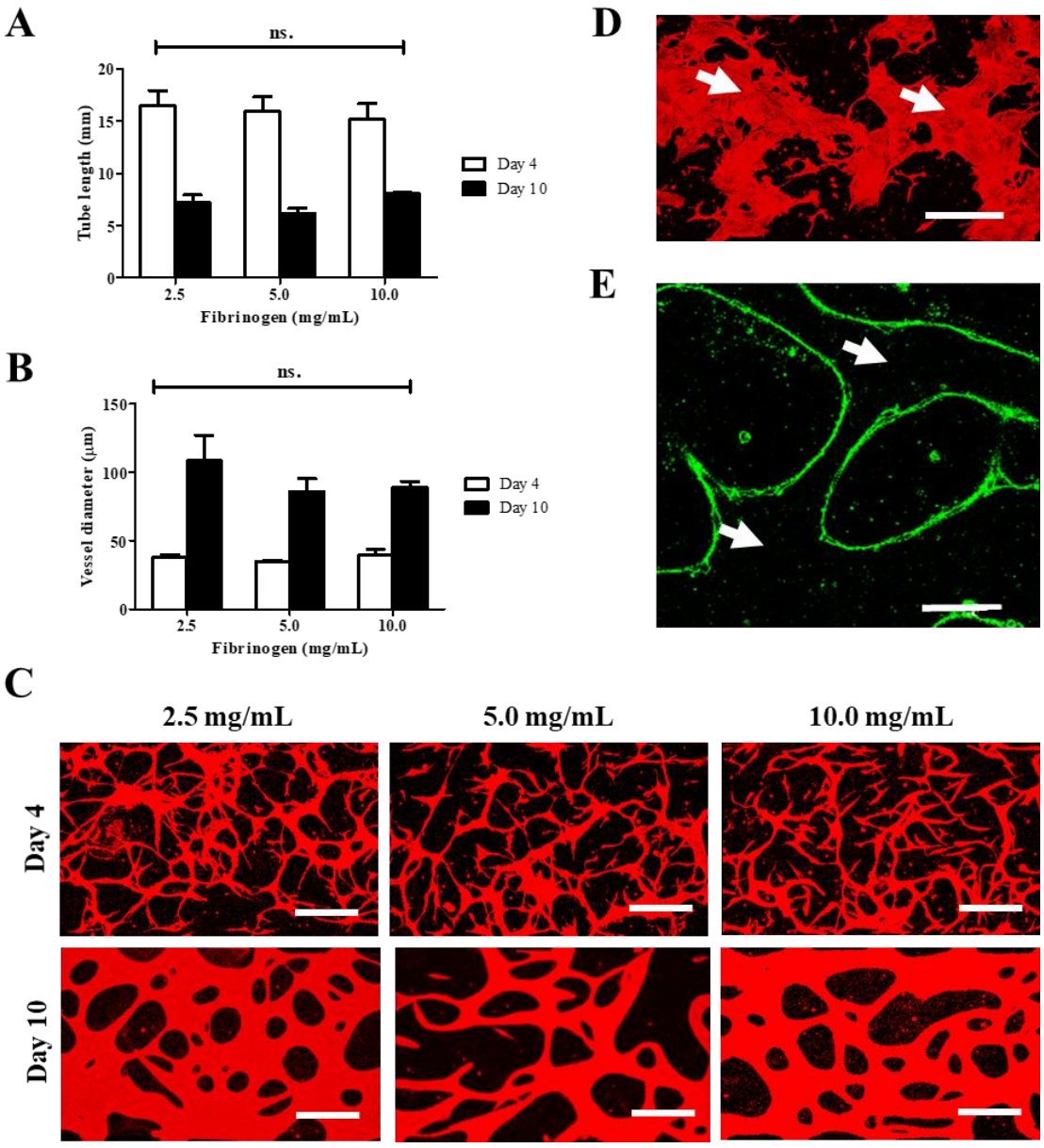

Figure 18. Impact of fibrinogen concentration on vessel formation. **A)** Impact of fibrinogen concentration on total tube length and **(B)** vessel diameter after 4 and 10 days of vasculogenesis. **C)** Representative images. Red, F-actin. Scale bar: 300 µm. **D)** Vessel formation in 1.25 mg/mL fibrinogen was investigated, these gels quickly degraded, with large areas of HUVECs adhering to the underlying glass substrate. Red, F-actin. Scale bar: 300µm. **E)** Image supporting lumen formation after 10-days vasculogenesis. Green, CD31. Scale bar: 75µm. Supplemented with 50 ng/mL VEGF. Statistics correspond to N=3.

Following 4-days vasculogenesis, vessels appear immature and largely non-lumenised according to non-quantified bright-field images. To promote the formation of a mature, perfusable, vascularised network the culture period was extended to 10 days. In this set of experiments, the impact of 2.5, 5.0 and 10.0 mg/mL fibrinogen on vasculogenesis was examined. However, following 10-days culture, increasing fibrinogen concentration still had no impact on either total tube length (mean total tube length ranging between 6.2 and 8.1 mm) or vessel diameter (mean diameter ranging between 89.8 and 113.4 μm). However, the time point significantly impacts the structure of the observed vessels. After 4-days vasculogenesis, vessels appear immature, characterised by extensive sprouting and low diameters. In contrast, by day 10, vessels appear much thicker, with extensive lumen formation, and reduced sprouting (Figure 18). This is believed to result from nascent vessels merging and endothelial cell proliferation, forming larger vessels, but leading to a reduced overall total tube length. Analysis between day-4 and day-10 samples was not statistically investigated as these represent separate experiments.

It was hypothesised that increasing fibrinogen concentrations would attenuate vessel formation, similar to observations made by Whisler *et al* [222]. Their experimental system used a five-channel microfluidic device, with a central vasculogenesis compartment separated by two, lateral medium channels from two stromal support compartments. They reported that increasing fibrinogen concentrations from 1.5 to 10.0 mg/mL led to an increased number of branches and branch length, a reduction in vessel diameter, but no overall difference in % area coverage. To promote vessel formation, they co-cultured HUVECs with NHLFs in stromal channels, and did not add further exogenous factors. However, a previous study by Ghajar *et al* suggests that the results observed by Whisler may be due to NHLF location and growth factor diffusion [243]. In their study, HUVEC-coated micro-beads were embedded within a fibrin gel, and fibroblasts were

suspended on-top or throughout the gel. When NHLFs were cultured on top of the gel, increasing fibrinogen concentrations (2.5-10.0 mg/mL) inhibited total network length and vessel segments, however, when NHLFs were seeded throughout the gel this inhibitory effect was not observed. Ghajar concluded that this observation was due to higher concentration fibrin gels restricting diffusive transport of growth factors and cytokines. Our system features a 1000 μm wide central channel, with lateral medium channels supplemented with exogenous VEGF. Due to the narrow width and presence of high concentrations of VEGF, no growth factor gradient is sustained. Hence, similarly to Ghajar, there is no observed difference in tube length or vessel diameter when fibrinogen concentration is increased.

8.11. Impact of channel width on vessel hyperplasia

Previous experiments used microfluidic devices with a central gel channel 75 μm high and 1000 μm wide, created according to the device manufacturing protocol described in the Materials and Methods section (p. 59). Device dimensions are an important consideration for the design of microfluidic systems, which is typically poorly discussed when describing new organ-on-chip models. The height of 75 μm was selected as similar heights are frequently reported in the literature, and because significantly thicker channels require thicker resists, which are notoriously difficult to pattern reliably (and lead to difficulty of PDMS stamp peel off) [215]. This height allows the formation of a 3D 'monolayer' vascular bed, enabling simple imaging and quantification of tube formation. According to the literature, channel widths typically range between 1000 - 1300 μm, these widths allow cells located in the centre of the channel to still receive sufficient nutrients to grow and proliferate [60, 213, 222, 244]. However, little has been reported on the use

of narrower channels (<1000 µm). This section investigates the impact of narrower channels on vessel formation.

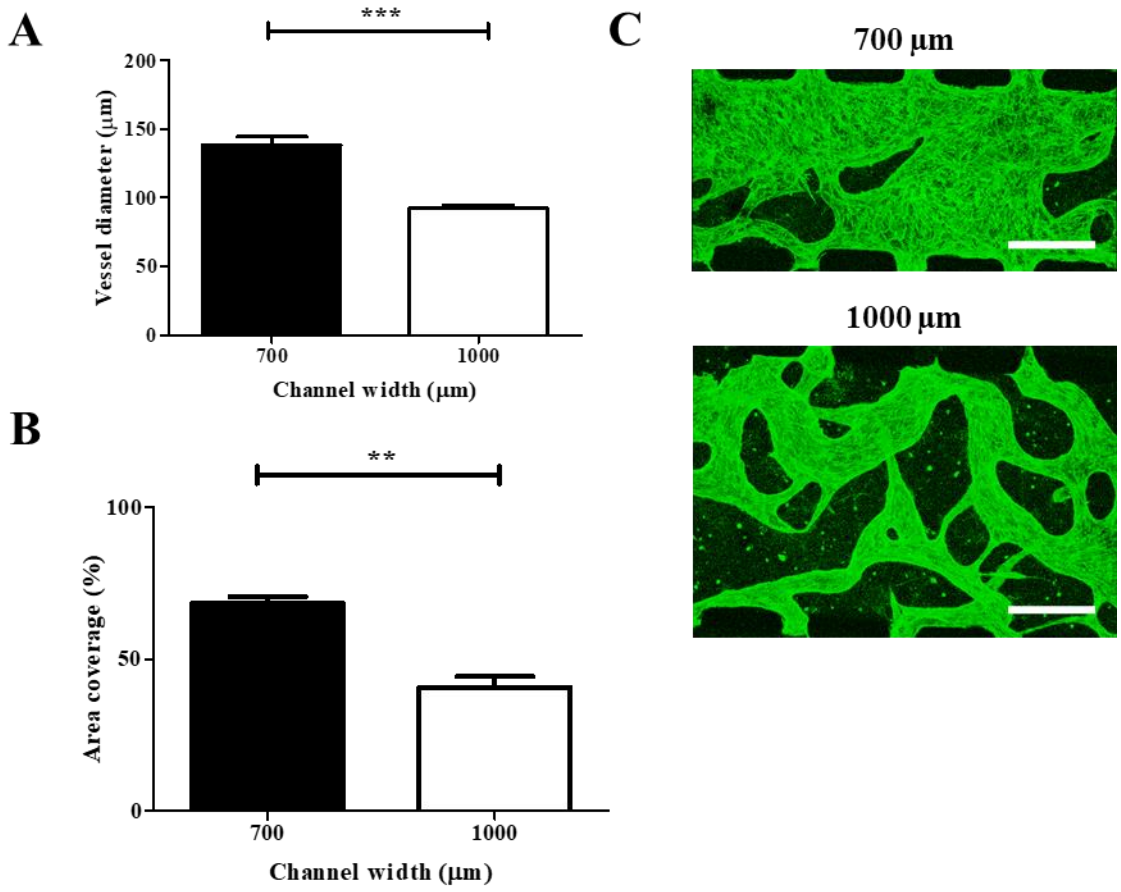

Figure 19. Impact of channel width on vessel hyperplasia. Vascular networks were formed in gel channels either 700 or 1000 µm in width. **A)** Narrow channels promoted the formation of vessels with significantly larger diameters, **B)** which more extensively cover the channel. **C)** Representative images. Time points: Day 10. Supplemented with 50 ng/mL VEGF. Green, CD31. Scale bar: 300 µm. Statistics correspond to N=3.

To investigate the importance of device dimensions on vasculogenesis, two chip designs were compared with different central gel channel widths: 700 and 1000 µm. Following gel injection with 6×10^6 HUVECs/mL, samples were cultured for 10 days. As seen in Figure 19, culturing samples in devices with 700 µm width central channels, compared with 1000 µm channels, led to the development of vessels with significantly larger diameters, 138.3 ± 5.9 and 92.5 ± 1.9, respectively. In addition, these larger vessels cover

a significant portion of the central channel, demonstrated by their overall channel area coverage of 68.5 ± 2.3%, compared with 40.7 ± 3.5% area coverage of vessels cultured in wider channels. This impact of channel width promoting vessel hyperplasia has not been previously described in the literature. It is not understood as to why this is observed, we hypothesised it could be due to vessels in closer proximity merging and forming larger, wider vessels. However, the same density of gel and HUVECs would be similarly injected into 1000 μm devices, suggesting there is an overlooked parameter which is currently unknown

8.12. Summary

The initial phase of this thesis aimed to establish a reproducible vasculogenesis model which could be adapted to more complex culture models. The final established system that will be used in subsequent sections is described in Table 4, and can be compared to what was initially investigated and used in Table 3. A number of components, including T1C and aprotinin, were shown to be superfluous to the assay, as they did not offer any key benefit when included and were thus phased out subsequent experiments. In addition, certain parameters which are frequently altered throughout the literature, such as the make-up of the thrombin solution, were shown to have no impact on angiogenesis and were thus dependent on the researchers own preference. However, if certain issues became a problem the knowledge gained from these experiments could be used, i.e. if vessel stability became a problem with long-term culture, aprotinin may be an appropriate compound to use to inhibit expansive vessel growth. Furthermore, we have established conditions to promote vessel formation that works within our laboratory, but these conditions may not be reproducible to all labs, due to individual handling techniques, different cell sources etc. However, the understanding of how these different parameters

impact vessel formation may be used. The next stage of this thesis will present the use of on-chip vascular networks to investigate interactions between endothelial cells and stromal cells, including pericytes and normal human lung fibroblasts.

Table 4. Standard fibrinogen gel components (final concentrations)

	Initial	***Finalised***
Component	**Concentration/time**	**Concentration/time**
HUVECs (Million/mL)	6	6
Fibrinogen (mg/mL)	2.5 (PBS)	10 (PBS)
Thrombin (U/mL)	2 (PBS)	2 (EGM-2)
Type 1 Collagen (mg/mL)	0.2	-
Aprotinin (U/mL)	0.15	-
VEGF (ng/mL)	50	50
Duration (Days)	4	10

9. Investigating HUVEC-stromal cell interactions

9.1. Introduction

Following the development of a reproducible vascular system described in section 8, the next phase was to investigate the interactions between the vasculature and various stromal cells, notably, normal human lung fibroblasts (NHLFs) and pericytes. These cells were chosen due to their current use in organ-on-a-chip studies to promote and stabilise vessel formation. To investigate the impact these cells had on the vasculature, various parameters were examined, including the total tube length, vessel diameter and junction marker expression.

9.2. Four-channel device used to investigate paracrine signalling

Experiments detailed in section 8, cultured cells in a three-channel PDMS device with a single gel channel. This section will explore stromal paracrine signalling which requires a different device design. Many studies have used stromal support cells to promote vessel formation and stabilisation, which are typically seeded in channels adjacent to the vascular compartment, separated by a medium channel [222, 245]. However, the device we designed to investigate paracrine signalling, unlike the aforementioned designs, features two gel channels directly parallel, with no separating medium channel - see Figure 20. This device was chosen as it may also allow the investigation of cell invasion into the parallel gel channel. The channel dimensions are 700 µm width, 75 µm height, with channels separated by posts 100 µm long with 100 µm gaps. As detailed in Figure 20, the two medium channels are labelled LM and RM, with the gel channels labelled LG and RG.

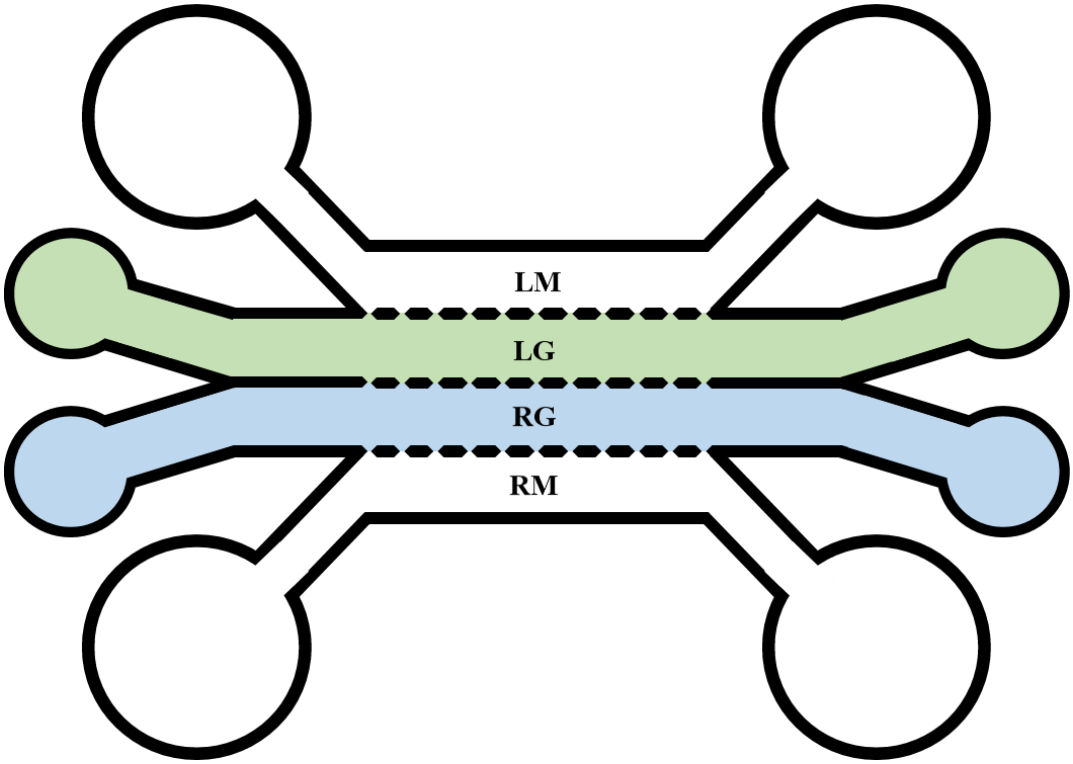

Figure 20. Schematic of four-channel device. Schematic representation of the four-channel device. This system has two central gel channels (LG and RG) and two lateral medium channels (LM and RM). Each channel is 75 µm in height and 700 µm in width. Posts are 100 µm in length with 100 µm gaps between posts. Schematics are not to scale.

9.3. Investigating the impact of NHLFs on HUVEC vessel sprouting

Fibroblasts are an ill-defined cell type with no reliable marker, instead they are largely defined by location and what they are not (e.g. non-endothelial, -smooth muscle or -epithelial cells) [241]. However, they are recognised as being important mediators of ECM synthesis and maintenance, and producers of various angiogenic growth factors [246-249]. It is through this combination of ECM remodelling and growth factor secretion that fibroblasts have been strongly linked with the promotion of vessel formation [222, 241], and have been extensively used in the promotion of angio- and vasculogenesis *in vitro* [215, 216, 243, 244, 250]. Indeed, the addition of NHLFs into *in vitro* culture systems has been shown to null the requirement of further exogenous growth factors to

promote vessel formation [199]. Analysis of the NHLF secretome by Hughes *et al* linked Ang-1, angiogenin, hepatocyte growth factor (HGF), TGF-α, and tumour necrosis factor (TNF) as being important mediators of endothelial sprouting [241]. In addition, collagen alpha 1, procollagen C-endo-peptidase enhancer 1, and transforming growth factor-β-induced protein ig-h3 were identified as important mediators of lumen formation [241].

Given the importance of fibroblasts in promoting vasculogenesis, the impact of co-culturing HUVECs and NHLFs was investigated. Though other fibroblast cell lines are also easily available, NHLFs were chosen due to their current use in organ-on-a-chip research, allowing for more direct comparisons with alternative studies. To investigate the impact of NHLFs on HUVEC tube formation the four-channel chip shown in Figure 20 was used. This chip design has four parallel channels, with two lateral media channels and two central gel channels. In this experiment, 6×10^6 HUVECs/mL and either 6×10^5 NHLFs/mL or an acellular fibrin gel was seeded in separate, parallel gel channels - allowing the investigation of paracrine signalling.

Due to experiments running in conjunction, the vascular system used in this experiment is different to what we proposed in section 8, as cells were cultured in 2.5 not 10.0 mg/mL fibrinogen gel. In addition, the end-point of this experiment was day 4. In our system, NHLFs significantly promote vessel formation in the absence of exogenous VEGF, with total tube length being 2.1 ± 0.7 and 4.9 ± 0.6 mm, for HUVEC mono-culture and HUVEC + NHLFs, respectively (see Figure 21). However, when EGM-2 was supplemented with 50 ng/mL VEGF, NHLFs had no significant impact on vessel formation (Figure 21). Suggesting, HUVECs supplemented with 50 ng/mL VEGF have already reached an optimum vessel coverage, as quantified by total tube length, and that further factors secreted by NHLFs do not promote further vessel growth. However, when

no exogenous VEGF is supplemented, the NHLFs secreted soluble growth factors are able to promote vessel sprouting and tube formation.

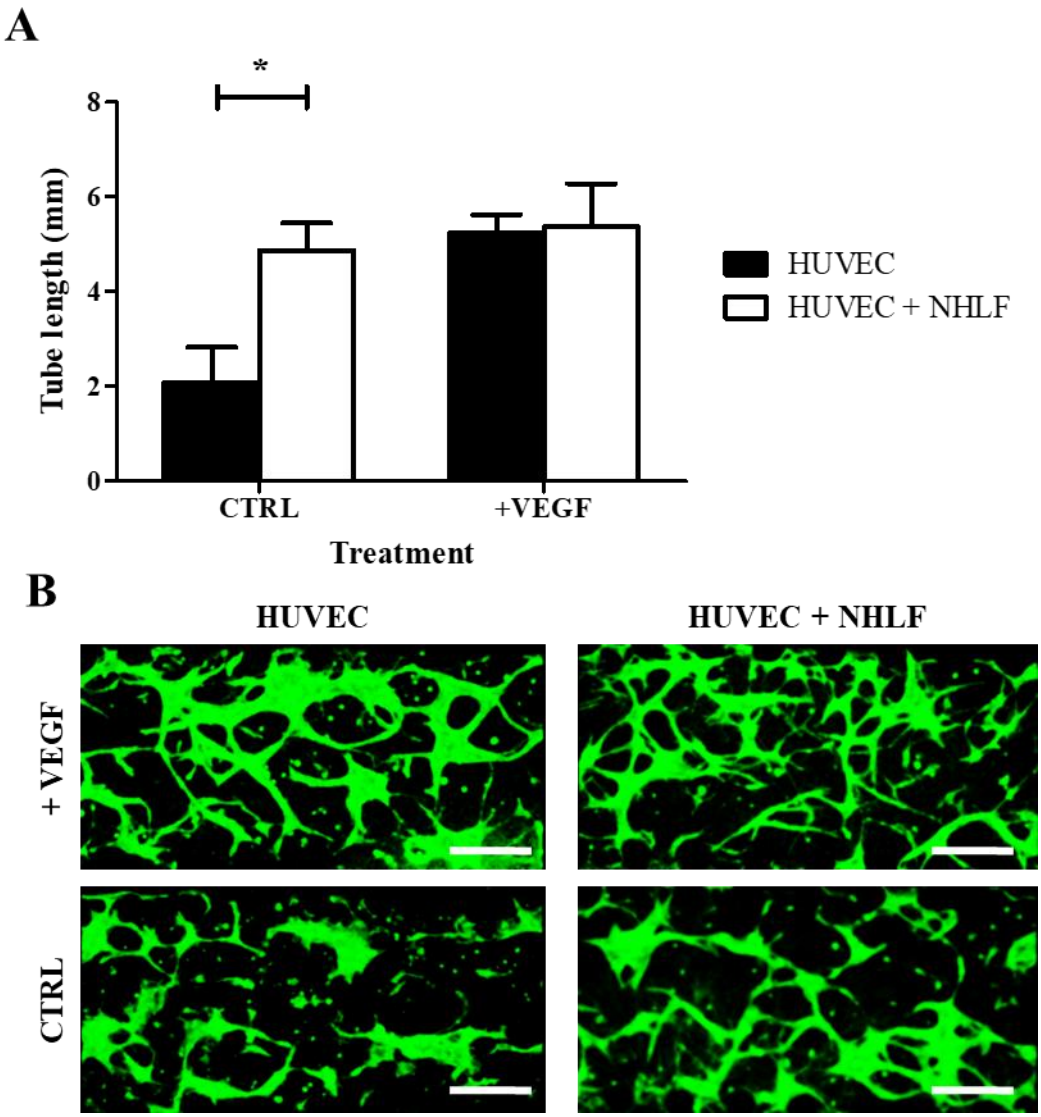

Figure 21. NHLFs promote short-term vessel formation. A) Impact of NHLFs on vessel formation, with and without exogenous VEGF (50 ng/mL). When VEGF is not present NHLFs promote a significant increase in total tube length (mm). This response is not observed in the presence of VEGF. **B)** shows representative images of samples. Green, CD31. Scale bar: 300 µm. Statistics correspond to N=3.

The end-point of this experiment is day 4. As mentioned in section 8, this time point does not allow the formation of mature, lumenised vessels. A shorter time point was used due to observed vessel regression at later points if samples were not further supplemented

with exogenous VEGF (data not shown). This is in contradiction to what has been previously reported in the literature, in that NHLFs promote the formation of an extensive, mature, stable vasculature [215, 244]. In these studies, NHLFs were typically seeded in a stromal compartment which is separated from the vascular compartment by a medium channel. This is unlike the devices used in this thesis which utilise directly adjacent gel channels. The use of a stromal compartment could perhaps enable a stronger concentration gradient promoting further vessel formation. In addition, alternative studies used much higher NHLF densities, between 1-8 × 10^6/mL, whereas in this thesis 6 × 10^5 NHLFs/mL were used. The increased number of NHLFs used in alternative studies may cause an increase in the secretion of angiogenic growth factors compared with our study - promoting the formation of a more extensive, mature vasculature than what is being reported in this thesis. The lower density of fibroblasts used in this thesis was due to potential comparisons between NHLF-HUVEC and G33-HUVEC interactions later. As such, 6 × 10^5 G33s/mL was seen as optimal as extensive fibrin gel degradation was otherwise observed, thus 6 × 10^5 NHLFs/mL were used.

Though NHLFs significantly promoted short-term vessel formation, they were not further investigated in this thesis. This is due to them being superfluous to forming a mature vasculature, as the addition of exogenous VEGF also significantly promotes vessel formation. Indeed, the addition of VEGF accounted for the greatest variance in results. Furthermore, the addition of NHLFs cannot be reversed, however, if desired, the concentration of VEGF is able to be manipulated during the duration of experiments. In addition, the use of NHLFs to promote vasculogenesis requires more time and is more expensive than using exogenous factors. Instead, pericytes were selected for further investigation.

9.4. Investigating the interactions between HUVECs and pericytes

Instead of further experiments investigating the interactions between NHLFs and the vasculature, studying pericyte-HUVEC interactions seemed more appropriate regarding the scope of this thesis. Pericytes, or 'Rouget cells' [251], are poorly described and recognised, with literature generally using the term pericyte to describe any microvascular peri-endothelial mesenchymal cell located within the vascular basement membrane [64]. Morphologically, pericytes often span and enclose multiple endothelial cells. They achieve this with primary cytoplasmic processes running along the length of the abluminal surface of the endothelium. From these primary processes, secondary processes run perpendicularly, encircling the endothelial tube [64]. Though pericytes are largely separated from endothelial cells by the basement membrane, there are areas of direct contact between the two cell types. These include gap junctions, peg-and-socket contacts and adhesion plaques, each of which have their own specific role in contributing to pericyte-endothelial signalling. Though not in direct contact, adhesion plaques, as the name suggests promotes adhesion between pericytes and endothelial cells, and are mainly composed of fibronectin [252, 253]. Gap junctions directly connect pericytes with endothelial cells, allowing the direct transfer of small molecules and ions [254-256]. Peg-and-socket junctions are pericyte projections, protruding into endothelial invaginations, which are linked with pericyte-endothelial juxtacrine signalling [257]. Indeed, Wakui revealed these invaginations are the location of endothelial EGF receptor (EGFR), which promotes angiogenesis when active [258]. In addition, N-cadherin is expressed in peg-and-socket junctions, further promoting pericyte-endothelial adhesion [259].

9.5. Determining the role of pericyte paracrine signalling on vessel formation

Though pericytes are typically found surrounding the endothelium, pericyte-HUVEC paracrine signalling was first investigated. This was to observe if similar effects were seen when investigating juxtacrine pericyte-HUVEC signalling. The role of pericyte paracrine signalling has been largely unexplored in humans, but some interesting ovine studies have suggested pericytes direct endothelial sprouting by acting as lead cells and subsequently secreting VEGF [260, 261]. In addition, the HUVEC-to-pericyte paracrine signalling system is essential for the recruitment of pericytes to immature, sprouting vessels. Though other proteins have been linked with pericyte recruitment, the PDGF-B - PDGFR-β axis is the most studied and believed to have the most importance in pericyte recruitment to vessels [155, 165, 262]. Indeed, PDGF-B or PDGFR-β null mutant mice feature many vascular abnormalities leading to oedema and embryonic lethality [155]. According to Armulik *et al*, endothelial cell-to-pericyte ratio is anywhere between 1:1 and 10:1 depending on the tissue of origin [64]. These ratios would allow sufficient abluminal coverall to promote proper endothelium function [64]. Therefore, a 10:1 ratio of endothelial cell-to-pericytes was used in this thesis to ensure pericyte coverage of the endothelium, though this is considerably lower than what has been previously used in literature [156, 207]. Pericyte-to-HUVEC paracrine signalling was investigated using a four-channel device (shown in Figure 20). 6×10^6 HUVECs/mL and 6×10^5 pericytes/mL were separately added to the central gel channels (LG and RG). The end-point of this assay was day 4, as similar difficulties were encountered as when co-culturing HUVEC-NHLFs in the absence of additional VEGF.

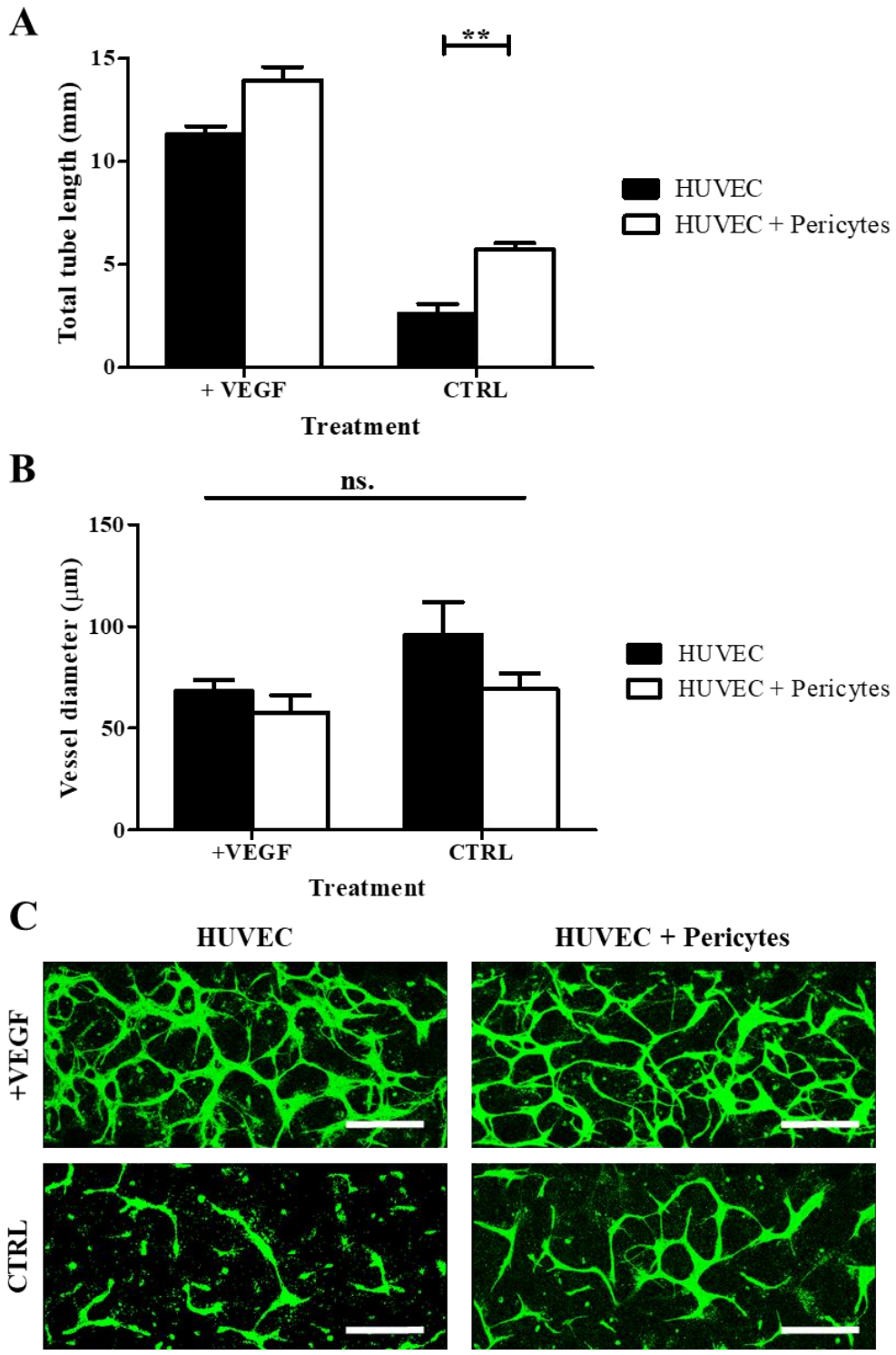

Figure 22. Pericyte paracrine signalling promote vasculogenesis. A) Pericyte paracrine signalling promotes a significant increase in total tube length (mm) when cultured in non-supplemented EGM-2, though no significant difference was observed when cultured 50 ng/mL with exogenous VEGF **B)** Additionally, pericytes had no significant impact on vessel diameter. **C)** Representative images. Green, CD31. Scale bar: 300 µm. Statistics correspond to N=3.

As shown in Figure 22, in the absence of exogenous VEGF, pericytes promote a significant increase in vessel formation compared with HUVEC mono-culture (5.8 ± 0.3 and 2.6 ± 0.5 mm, respectively). In addition, pericytes had no significant impact on vessel formation when exogenous VEGF was added, compared with HUVEC mono-cultures, similarly to what was observed with NHLFs. To observe if the pericytes reported impact on vessel hyperplasia requires direct contact, vessel diameter was also examined. As shown in Figure 22, pericyte paracrine signaling had no impact on vessel diameter when cultured with or without exogenous VEGF. These results suggest pericytes, like NHLFs, are able to promote vasculogenesis through paracrine signaling. This could be through the release of various angiogenic growth factors, such as VEGF, though this was not further examined. Interestingly, these results suggest that pericyte paracrine signaling does not impact vessel morphogenesis, which was demonstrated by the lack of difference in vessel diameter. Rather, vessel morphology may be more tightly regulated by juxtacrine pericyte signaling. This was further examined by the co-culture of HUVECs and pericytes within the same gel channel.

9.6. Investigating the role of pericytes on vessel sprouting and vessel diameter

Pericyte paracrine signalling promoted vasculogenesis, but had no impact on vessel morphology. As discussed, pericytes are normally found in direct contact with endothelial cells through three main interactions; adhesion plaques, gap junction and peg-and-socket junctions [263]. These interactions were further examined by co-culturing HUVECs and pericytes in the same microfluidic channel.

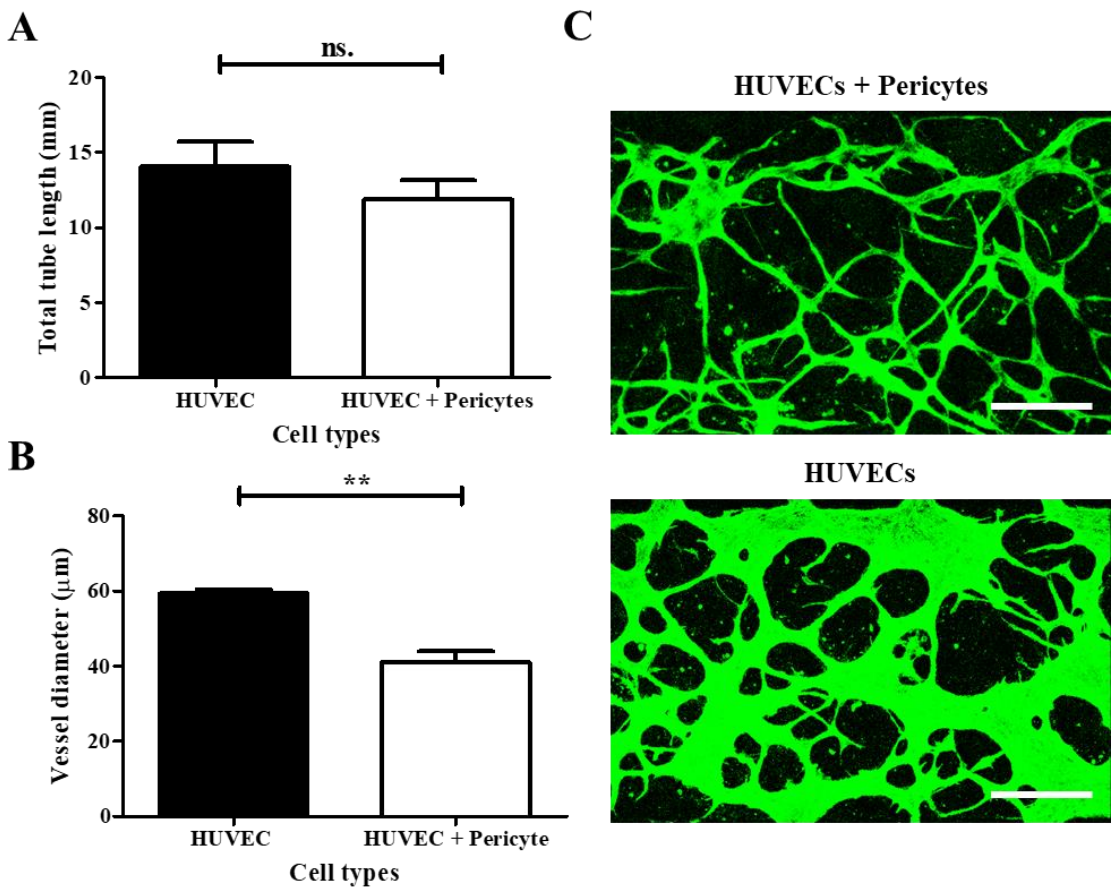

Figure 23. Short-term impact of pericytes on endothelial morphology and vasculogenesis. A) Pericytes do not significantly impact HUVEC sprouting after 4-days direct co-culture. **B)** However, they do significantly reduce vessel diameter when compared with HUVEC mono-culture. **C)** Representative images. Green, CD31. Scale bar: 300 µm. Statistics correspond to N=3.

The impact of pericytes on vessel formation was investigated at two different time-points (days 4 and 10) to examine any differences in vasculogenesis or vessel diameter between these time-points. These experiments were conducted in a three-channel microfluidic device, with a fibrin gel embedded with the respective cells in the central channel. As stated previously 6×10^6 HUVECs/mL and 6×10^5 pericytes/mL were used for this experiment. However, these experiments were conducted in the presence of VEGF due to vessel regression at later time points (beyond 4-days) if absent.

Co-culturing HUVECs and pericytes had no significant impact on total tube length when compared with HUVEC mono-cultures following 4-days culture (Figure 23, mean total tube lengths between 11.9 - 14.0 mm). However, the addition of pericytes led to a significant reduction in vessel diameter when compared with HUVEC mono-cultures, vessel diameters being 41.1 ± 2.9 and 59.4 ± 1.1 μm, respectively.

As described in Figure 18, following 10-days culture HUVECs undergo extensive vessel hyperplasia, concurrently a clear reduction in overall tube length is observed. Pericytes, which are known to inhibit vessel hyperplasia, were hypothesised to stabilise vessel growth. This can be seen in Figure 24, with pericytes significantly promoting total tube length when compared with HUVEC mono-culture, following 10 days of culture. Concomitantly, pericytes significantly reduce vessel diameter and hyperplasia compared with HUVEC mono-cultures (48.06 ± 3.0 and 112.7 ± 12.3 μm, respectively). Conducting statistical quantitative analysis between day 4 and day 10 conditions is not possible, due to them being separate, unrelated repeats. However, this trend would suggest that at day 4, HUVEC vessels are being restricted by the pericytes, which inhibit their diameter, but not actual vessel formation. However, by day 10, HUVEC vessels undergo continued proliferation and growth, promoting vessel diameter and eventually causing vessel merger - leading to a reduction in total tube length. Whereas, pericytes restrict vessel diameter, preventing vessel merger and therefore maintain overall vessel length. In addition, pericytes appear to be directly interacting with HUVECs (see Figure 24), with single pericytes interacting with multiple endothelial cells. Similar interactions are reported in the literature, with single pericytes coordinating signalling between multiple endothelial cells [264]

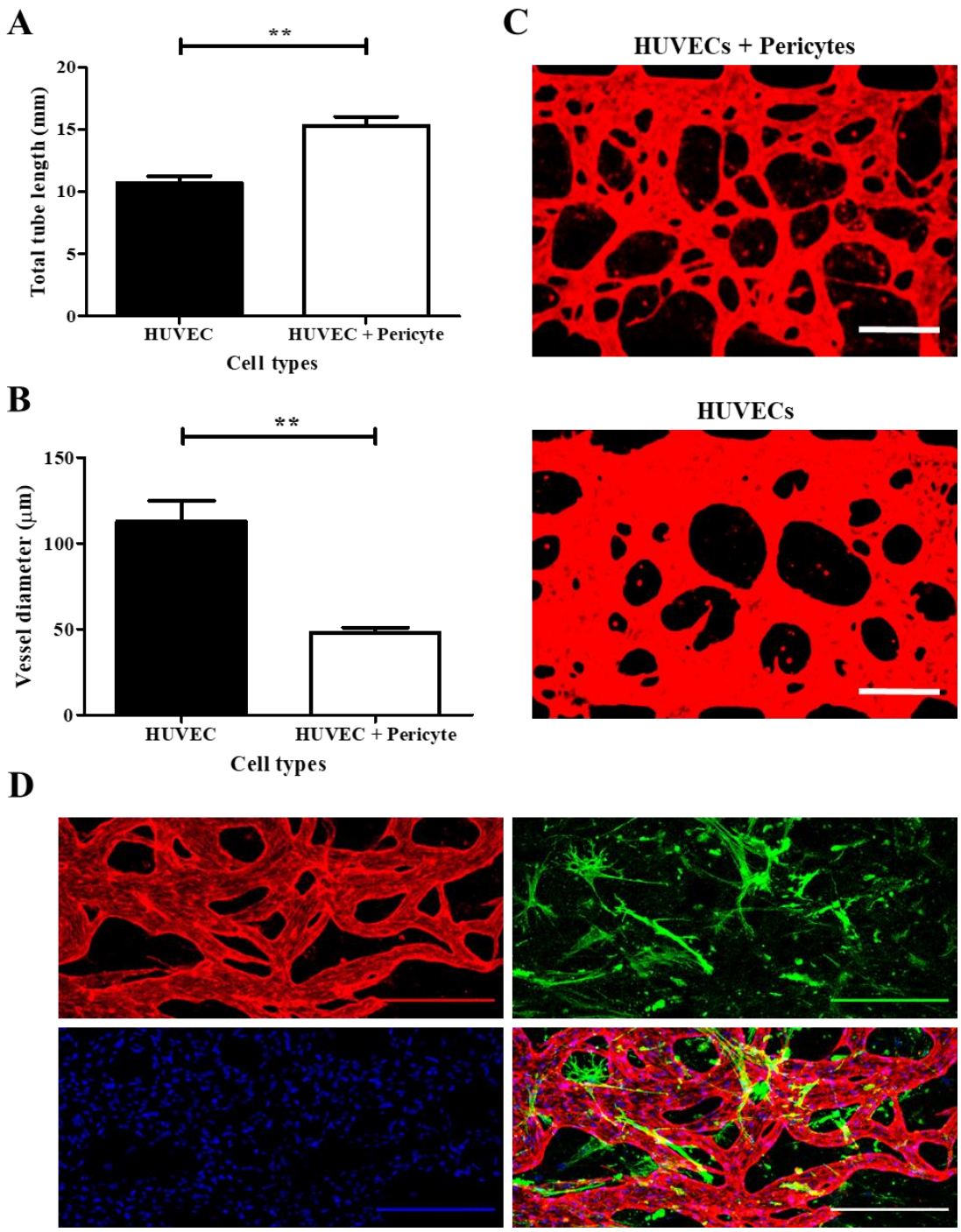

Figure 24. Long-term impact of pericytes on endothelial morphology and vasculogenesis. A) Pericytes led to a significant increase in vessel length after 10 days of co-culture, compared with HUVECs in mono-culture. **B)** In addition, they significantly inhibit vessel hyperplasia and restrict their diameters. **C)** Representative images. **D)** Representative images of HUVECs co-cultured with pericytes in VEGF-supplemented EGM-2. Red, CD31. Green, α-SMA. Blue, DAPI. Scale bar: 300 µm. Statistics correspond to N=3.

In agreement with our results, pericytes and other stromal support cells have been reported to limit vessel hyperplasia *in vitro* [156, 207, 265]. However, pericytes impact on overall vessel formation is less well-documented and somewhat contradictory. Pericytes have been reported to promote the number of branch points and junctions within an endothelial network, to have no impact no impact on total vessel area, and to inhibit total tube length [156, 207, 265]. Interestingly, Lee *et al* report how pericytes significantly reduce the vessel area of networks at day 3, however by day 7 no difference is observed, when compared with HUVEC mono-cultures [207]. If Lee extended these experiments past day 7, perhaps pericytes would promote vessel formation, as we report in this thesis.

This thesis proposes that pericytes significantly reduce vessel diameter and increase vessel length. We believe that these results are correlated, as through the inhibition of vessel hyperplasia, pericytes prevent the fusion of vessels - inhibiting the reduction in overall tube length. Interestingly, Hellström *et al* revealed that abrogation of endothelial-pericyte interactions *in vivo* does not lead to any changes in micro-vessel density, length, and number of branch points [166]. However, a significant increase in vessel diameter was observed. This would suggest that *in vivo* loss of pericytes is not commonly associated with a reduction in vessel density or length - contradicting what we observe in Figure 24. However, compared with Hellström, we observe a larger change in vessel diameter in a smaller environment - promoting vessel merger and reduction in vessel length. The precise mechanism behind pericytes inhibition of vessel hyperplasia has not been elucidated, but two prevailing theories exist; inhibition of endothelial proliferation and physical contraction [253]. Orlidge *et al* revealed that direct co-culture of endothelial cells and pericytes, at a 10:1 ratio, significantly inhibited endothelial cell proliferation [266]. However, this inhibition was not observed if pericytes were cultured in separate, but connected, chambers. This is supported by Hirschi *et al*, who, using a similar assay,

demonstrated endothelial-pericyte heterotypic contact led to a 43% growth inhibition of endothelial cells [267]. Using electrophysiological recordings, Sakagami *et al*, revealed that pericytes action as contractile cells may also inhibit endothelial hyperplasia, via the PDGF-B - PDGF-β1 axis [160, 262]. These studies suggest that pericytes inhibit endothelial proliferation and reduce vessel diameter via direct or juxtacrine signalling - in agreement with what is reported in this thesis.

9.7. Impact of pericytes on vessel permeability

Pericytes play an essential role as support cells in the vasculature. Interestingly, the tissues with the highest densities of pericytes are neural tissues, with a clear positive correlation between pericyte coverage and endothelial barrier function [64]. This effect has been translated by a number of advanced *in vitro* models, which demonstrate enhanced barrier function when endothelial cells are co-cultured with pericytes [156, 268]. Analysis of human tissues has further demonstrated that the germinal matrix, an area of the brain vulnerable to haemorrhage in premature infants, contains significantly fewer pericytes than the neocortex and white matter, highlighting the important role pericytes play in inhibiting vessel hyper-permeability [269].

To further examine the impact of pericytes on vessel permeability, an assay was established based upon a similar technique reported in the literature, and is discussed in greater detail in the Materials and Materials section of this thesis (p.60). Briefly, this assay compared HUVEC mono-culture with HUVEC and pericyte co-culture (6×10^6 HUVECs/mL and 6×10^5 pericytes/mL). Following 10-days cell culture, medium was aspirated from the reservoirs and 70 kDa FITC-dextran was added to one of the side-channels. FITC-dextran perfused through the vessel network and using real-time live

imaging, leakage from the intravascular to extravascular compartments over 30 min was analysed. Quantification of fluorescence intensity in the vessel lumen and in extravascular compartments, at different time points, enabled the monitoring of the permeability of the vessels formed to dextran macromolecules. This assay analysed three ROI per chip, plotting each ROI separately (N=4). In agreement with the literature, as shown in Figure 25, pericytes significantly reduced vessel permeability in this system. The mean net-fold intensity change was 1.25 ± 0.18 in endothelial mono-cultures and 0.80 ± 0.14 in pericyte co-cultures. Pericytes are known to be an important regulator of vessel permeability, however this has not been quantitatively demonstrated in an advanced microfluidic system previously. Rather, many studies typically demonstrate that the vascular network is perfusable, using 70 kDa FITC-dextran, but do not attempt to quantify this process [156, 207]. This is perhaps a result with the difficulty of limiting leakiness at the point of opening between the side channels (in which media containing dextran is supplemented) and the vascular network. Indeed, when adding 70 kDa FITC-dextran to the side-channel of a microfluidic device, the dye will enter the vasculature through vessel lumen openings, between posts. If any fibrin gel is left exposed, the FITC-dextran will enter the gel, as well as the vessels, and perfuse through the system relatively fast, preventing vessel leakage analysis. Due to this, obtaining reproducible results is challenging, as such, groups have often shown qualitative rather than quantitative data when discussing vessel permeability [156]. To overcome this, only chips which had clear vessel openings in the gaps between posts were selected for further study. This technique could be optimised via the improvement of endothelial coverage of the side-channels, limiting fibrin gel exposure. An interesting study by Hughes *et al* coated the side-channels with laminin, reporting that this improved anastomosis and hence reduced FITC-dextran dye diffusing directly into the gel [159].

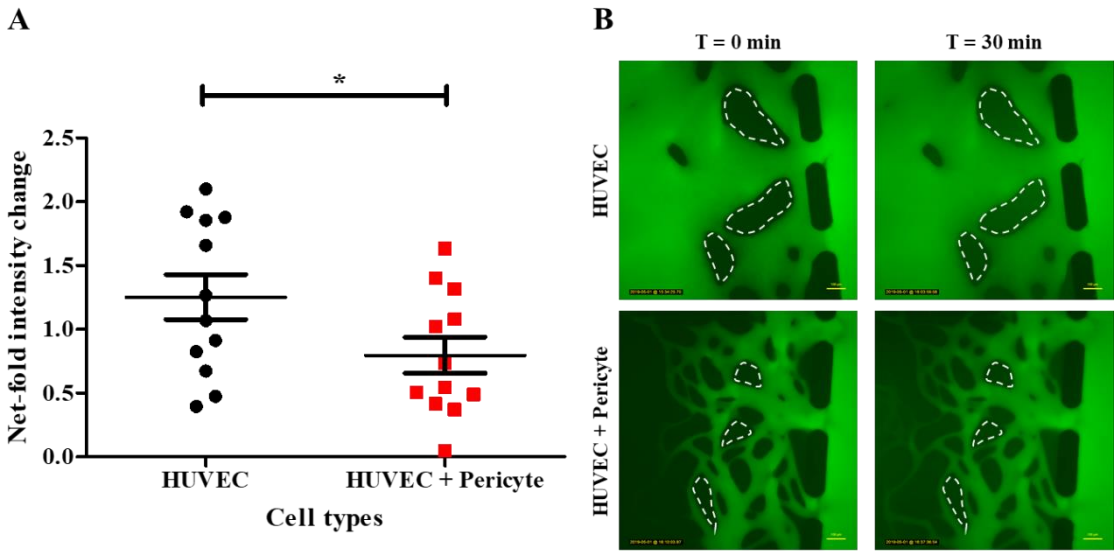

Figure 25. Pericytes inhibit vessel permeability. A) Real-time, live-imaging measuring 70 kDa FITC-dextran leakage from the intravascular to extravascular compartments, reveals that pericytes significantly inhibit vessel permeability **B)** Representative images. Areas within the dashed line are examples of ROI's which could be analysed. Green, 70 kDa FITC-dextran. Scale bar: 100 µm. Statistics correspond to N=4, with triplicates per repeat.

9.8. Vascular networks express multiple junction markers

Pericytes are known to reduce vascular permeability through a number of mechanisms, including the inhibition of transcytosis and paracellular transport, via reducing the number of endothelial cytoplasmic vesicles and regulation of tight junctions, respectively [167, 270, 271]. Tight junctions are composed of a number of transmembrane spanning proteins which act as a barrier, preventing the diffusion of polar substances from the blood, with ZO-1 playing an integral role in tight junction formation and stability [167]. Many organ-on-a-chip studies use junction marker expression to indicate vessel maturation [198, 207, 213]. However, few organ-on-a-chip studies quantify junction marker expression, and link these results with vessel permeability. This is perhaps due to the difficulties involved in removing the cells from within PDMS devices, limiting the molecular biological techniques available to researchers. To overcome this issue, Jeon *et*

al designed a novel microfluidic system which incorporated a PDMS construct non-covalently bound to an underlying PSA film, when the experiment is completed the chip can be deconstructed and the cell-laden hydrogel removed [207]. With this device, Jeon demonstrated that pericytes significantly increase endothelial ZO-1 expression when compared with endothelial mono-culture.

To investigate the role pericytes play in junction marker expression, we compared the expression of three separate junction markers, VE-cad, β-catenin and ZO-1 (in addition to CD31). These markers were selected due to their role in the establishment of adherens and tight junctions. The same cell densities as previously reported were used, 6×10^6 HUVECs/mL and 6×10^5 pericytes/mL, with the end-point being day 10. As shown in Figure 26, both HUVEC mono-culture and HUVEC-pericyte co-culture vessel networks displayed clear expression of VE-cad, β-catenin and ZO-1 at cell-cell junctions, suggesting these vessels, even without pericytes, have achieved maturity and stability. This is in agreement with results presented in Figure 25, which show that HUVEC mono-culture vessels still maintain a barrier function - though this is enhanced when co-cultured with pericytes.

This experiment was able to demonstrate the expression of various junction markers in both HUVEC, and HUVEC and pericyte cultures. However, it was unable to investigate the relative expression of these markers. Future experiments could develop a chip with a PSA substrate to replace the underlying glass, similar to what was proposed by Jeon *et al* [207]. Using this system, we could investigate the expressions of different junction markers in comparison with the ubiquitous CD31 - with high expressions suggesting a more mature, developed vasculature.

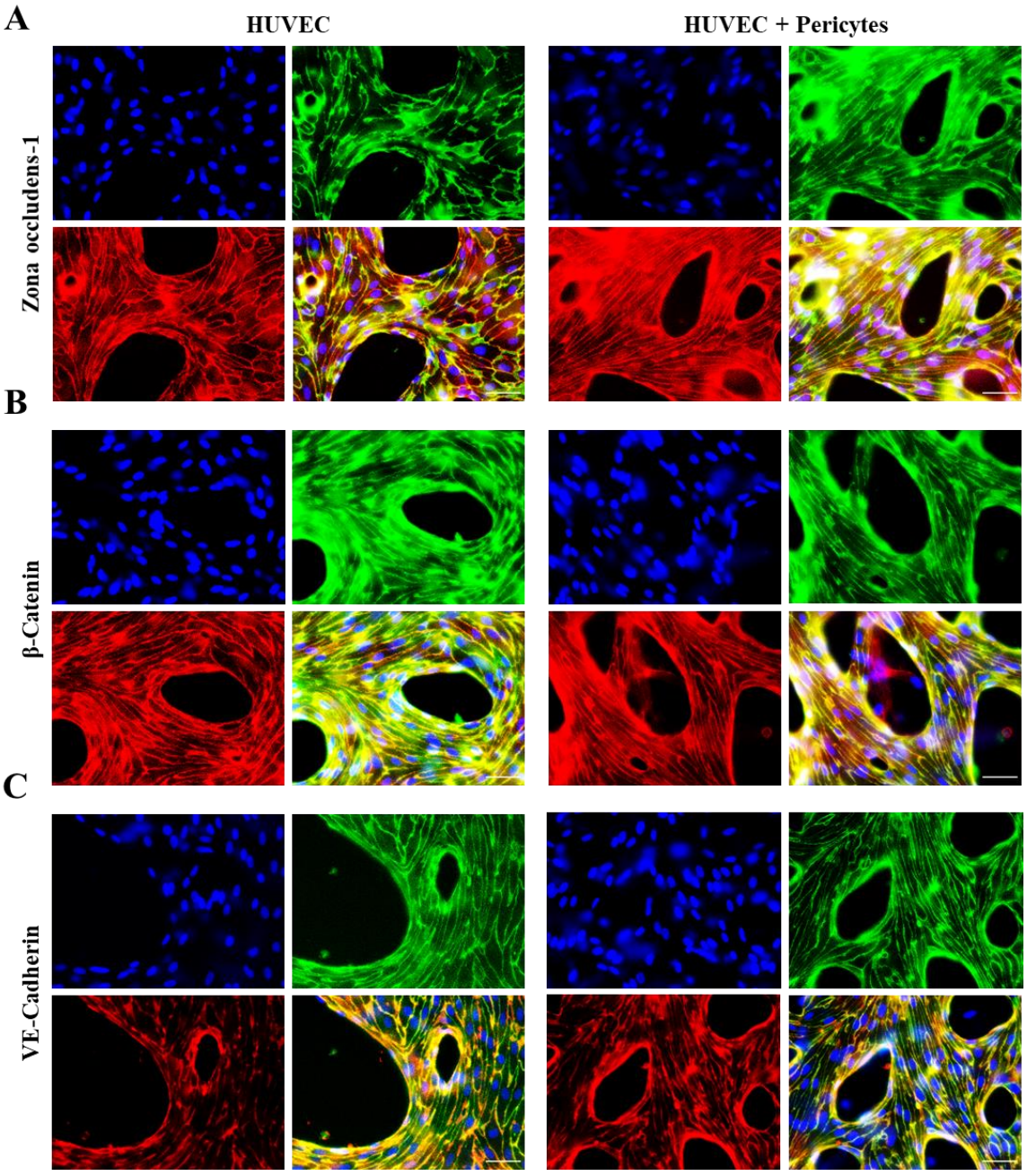

Figure 26. Junction marker expression in vessels cultured with and without pericytes. Epifluorescence microscopy images of HUVECs or HUVEC and pericytes vascular networks following 10-days culture. These images display single Z-frames of the respective channels and a final merged Z-stack. **A)** β-cat expression. Red, β-cat. Green, CD31. Blue, DAPI. **B)** VE-cadherin expression. Green, VE-cad. Red, CD31. Blue, DAPI. **C)** ZO-1 expression. Red, Z01. Green, CD31. Blue, DAPI. Scale bar: 50 µm. Images represent N=3.

9.9. Impact of pericytes on vessel regression following induced stress

As demonstrated so far, pericytes play an essential role within the vasculature, promoting endothelial sprouting through paracrine and juxtacrine signalling, inhibiting vessel hyperplasia, and reducing endothelium permeability. In addition to these effects, pericytes are also known to promote endothelial cell survival, with multiple pathways being linked with this effect, with the VEGF and Ang-1 pathways being particularly notable [154, 272, 273]. VEGF is recognised as being the most important angiogenic factor impacting the development and homeostasis of the vascular network. As such, it is unsurprising it has also been demonstrated to hugely impact endothelial cell survival. *Ex vivo* studies have shown that VEGF withdrawal from tumour samples leads to the selective apoptosis of endothelium unsupported by perivascular cells [274], indicating that pericytes play an important role in endothelial cell survival, perhaps through the local release of VEGF. This is further supported by Darland *et al*, who demonstrated that co-culturing endothelial cells with pericytes promotes endothelial cell survival through a TGF-β1 dependent VEGF pathway [154]. VEGF promotes cell survival through the increased expression of B-cell lymphoma 2 (Bcl-2), in turn inhibiting caspase-3 expression and its downstream apoptotic pathway including DNA fragmentation and activation of endonucleases [275]. In addition, Ang-1 has been linked with endothelial cell survival and vessel stabilization [273, 276, 277]. Interestingly, in a serum deprivation study Ang-1 was shown to attenuate endothelial apoptosis via TIE-2 stimulation - leading to the inhibition of caspases -3, -7 and -9 [273, 276].

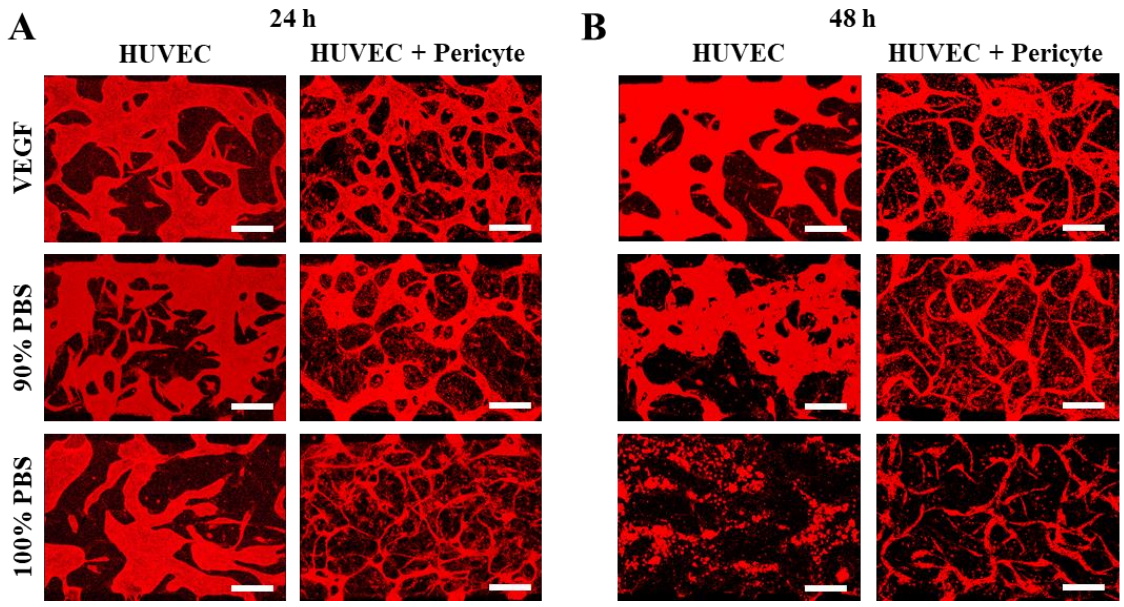

Figure 27. Impact of nutrient deprivation on vascular networks. The impact of nutrient stress on vessel survival and stability was investigated using DPBS-medium solutions. **A)** Following 24 h, 90% DPBS does not have a clear impact on vessels. However, vessel regression and vessel thinning are observed in HUVEC mono-cultures and pericyte co-cultures, respectively, when cultured in 100% DPBS. **B)** Following 48 h HUVEC vessels are beginning to break-down, with further vessel thinning observed in pericyte co-cultures, when cultured in 90% DPBS. However, complete vessel regression is observed in HUVEC mono-cultures following 48 h in 100% DPBS. With pericyte co-cultures beginning to break-down. Red, CD31. Scale bar: 300 µm. Images represent N=1.

To further investigate the impact of pericytes on HUVEC survival an assay was established which used nutrient deprivation of established vascular networks. The induction of nutrient deprivation is a well-established technique to induce cellular stress. One particularly interesting study induced extreme stress in HUVECs by replacing medium with 90% DPBS for 4 days [216]. Due to the similarities between our systems, this technique of nutrient deprivation was further investigated. A similar co-culture as that previously described was employed, which used 6×10^6 HUVECs/mL and 6×10^5 pericytes/mL cultured in the same gel channel for total period of 10 days. Firstly, comparisons were made between HUVECs or HUVEC and pericytes cultured in VEGF, 90% PBS or 100% PBS for 24 h and 48 h culture. As shown in Figure 27, following 24 h culture PBS treatments appear to be promoting vessel regression in both mono- and co-

cultures (images represent N=1). Following 48 h culture, 90% PBS treatment is causing vessel breakdown in mono-cultures, and further vessel regression in co-cultures. However, 100% PBS treatment has promoted the complete breakdown of the endothelium in HUVEC mono-cultures. Whereas, co-cultures still have vessel structure, though extensive vessel regression is observed and cell-cell adhesion appears disrupted. This would qualitatively suggest that pericytes are promoting vessel stability, however no quantification was conducted as this experiment was not repeated.

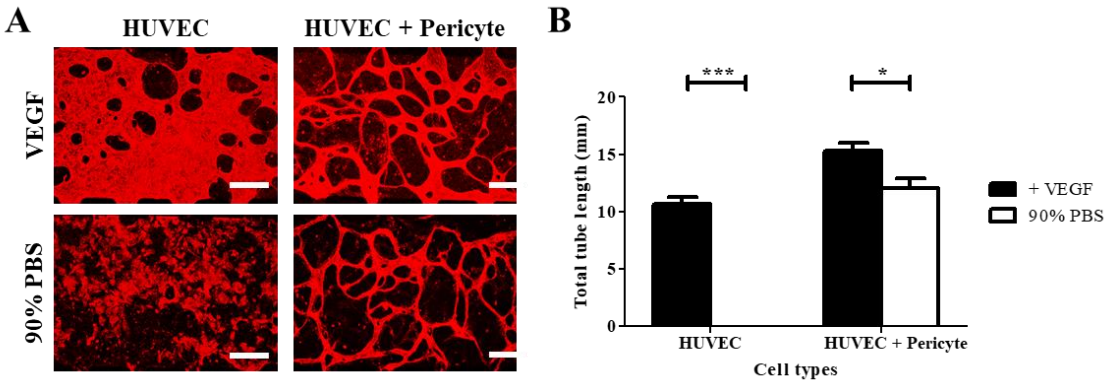

Figure 28. Impact of nutrient deprivation on vascular networks after 72 h. A) Following 72 h in 90% PBS HUVEC mono-cultured vessels have completely regressed. However, pericytes appear to maintain vessel structure. **B)** Quantitative analysis reveals nutrient stress led to a significant reduction in total tube length in HUVEC and pericyte co-cultures when compared with control. Red, CD31. Scale bar: 300 µm. Statistics correspond to N=3.

Next, the impact of 90% PBS treatment on vessel stability following 72 h culture was studied (Figure 28). 100% PBS was not used for this time-point as it had already been demonstrated that by 48 h in HUVEC mono-culture, vessel integrity had entirely collapsed and was judged too harsh a condition. As shown in Figure 28, pericytes appear to promote vessel stability and cell survival from nutrient stress. 90% PBS treatment causes significant vessel regression in HUVEC and pericyte co-cultures when compared with VEGF supplemented medium, with mean total tube length reducing to 12.1 ± 0.8

mm compared to 15.3 ± 0.7 mm for VEGF supplemented medium. However, when HUVEC networks were mono-cultured in 90% PBS treatment, complete vessel breakdown was observed. These results highlight the protective impact of pericytes during serum deprivation and nutrient stress on the endothelium.

Previous studies did not report the impact of PBS treatment and nutrient deprivation on the vascular networks, instead, they described the impact of stress on spheroids embedded within the vascular network [216]. However, pericytes have been repeatedly shown to promote endothelial cell survival *in vitro* [154, 272, 274]. Though our assay did not directly analyse apoptosis, it did demonstrate that pericytes promote vessel stability under induced nutrient stress. Ramsauer *et al* also describe how the addition of pericytes to an *in vitro* model promotes endothelial resistance to apoptotic stimuli and maintains vessel integrity [278]. Perhaps the most elegant and in depth study concerning pericyte-induced endothelial cell survival, was conducted by Franco *et al* [272]. They proposed endothelial cells recruit pericytes through PDGF-BB secretion. Pericytes subsequently deposit vitronectin which stimulates the endothelial integrin α_v, leading to downstream activation of NFκB. This promotes autocrine VEGF-A signalling and Bcl-w expression, and promotion of endothelial cell survival.

9.10. Summary

This section describes the interactions between endothelial cells and two different regulators of vasculogenesis; fibroblasts and pericytes. NHLFs were selected due to their ubiquitous use in other advanced *in vitro* microfluidic models and their reported ability to significantly enhance vessel formation [199, 222]. The ability of NHLFs to promote vasculogenesis via paracrine signalling was demonstrated, however, this appeared as a

short-term effect and did not promote the formation of mature, stable vessels. Instead, pericytes ability to promote stable vessel formation was further evaluated. As shown, pericytes promoted short-term vessel formation through paracrine signalling. However, it was through juxtacrine signalling that pericytes had the most significant impact, demonstrably inhibiting vessel hyperplasia, promoting total tube length, and reducing vessel permeability. The addition of pericytes to vascular networks was also shown to significantly inhibit vessel regression following nutrient deprivation, when compared with mono-cultured HUVEC vessels. These effects are in agreement with the literature which shows pericytes play an important role regulating vascular maturation [155, 156, 165, 166, 207].

10. Investigating the interactions between endothelial and high-grade serous ovarian cancer cells

10.1. Introduction

Angiogenesis plays an essential role in tumour development. Indeed, tumours may only reach 1-2 mm diameter before requiring a vascular network to supply the proliferating cells with oxygen and nutrients, and to remove waste products [60]. Angiogenesis has therefore become a key target in cancer therapy, including HGSOC therapy. This has led to the successful incorporation of bevacizumab, a VEGF-A blocking antibody, into ovarian cancer adjuvant and neo-adjuvant treatment [91, 92]. However, the exact role the vasculature plays in ovarian cancer progression is contentious, due to the mechanism behind ovarian cancer spreading/metastasis being disputed. As discussed more extensively in the introduction (p. 20), HGSOC is typically regarded to spread through direct transcoelomic dissemination, aided by the peritoneal circulation [38, 40]. However, HGSOC may also spread via hematogenous metastasis [45]. Regardless of the prevalent mechanism of disease spreading, angiogenesis is an important mediator of disease progression, with high micro-vessel density an independent marker for poor overall and progression-free survival in patients with epithelial ovarian cancer [89]. In addition, high tissue expression of VEGFR-2 has been positively correlated with aggressive tumour invasion in ovarian carcinoma [279]. These studies highlight the importance of an extensive vascular network in disease progression.

10.2. G33 viability within fibrin gels

As discussed in the introduction of this thesis, many commonly used HGSOC cells lines are genetically non-representative of the disease, including SKOV3 and IGROV1 [181]. As such, investigating cell behaviour and novel chemotherapeutic agents on these cells may give misleading results. Due to this alternative cell sources were explored. G33 cancer cells, a primary cell line generated by the Balkwill lab, are a much improved option as they were isolated from the omentum of a patient with advanced HGSOC. G33 cells were extensively characterised, confirming the expression of various HGSOC genetic and protein markers, including TP53 over-expression and PAX8 expression, and characterised as a genetically distinct cell line by short-tandem repeat sequencing. Hence, G33 cells were selected for this study owing to their relevance to HGSOC.

The impact of embedding G33 cells in fibrin gels was assessed. This was to ensure that the culture conditions in microfluidic chips were suitable for further co-culture experiments with HUVECs, to investigate endothelial-HGSOC cell interactions. G33 cells were cultured in PDMS well, as described in p 56, mimicking exposure to the PDMS channels of chips. G33 cells were cultured in 2.5 mg/mL fibrin gel, with additional 0.15 U/mL aprotinin and 0.2 mg/mL T1C. The impact of cell density on viability was investigated with 1, 2.5 and 5×10^5 G33s/mL fibrin gel being explored. Cells were cultured in EGM-2 for 4 days before carrying out a LIVE/DEAD^{TM} assay, as described in the Materials and Methods section (p. 56). Day 4 was selected as the endpoint as this was the initial endpoint for concurrent vasculogenesis experiments. As shown in Figure 29, G33 cells maintain a high viability at day 4, with mean cell viabilities between 76.2 and 80.7%. G33 density had no significant impact on cell viability.

The impact of VEGF on G33 viability was also examined, this was to observe whether HUVEC culture medium had any impact on G33 viability. 2.5×10^5 G33s/mL were

selected and cultured for 4 days in basal EGM2 or 50 ng/mL VEGF supplemented EGM-2. The addition of VEGF had no significant impact on cell viability, see Figure 29, with mean cell viabilities of 84.5 ± 3.9 and 79.5 ± 1.7 for CTRL and VEGF-supplemented conditions, respectively. In addition, VEGF had no significant impact on total number cells counted, with mean cell number ± SEM: 86.7 ± 7.8 and 79.0 ± 7.8 for control (CTRL) and VEGF-supplemented conditions, respectively.

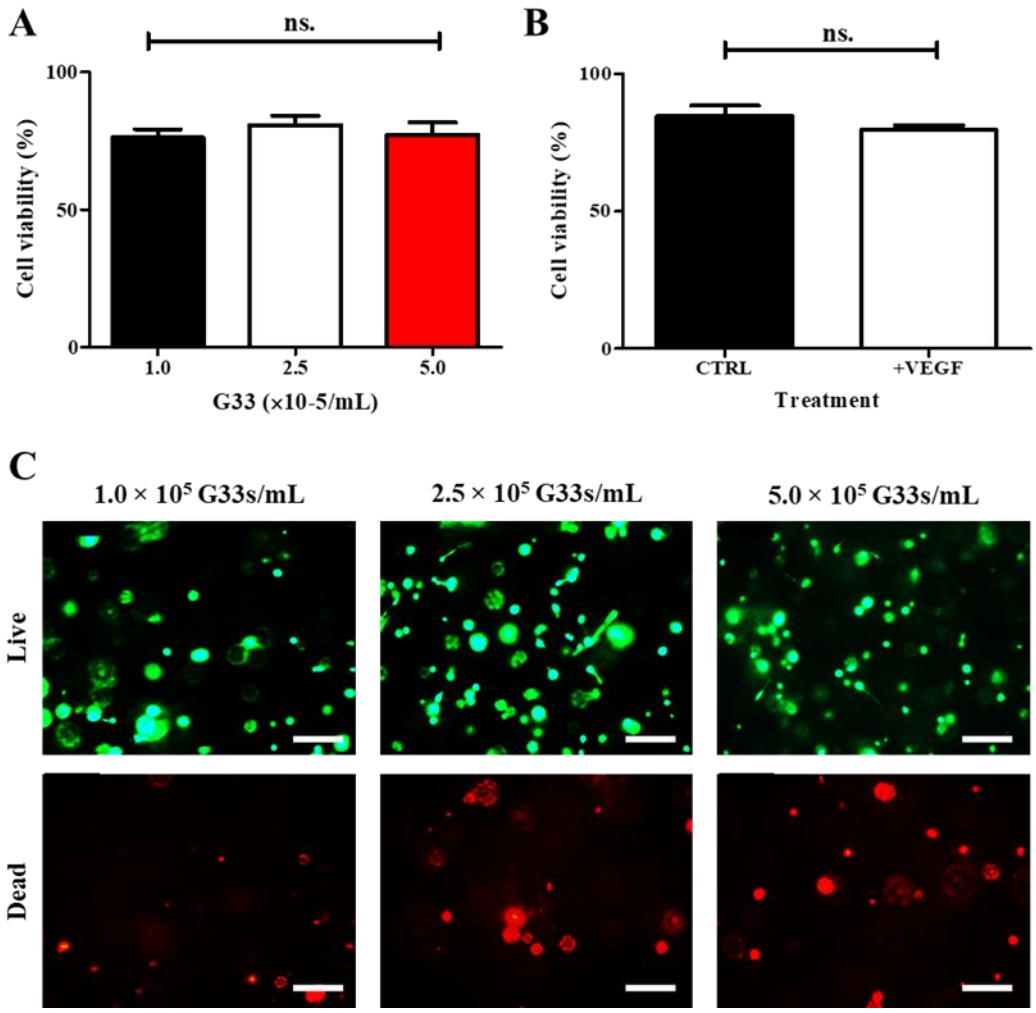

Figure 29. Investigating G33 viability within fibrin gel. A) Cell density has no significant impact on G33 viability following 4-days culture. **B)** No significant difference in G33 viability is observed between culturing G33s in the presence of 50 ng/mL VEGF in EGM-2 culture medium. Green, calcein AM (live cells). Red, ethidium homodimer (dead cells). Statistics correspond to N=3. Scale bar: 200 µm.

Our results reveal G33 culture conditions are fairly robust, with no observed significant differences in cell viability across the conditions tested. In addition, G33s are suitable to culture with VEGF-supplemented EGM-2, alongside HUVECs. Interestingly, HGSOC cells were previously reported to have high-to-moderate expression of VEGFR-2 [280]. Spannuth *et al* report that the administration of a VEGFR-2 blocking antibody to mice injected with SKOV3ipl and A2774 cells, promoted cell apoptosis and decreased the proliferative index. Though SKOV3ipl cells are reported as 'probably not HGSOC' by Domcke *et al*, the importance of VEGFR-2 activity on cancer cell proliferation and survival is evident [181]. However, the VEGFR-2 expression profile of G33 cells is not currently known. The observed cell viability of G33s within this system is similar with other reported 'high viability' fibrin gel models, with reported cell viabilities between 71-85% [185, 281].

10.3. Impact of G33s on short-term vessel formation

As described in section 9 of this thesis, short-term vasculogenesis can be enhanced with the addition of stromal cells in parallel gel channels to the HUVECs. This is believed to be through the release of various growth factors, cytokines and signalling molecules - though the full nature of these interactions has not been elucidated in this thesis. Ovarian cancer cells are known to enhance vessel formation [282-284], this is to supply the proliferating ovarian cancer cells with nutrients and oxygen, and to remove waste products [60]. In addition, typical carcinomas are believed to metastasize through this tumour induced vasculature to a secondary site.

The ability of HGSOC cells to promote short-term vessel formation was investigated. This assay used the same four-channel device discussed previously in Figure 20, with

HUVECs (6×10^6 HUVECs/mL) cultured in a gel channel, and either G33s (6×10^5 G33s/mL) or an acellular fibrin gel in the opposing gel channel. Cells were cultured for 4 days in the presence of EGM-2. As shown in Figure 30, co-culturing HUVECs with G33 cells significantly promoted vessel formation when compared with HUVEC mono-cultures, with total tube lengths of 3.8 ± 0.9 and 1.5 ± 0.2 mm, respectively.

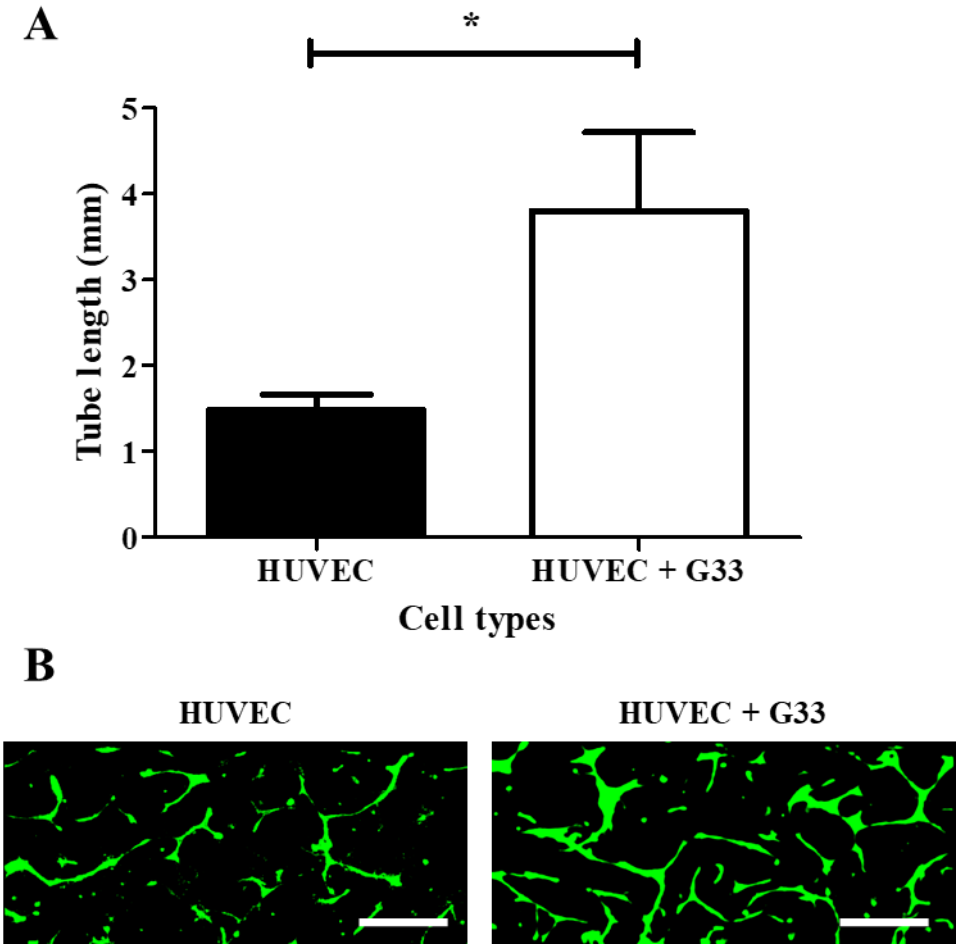

Figure 30. Impact of G33s on short-term vessel formation. A) G33 paracrine signalling promotes a significant increase in vessel formation when compared with HUVEC mono-culture. **B)** Representative images. Green, CD31. Scale bar: 300 µm. Statistics correspond to N=3.

In the literature, co-culturing endothelial cells alongside HGSOC cells, or treating with conditioned medium, promotes vessel formation and endothelial cell proliferation. A

study by Wan *et al* details the development of a novel co-culture system, involving the culturing of HUVECs and OVCAR8 ovarian cancer cells in Matrigel [282]. This system demonstrated that OVCAR8 clusters were able to maintain endothelial networks for 10 days, whereas, significant vessel regression was observed in HUVEC mono-cultures following day 2. No quantification of total vessel formation was reported for the 2-day period when both systems promoted vasculogenesis, although the maintenance of networks in co-cultures suggests a positive impact of OVCAR8 cells on microvasculature stability. It was not reported why vessel regression was observed following 2-days culture. However, there is debate regarding the validity of some ovarian cancer cell lines, including OVCAR8, which was described as 'possibly HGSOC' due to some reported differences in the genome vs primary human HGSOC cells [181]. Another study by Li *et al* used a similar system in which they seeded HUVECs directly on growth factor-reduced Matrigel and were able to investigate ovarian cancer cell paracrine signalling [283]. Using this system, Li *et al* demonstrated that conditioned medium from PA-1 and SW626 ovarian cancer cells promotes HUVEC tube formation, which is inhibited with the upregulation of SOX6. Al Thawadi *et al* proposed a novel mechanism of ovarian cancer induced angiogenesis [284]. They revealed endothelial cells cultured on Matrigel underwent angiogenesis following ovarian cancer derived microparticle treatment. Microparticles interacted with endothelial integrin subunits αV and β3, inducing β-cat dependent up-regulation of downstream Wnt/β-cat target genes, including VEGF and cyclin D1. These results are in good agreement with our observations that G33 ovarian cancer cells act to promote tube formation, which mimics the high micro-vessel density observed in poor prognosis epithelial ovarian cancer [89].

Interestingly, Kaneko *et al* demonstrated Bcl-2, the apoptotic regulator, is significantly upregulated in endothelial cells associated with head and neck carcinoma, and when

down-regulated, a significant reduction in micro-vessel density is observed [285]. In addition, it has been further demonstrated that human dermal microvascular endothelial cells (HDMECs) over-expressing Bcl-2 show a significant increase in vessel sprouting, increased cell number and protection against apoptosis [275]. Furthermore, Bcl-2 protein expression was induced by the addition of VEGF to *in vitro* cultures. To further elucidate the role of G33s, or HGSOC cells, are having on HUVECs, further studies should be conducted investigating the evolution of cell densities, endothelial cell viability and the regulation of apoptosis.

10.4. Impact of G33s on long-term vessel formation

As shown in Figure 30, G33 cells promote vessel formation over a 4-day period. Following this, the impact of G33s on endothelial tube formation, up to 10 days, was assessed. These experiments used microfluidic devices with 1000 µm channel widths.

To investigate the long-term impact of G33s on vasculogenesis, we compared mono-cultured HUVECs with HUVECs co-cultured with G33s, with 6×10^6 HUVECs/mL and 6×10^5 G33s/mL. Cells were cultured in four-channel devices, shown in Figure 20, with HUVECs and G33s cultured in separate, parallel gel channels. Cultures were maintained with 50 ng/mL VEGF supplemented EGM-2. As previously described, vessels grown in this system up to 10 days, undergo extensive vessel regression if they are not further supplemented with VEGF, independent to co-culture with stromal cells, thus a basal EGM-2 condition was not further investigated. As shown in Figure 31, no significant difference in total tube length (mm) is observed between groups, with total vessel length ± SEM being 11.8 ± 1.9 and 12.2 ± 2.2 mm for HUVECs and HUVECs + G33s respectively. Furthermore, no significant difference in vessel diameter is observed when

co-culturing HUVECs with G33s, as compared with mono-cultured vessels, with vessel diameters of 94.9 ± 14.2 and 108.2 ± 16.4 μm, respectively.

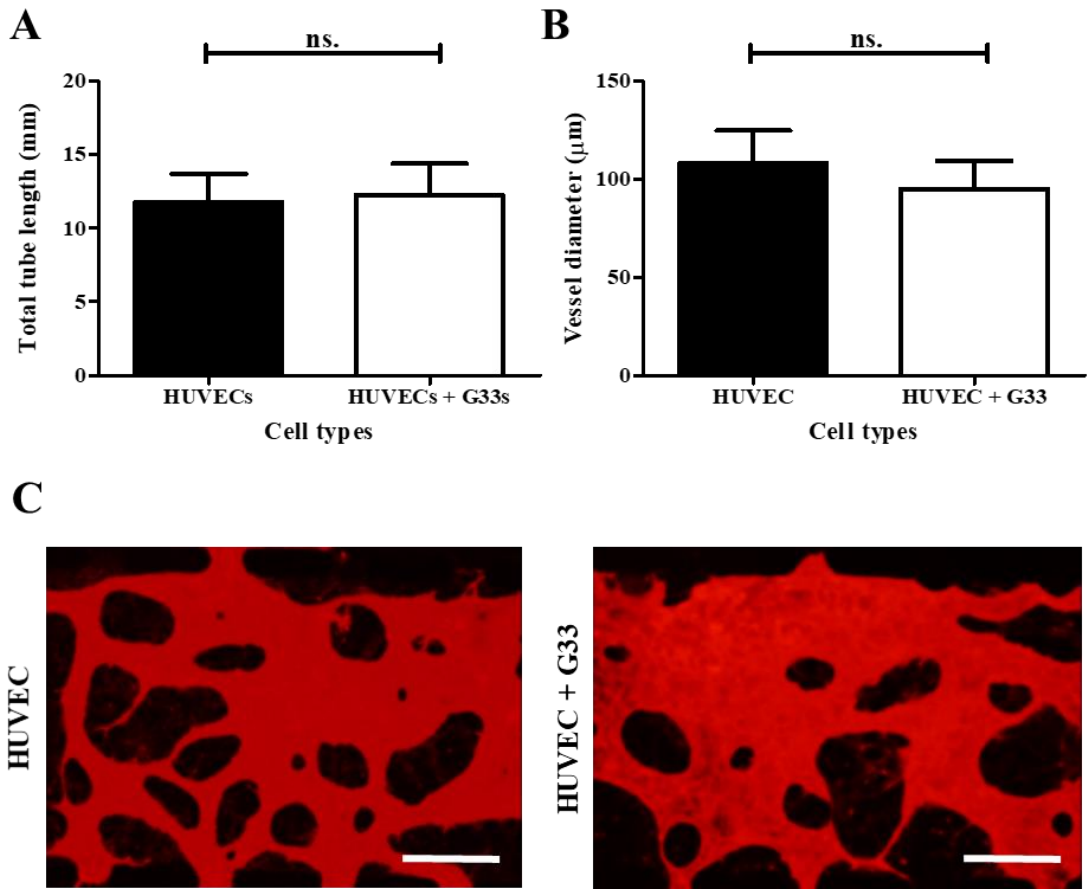

Figure 31. Impact of G33s on long-term vessel formation. A) G33s have no significant impact on HUVEC tube formation. **B)** Additionally, no significant impact on vessel diameter was observed when HUVECs were co-cultured with G33s. **C)** Representative images. Red, CD31. Scale bar represents 300 μm. Statistics correspond to N=3.

Within the context of this thesis it is unsurprising that G33 cancer cell paracrine signalling did not promote any increase in vessel formation, as supplementing cultures with 50 ng/mL VEGF appears to promote optimal vasculogenesis. This was also demonstrated in Figure 21 and 22, with NHLF and pericyte paracrine signalling having no significant impact on vessel formation, when compared with monocultures supplemented with VEGF. The impact of cancer cells on vessel morphology was examined in a microfluidic

co-culture model of breast cancer and endothelial cells [214]. In this study HUVECs were co-cultured with two commonly used breast cancer cell lines, MCF7 and MDA-MB-231, with the latter being recognised as having a particularly metastatic and invasive phenotype. When co-culturing with MDA-MB-231 cells, a significant reduction in vessel diameter was observed, however a similar result was not observed when culturing with MCF7 cells. The mechanism behind this was not further investigated, however, citing the work by Watson *et al* [286], the authors concluded that this reduction in vessel diameter could be due to increased endothelial apoptosis - though this was not further elucidated. However, G33s had no significant impact on vessel diameter in our study.

10.5. Impact of HUVECs on G33 proliferation and morphology

Following the characterisation of G33s on HUVEC vascularisation, the impact of HUVECs on G33 phenotype was investigated. Specifically, the impact of HUVECs on G33 cell number, cluster size and cluster circularity was studied. Culture conditions were the same as reported when investigating the role of G33s on HUVEC tube formation at day 10, though the impact of EGM-2 basal medium was also further studied. Representative images of these samples are shown in Figure 32, which clearly depict morphological differences in G33 cells when HUVECs are present. However, the impact of VEGF on G33s is less pronounced, if any.

As observed in Figure 32, HUVECs appear to increase the number of G33s. Indeed, quantification confirmed that the number of G33s increased when co-cultured with HUVECs, from 77.0 ± 11.4 and 66.7 ± 18.3 cells/mm^2, for EGM-2 and VEGF-supplemented monocultures, to 112.9 ± 21.6 and 133.6 ± 15.4 cells/mm^2 for EGM-2 and VEGF-supplemented co-cultures, respectively (Figure 33). VEGF had no significant

impact on G33 cell number, suggesting the observed increase in G33 number with the addition of HUVEC is through a VEGF independent pathway of cell proliferation, or inhibition of G33 apoptosis. In addition to the observed increase overall G33 cell densities in co-cultures, there is a significant increase in G33 cell clusters (cell clusters being defined as 2+ cells). The total number of cell clusters increased from 8.6 ± 1.1 and 6.2 ± 0.5 clusters/mm^2, for EGM-2 and VEGF-supplemented monocultures, to 15.1 ± 2.7 and 14.5 ± 2.5 clusters/mm^2, for EGM-2 and VEGF-supplemented co-cultures, respectively. Interestingly, whereas there was no significant difference in the number of small clusters, the number of large cell clusters (containing at least 5 cells) was significantly increased (Figure 33).

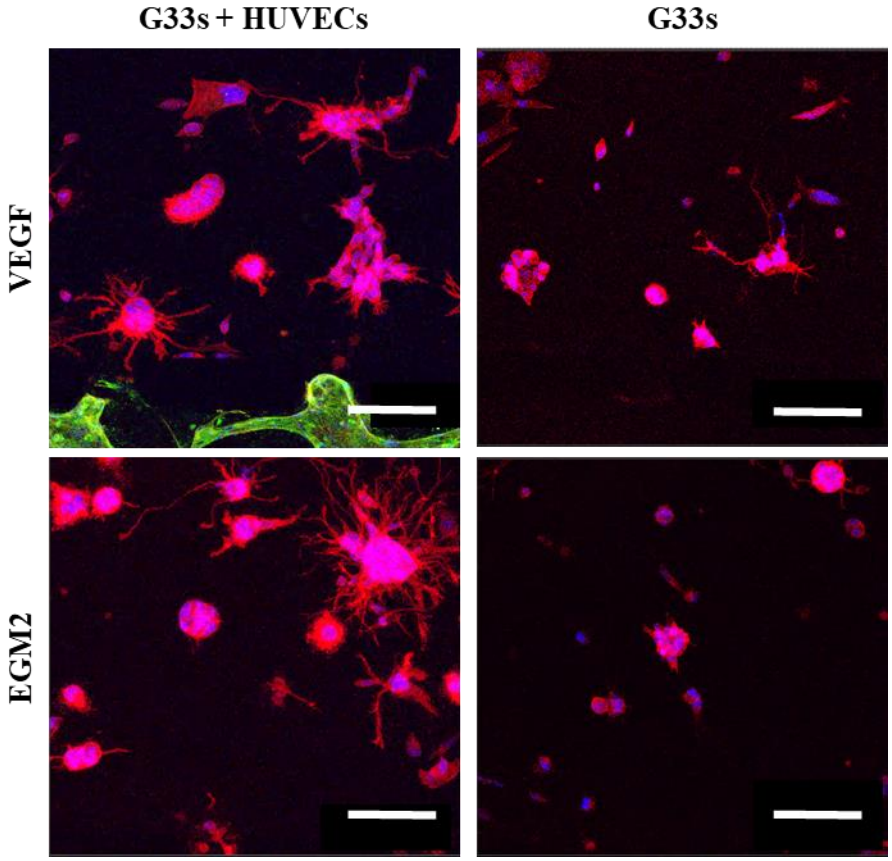

Figure 32. G33s co-cultured with HUVECs. Representative images of G33s when cultured with HUVECs or separately. When cultured with HUVECs G33 cells appear to grow into larger clusters. In addition, cells appear as more irregular and less rounded. Green, CD31. Red, F-actin. Blue, DAPI. Scale bars are 300 µm.

As well as increasing the number of G33 cells through an increase in cell clusters, Figure 32 also indicates a morphological change in G33s in co-cultures with HUVECs. This was further analysed in Figure 34, in which cluster circularity and area are quantified - perfect circularity corresponds to a value of 1. Interestingly, HUVECs promoted a less circular phenotype in G33 clusters, with circularity decreasing to 0.3 ± 0.1 and 0.2 ± 0.0 in co-cultures in EGM-2 and VEGF-supplemented media, respectively. In addition, the average area of G33 clusters was found to increase in co-cultures, which is unsurprising considering that HUVECs promote the formation of large (5+ cells) G33 clusters. Furthermore, correlations of area and circularity indicated that larger clusters displayed the most irregular shapes, consistent with the high number of protrusions displayed by these aggregates. Analysis of these parameters using the Pearson correlation coefficient confirmed a significant negative correlation between these values, shown in Figure 34. This suggests that as G33 clusters become larger they concomitantly become less circular. The addition of VEGF in the medium had little impact on cluster size or shape. These results suggest that HUVECs promote G33 proliferation and/or survival, concurrently promoting a phenotypic change.

Endothelial cells are typically regarded to have an impact on the tumour microenvironment, via the formation of vessels that deliver nutrients and constitute "highways" for metastasis. Though these are important mechanisms for tumour growth there is a growing body of evidence that demonstrates endothelial cells actively signal to tumour cells, promoting a change in behaviour [287]. This paracrine signalling, though not well-studied in ovarian cancer, has been better evidenced in other cancers such as head and neck squamous carcinoma [288]. Endothelial derived chemokine (C-X-C motif) ligand 1 (CXCL1) and CXCL8 was shown to be an important mediator of tumour cell motility and invasion via activation of the CXC receptor 2 (CXCR2). Interestingly, the

addition of VEGF, and Bcl-2 over-expression, promotes downstream activation of NFκB, which increases CXCL1 and CXCL8 expression in endothelial cells [289]. However, we observe no difference in cancer cell number and morphology with the addition of VEGF, which may imply that there is a different axis responsible for the increased number and morphology change of G33 cells that we observe.

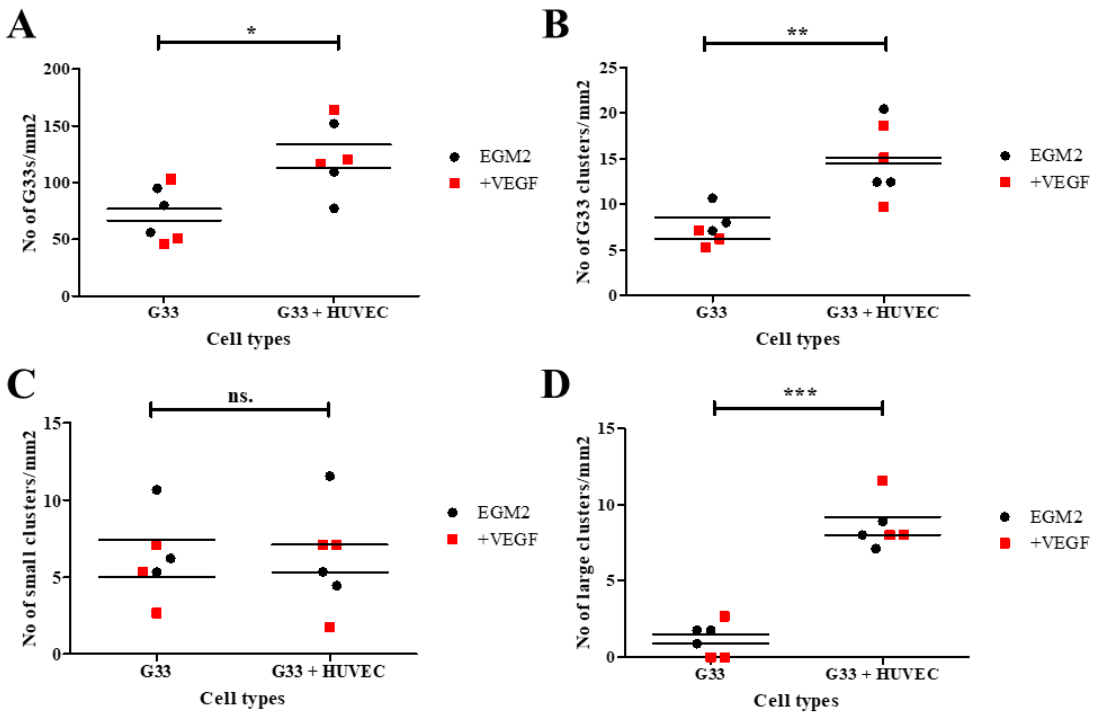

Figure 33. Impact of HUVECs on G33 cell number. A) HUVECs significantly promote the number of G33s/mm^2. **B)** In addition, HUVECs significantly increased the number of G33 cell clusters. **C)** However, HUVECs had no significant impact on the number of small G33 clusters, defined as 2-4 cell, with mean number of small cluster/mm^2 ranging from 5.0-7.4. **D)** But, HUVECs do promote the formation of large clusters (defined as 5-15+ cells) - increasing from 1.5 ± 0.3 and 0.9 ± 0.9 clusters/mm^2 for EGM-2 and VEGF-supplemented mono-cultures, to 8.0 ± 0.5 and 9.2 + 1.2 clusters/mm^2 for EGM-2 and VEGF-supplemented co-cultures. Statistics corresponds to N=3.

G33 clusters becoming more irregular may indicate they are undergoing EMT. This is in agreement with what is reported within the literature, as epithelial cells are regarded to have a ‘cobblestone’ appearance, becoming more elongated when transitioning to a

mesenchymal phenotype - as observed in MDCK cells - a commonly used epithelial cell line [290]. However, to further confirm that HUVECs are promoting this EMT phenotype, further characterisation will have to be carried out. Commonly associated hallmarks of EMT are loss in epithelial markers, such as E-cadherin, and gain in mesenchymal markers, such as vimentin [291, 292]. These are both widely used markers and would be suitable to further investigate the potential loss in epithelial function of G33s, when co-cultured with HUVECs [293, 294]. In addition, further *in vitro* experiments using HUVEC conditioned medium to culture 2D G33 cells, may allow the visualisation of HUVEC induced EMT via paracrine signalling. Furthermore, seeding HUVECs and G33s in the same channel will also allow studying of endothelial and HGSOC cell juxtacrine signalling.

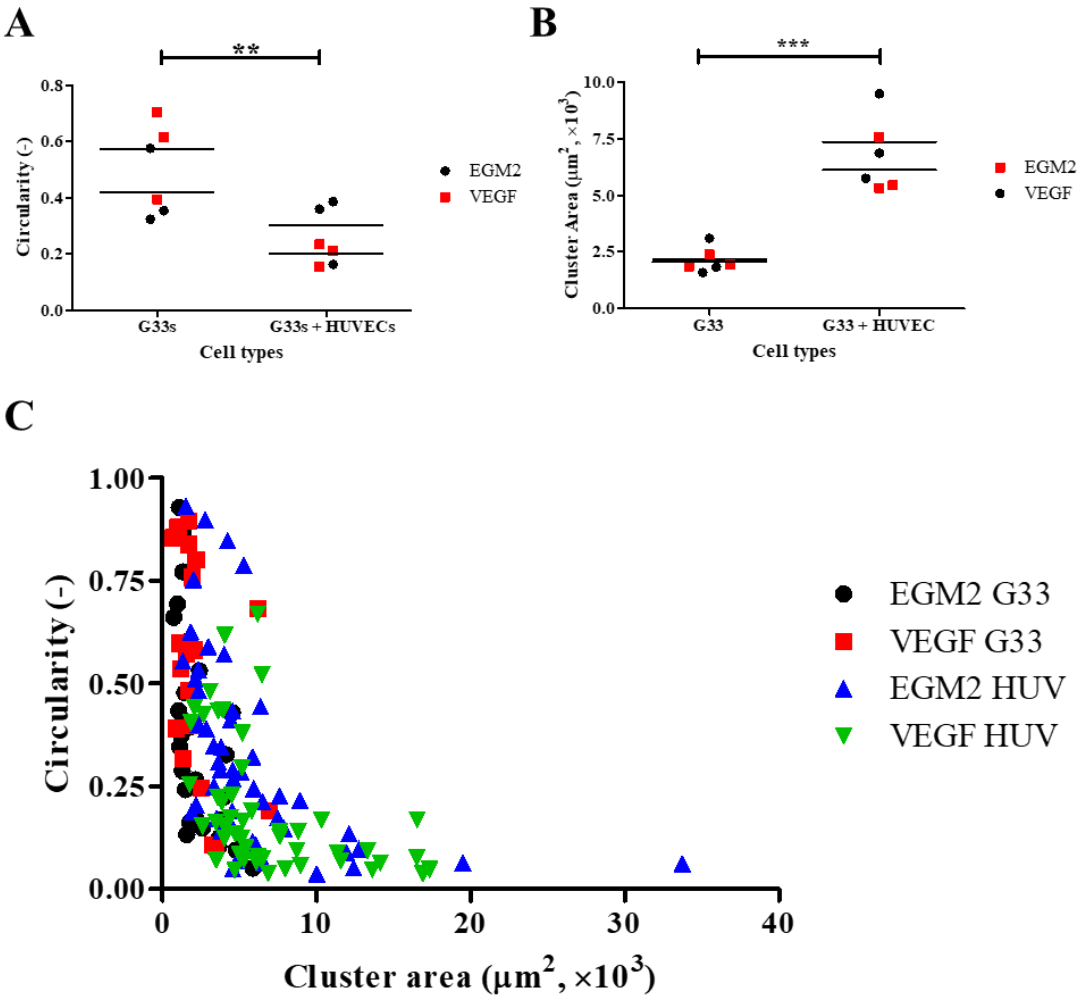

Figure 34. Impact of HUVECs on G33 circularity and perimeter. A) When co-cultured with HUVECs, G33 cell clusters become significantly less circular and more irregular in shape. **B)** Concurrently, they become much larger, occupying an area of 6.11 ± 0.7 $\times 10^3$ and 7.4 ± 1.1 $\times 10^3$ μm^2 when cultured with EGM-2 and VEGF, respectively, compared with 2.1 ± 0.2 $\times 10^3$ and 2.2 ± 0.5 $\times 10^3$ µm for mono-cultures supplemented with EGM-2 or VEGF, respectively. **C)** Furthermore, using the Pearson correlation coefficient to correlate cluster circularity with size reveals an *r* value of -0.51. Demonstrating that as G33 clusters become larger they concurrently become less circular. Statistics correspond to N=3.

10.6. Summary

This section studied the paracrine interactions between HUVECs and G33 HGSOC cells.

G33 cells were shown to promote HUVEC vessel formation following 4 days when

cultured with basal EGM-2, via paracrine signalling. However, when cultured for 10 days with VEGF supplemented EGM-2, no statistical differences were observed in vessel formation and diameter between HUVEC and G33 co-cultures and HUVEC mono-cultures. Interestingly, HUVECs were shown to significantly impact G33 cells through paracrine signalling. This has not previously been demonstrated using microfluidics and such interactions have not been evidenced in the context of ovarian cancer. But as shown, when co-cultured with HUVECs, G33 numbers are significantly increased through either increased proliferation or improved survival. In addition, G33 clusters are more irregular when co-cultured with HUVECs, which is suggestive of an EMT phenotype - though further experiments are required to confirm this observation. The next stage of this thesis will be focus on developing a novel spheroid-on-a-chip system that will allow the integration of a cancer spheroid within a vascularised spheroid gel, this will then undergo chemotherapy treatment to observe how HUVECs impact drug response.

11. Development of ovarian cancer spheroids on-a-chip

11.1. Introduction

HUVEC-G33 paracrine signalling was investigated using a four-channel PDMS device (see Figure 20). Though this better mimics the *in vivo* environment compared with culturing cells in 2D, this system still does not fully recapitulate cell-cell bonding experienced *in vivo* due to the dispersed nature of cell seeding [295]. Due to the limited size of G33 cell clusters, gradients of oxygen, nutrients and waste do not develop. These are important contributors to the formation of a hypoxia environment - known to be important regulator of HGSOC chemo-resistance [296-298]. Cancer spheroids, compared with dispersed culture, are recognised as being more physiologically relevant when recapitulating the tumour microenvironment [295, 299]. This is due to spheroids promoting extensive cell-cell interactions and cell-matrix interactions, which influences drug response [295]. In addition, tumour spheroids larger than 400-600 μm diameter, allow the development of oxygen, nutrient and waste gradients. This in turn promotes an architectural change in which the outer 100-300 μm cells are proliferative and viable, surrounding a necrotic, hypoxic core [300]. It is recognised that the hypoxic core of spheroids plays an important role in drug resistance, particularly therapies which target rapidly proliferating cells [295, 301].

Nashimoto *et al* developed a microfluidic device that allowed the embedding of a lung fibroblast spheroid within a fibrin gel [216]. Their system incorporated three parallel channels, a central gel/spheroid channel and two lateral medium channels. To seed their device, they first injected the central channel with a fibrin gel embedded with a NHLF

spheroid. Following this, HUVECs suspended in EGM-2 medium were added to the lateral side-compartments and the device tilted at 90 ° for 30 min to allow cells to adhere to fibrin gel. This allowed HUVECs, over a period up to 14-days, to invade through the fibrin gel towards the spheroid, allowing them to perfuse solutions, including labelled-dextran and microbeads, through the vasculature and into the spheroid. Interestingly, MCF7 breast cancer spheroids were tested but did not promote angiogenesis in this system. We designed a similar system, combining the advantages of spheroid and organ-on-a-chip culture. This system incorporates a cancer spheroid embedded within a fibrin gel seeded with HUVECs, and will use the vascular system designed in this thesis to deliver chemotherapeutic agents to the cancer spheroid.

11.2. Microfluidic device design

The microfluidic device design initially used to investigate interactions between HUVECs and a G33 spheroid is shown in Figure 35. This design, as stated, is inspired by Nashimoto *et al* [216], though with some key differences. Firstly, Nashimoto used a three-channel device, whereas this device incorporates five channels, including additional lateral vascular compartments (LC and RC). Secondly, our system embeds HUVECs within fibrin gels injected into the vascular channels (LC and RC), whereas Nashimoto seeds HUVECs on the outer-sides of the central channel. This design difference was partly due to our previous work focusing on developing a vasculogenic approach to cell seeding, whereas little work has focused on an angiogenic approach, which may require different conditions. In addition, this design allows the incorporation of different pre-metastatic niches within the same device, allowing the study of metastasis.

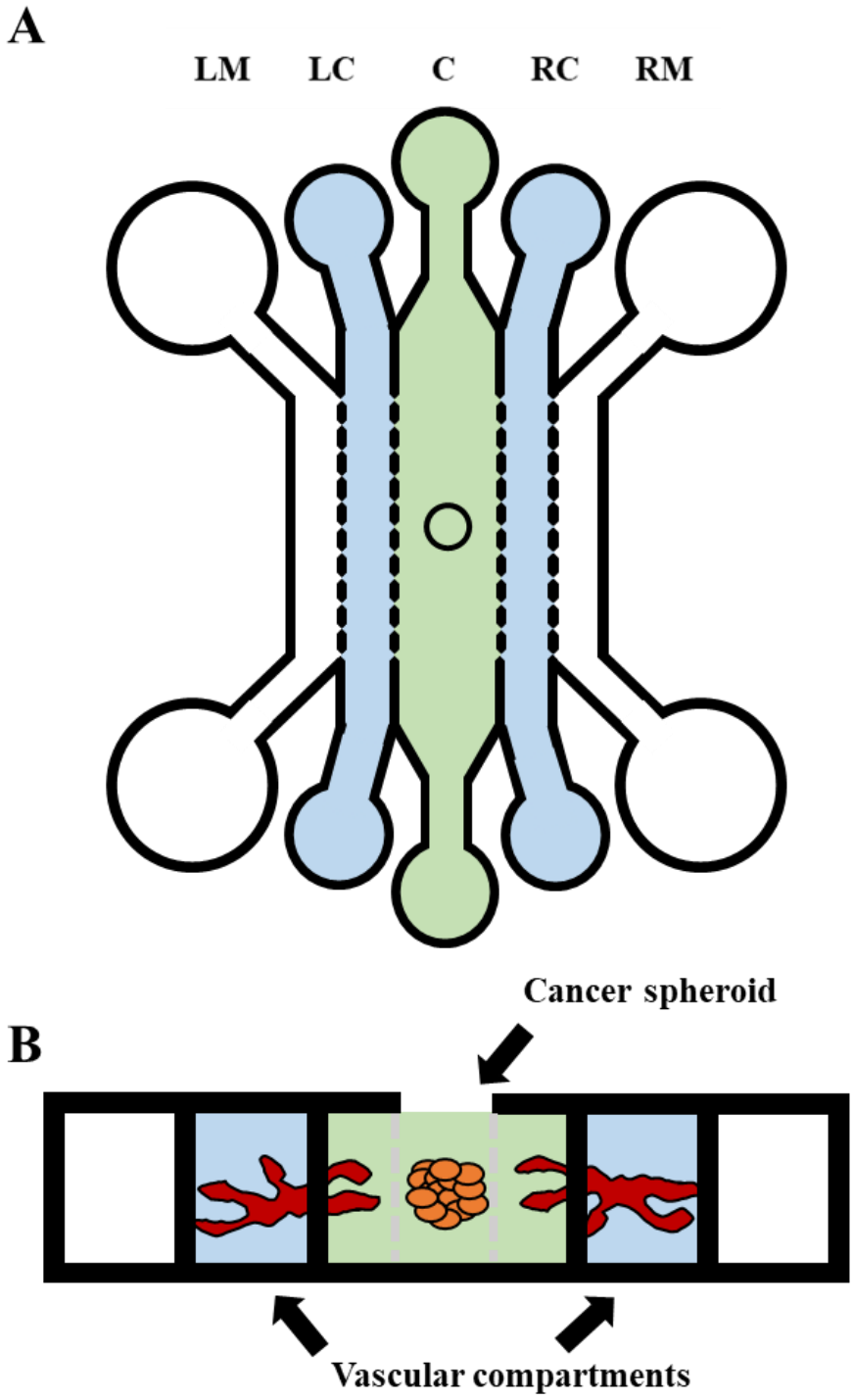

Figure 35. Design of five-channel spheroid chip. A) Schematic representation of the spheroid device. This system has two lateral medium channels (LM and RM), two lateral gel channels (LC and RC), and a central spheroid channel. Each channel is 75 µm in height, the LM, RM, LC and RC channels are 1000 µm in width and the central channel is 2000 µm in width. **B)** Depicts the cross-section of the device. Spheroids are injected into the central gel channel, through the central well, and HUVECs injected into lateral gel channels LC and RC - and allowed to undergo angiogenesis towards spheroid. Schematics are not to scale.

11.3. Methods for creating spheroids

A method for creating reproducible spheroids, to be seeded in microfluidic devices, was established. Many protocols exist for spheroid formation, these typically encourage cell-cell bonding, rather than cell-substrate bonding, which is commonly observed in 2D culture. Coating plasticware with non-adhesive compounds, such as poly-HEMA, inhibits cell adhesion to the underlying substrate and encourages spheroid formation [299, 302]. The hanging drop method is another commonly used spheroid formation technique [303]. As the name would suggest, cells are seeded from a hanging drop, typically on the underside of the lid of cell culture plasticware. As there is no underlying substrate, when using the hanging drop method, cell-cell adhesion is encouraged.

Different techniques for forming spheroids were investigated. U-bottomed 96 well plates were coated with poly-HEMA (2% w/v solution, 95% ethanol solvent) for 10 min, before the solution was aspirated, and plates dried at RT for 1 h, before washing with DPBS. 5×10^3 and 2×10^4 G33 cells were seeded in poly-HEMA coated U-bottomed 96 well plates and cultured for 48 h before imaging. Poly-HEMA coating damages the surface of the substrate, making visualisation and imaging challenging (see Figure 36). In addition, poly-HEMA coating appears to promote the formation of multiple small clusters, but not a single large spheroid. The hanging drop method of spheroid formation was also evaluated. We seeded 5×10^3 and 1×10^4 G33s in 20 µl and 40 µl droplets, respectively. This technique allowed the establishment of loosely formed spheroids, with clear gaps between cells - particularly in 5×10^3 G33 spheroids (see Figure 36). In addition, replacing medium in this technique is challenging due to interference with the nascent spheroids. Due to the difficulties with the poly-HEMA and hanging drop methods, 96-well clear ultra-low attachment well plates were used to form spheroids. As shown in Figure 36, these plates allowed the establishment of well-formed 5×10^3 and 2×10^4 G33

spheroids. These spheroids were stable and able to be handled using a pipette, which is essential when embedding in a fibrinogen gel. This technique is further described in the Materials and Methods section of this thesis (p. 56).

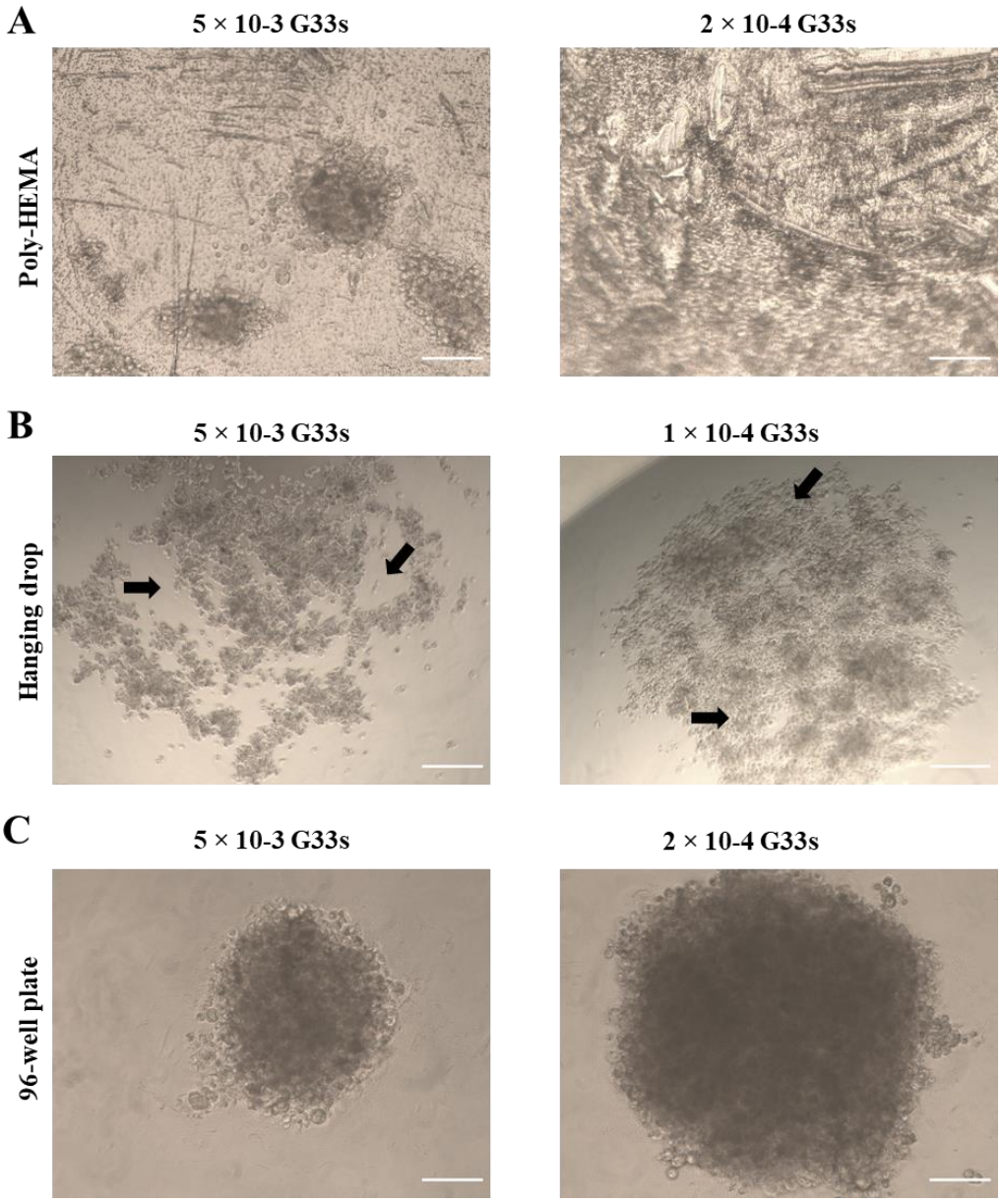

Figure 36. Establishing spheroid seeding method. A) Spheroids grown in poly-HEMA coated wells do not establish well structure vessels. In addition, the poly-HEMA solution damages the surface of the well, making visualisation and imaging difficult. **B)** The hanging drop method does not form well-structured spheroids, with gaps observed in the structure (arrows). **C)** Culturing G33 cells in 96-well clear ultra-low attachment well plates allow the formation of stable spheroids. Scale bar: 100 µm.

Nashimoto *et al* describes forming vascularised spheroids using a combination of lung fibroblasts and HUVECs, allowing the vascular network to perfuse through the spheroid [216]. We replicated this in G33 spheroids, using a 4:1 ratio of G33-to-HUVECs, thus 2 × 10^4 G33s and 5 × 10^3 HUVECs were seeded per well in the aforementioned 96-well plates, these spheroids are referred to as micro-tumours (MCT). Following 72 h culture in EGM-2, MCTs were removed and embedded within fibrinogen gels and injected into PDMS devices and cultured for a further 10 days (see Figure 37). These MCTs form clear spheroid structures, with a visible vasculature around the periphery. In addition, G33 cells adhere to the underlying glass substrate and migrate from the bulk spheroid. Interestingly, G33s appear to migrate along a boundary with a clear outer ring of cells, suggesting they are degrading the fibrinogen gel - though this needs to be confirmed.

As seen in Figure 37, an issue with diffusion gradients of staining reagents is observed, as particular stains (phalloidin) show a clear ring structure as the stain has failed to diffuse into the centre of the MCT, however another stain (DAPI) has clearly diffused and stained throughout the spheroid. This problem is likely the result of high cell density and staining agents unable to diffuse to the centre of the MCT. Increasing the exposure time of permeabilization and staining reagents may resolve this issue. In addition, developing a method to remove the MCT from the chip will allow researchers to perform immunohistochemistry on the sample, which will provide further structural analysis on the MCT interior. Nashimoto *et al* spin coats a 100 µm thick PDMS layer onto a glass substrate, before curing, and bonding to the micropatterned PDMS stamp using oxygen plasma treatment - this allows spheroid retrieval from the device using a biopsy punch [216].

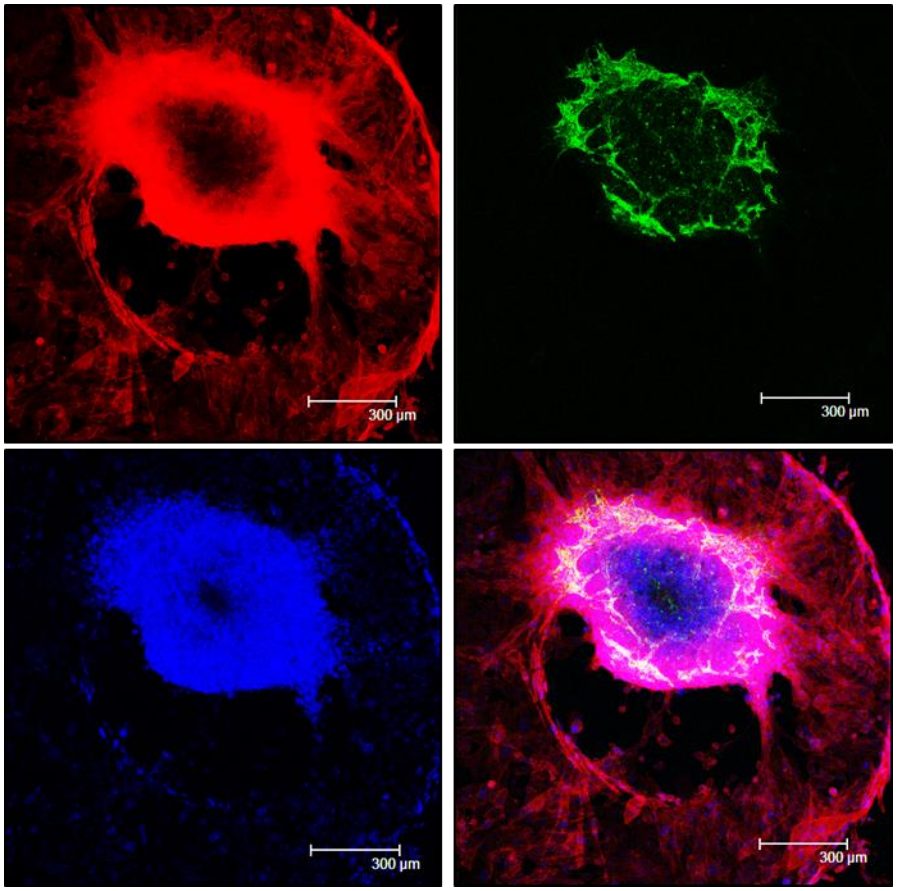

Figure 37. Culturing micro-tumour spheroids. G33s and HUVECs were cultured in 96 well-plates for 72 h, before embedding within fibrinogen gel and cultured for a further 10 days in a microfluidic device. As shown, these MCTs form clear spheroid structures with vasculature around the periphery. Red, Phalloidin. Green, CD31. Blue, Dapi. Scale bar: 300 µm.

11.4. Spheroid angiogenesis in five-channel devices

A method for injecting MCTs into devices five-channel spheroid devices was developed, following the establishment of the MCT formation protocol. Firstly, the vascular compartments (LC and RC) were injected with a 10 mg/mL fibrin gel embedded with 6 × 10^6 HUVECs/mL before gel curing, VEGF-supplemented medium was then added to the lateral medium channels (LM and RM) and the device incubated for 1 hr at 37 °C. An MCT spheroid was then embedded within a fibrin gel and injected into the central channel

(C), forming an interface with the parallel vascular compartments. The end-point of these experiments was day 10.

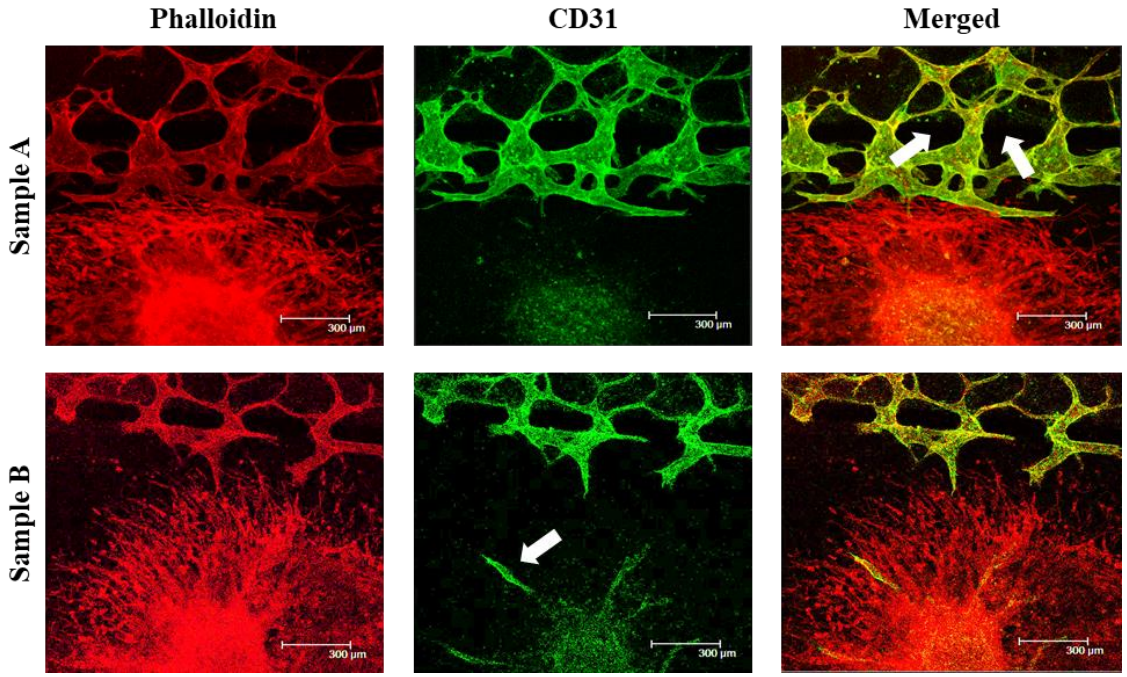

Figure 38. HUVEC angiogenesis in five-channel spheroid device. Two separate repeats, with the same conditions are presented (samples A and B), with HUVECs co-cultured with MCT spheroids. In sample A, the vasculature has invaded into the central gel channel; arrows indicate post location. In sample B, the CD31 staining indicates the sprouting and migration of endothelial cells to the MCT spheroid (see arrow). Red, phalloidin. Green, CD31. Scale bar: 300 µm.

This method for developing vascularised spheroids had mixed success. As shown in Figure 38, HUVECs initially underwent vasculogenesis within their respective compartments, followed by angiogenesis towards the MCT spheroid (as evidenced by the crossing of the post delimitation of the channel within which endothelial cells were initially seeded). Concurrently, the HUVECs within the MCT formed vessels which projected outwards. However, in the multiple repeats of this experiment HUVEC vessels were not found to perfuse through the MCT spheroid, failing to connect the vasculatures

in the LC and RC channels. Without this perfused system drugs would be unable to be delivered to the MCT through the vasculature.

The system used in this thesis cultures cells for a total of 10 days in the microfluidic device, compared with 14 days culture reported by Nashimoto *et al* [216]. If these experiments were extended to > 14 days, further vessel formation may be observed, however extensive vessel hyperplasia may then become an issue. This could be resolved with co-culturing HUVECs with pericytes, as reported in Figure 24 of this thesis. However, HUVEC angiogenesis into the central channel, as well as being inadequate, was also unreliable with some repeats showing little signs of angiogenesis. Thus, extending culturing time may not be suitable. In addition, MCF7 cells were shown not to promote HUVEC angiogenesis into the central compartment by Nashimoto - though the reason behind this was not further elucidated [216]. Highlighting, that perhaps not all cell types are suitable to promote sufficient angiogenesis to allow MCT vascularisation. Perhaps other ovarian cancer cell types would be more suitable, but this then questions the relevance of this model to a broad range of tumours and its patient specificity. An alternative chip design and seeding strategy was then established which uses a simpler three-channel spheroid chip and embeds the MCT spheroid directly together with HUVECs.

11.5. Spheroid three-channel device design

Due to the difficulties in culturing reproducible, vascularised MCTs using the five-channel chips, we developed a three-channel spheroid device (see Figure 39). This device incorporates 3 parallel channels: a central gel channel, and two lateral medium channels, separated by hexagonal posts. This device allows HUVEC vascularisation within the

same channel as the MCT, encouraging spheroid perfusion and drug delivery. However, unlike the five-channel device, this design will not allow the study of different pre-metastatic niches and will not allow quantification of angiogenesis directionality, as described by Nashimoto [216].

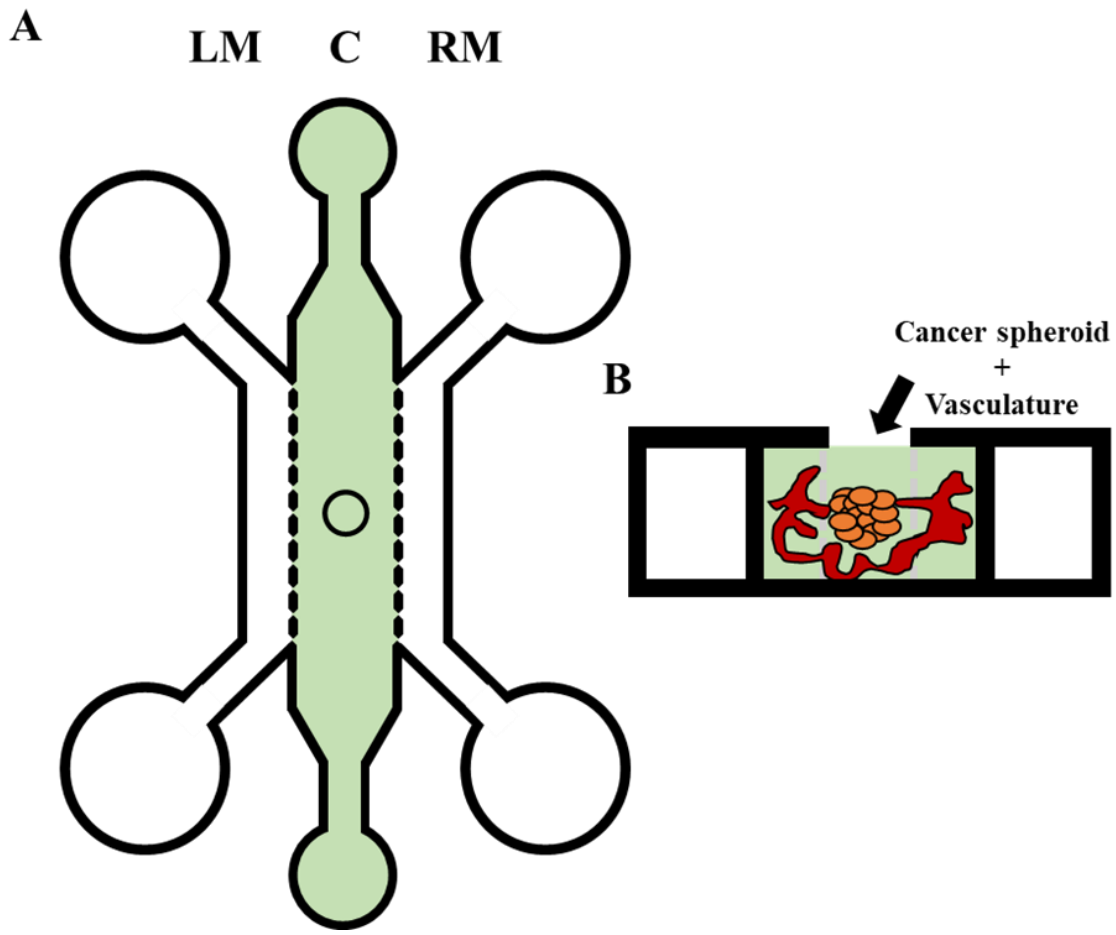

Figure 39. Design of three-channel spheroid chips. This device was designed to allow the seeding of HUVECs and MCTs in the same central chamber. **A)** Two lateral medium channels, LM and RM, delimitate a central gel channel (C, 2000 µm width, 75 µm in height), with posts (300 µm in length with 75 µm gaps) enabling the retention of fibrin gels in C. **B)** Cross section of device. HUVECs and spheroids embedded in the same fibrin gel. Schematics are not to scale.

11.6. Spheroid vasculogenesis in three-channel device

The five-channel device was unsuitable for drug delivery studies, as the MCT remained non-vascularised following 10-days culture. To address this, HUVECs were directly

embedded within the fibrin gel alongside the MCT. HUVECs were expected to vascularise around and through the spheroid, allowing drug delivery through the vascular network. A similar system has since been adopted by Kamm *et al*, who seed neural spheroids alongside endothelial cells in a 3D gel [304].

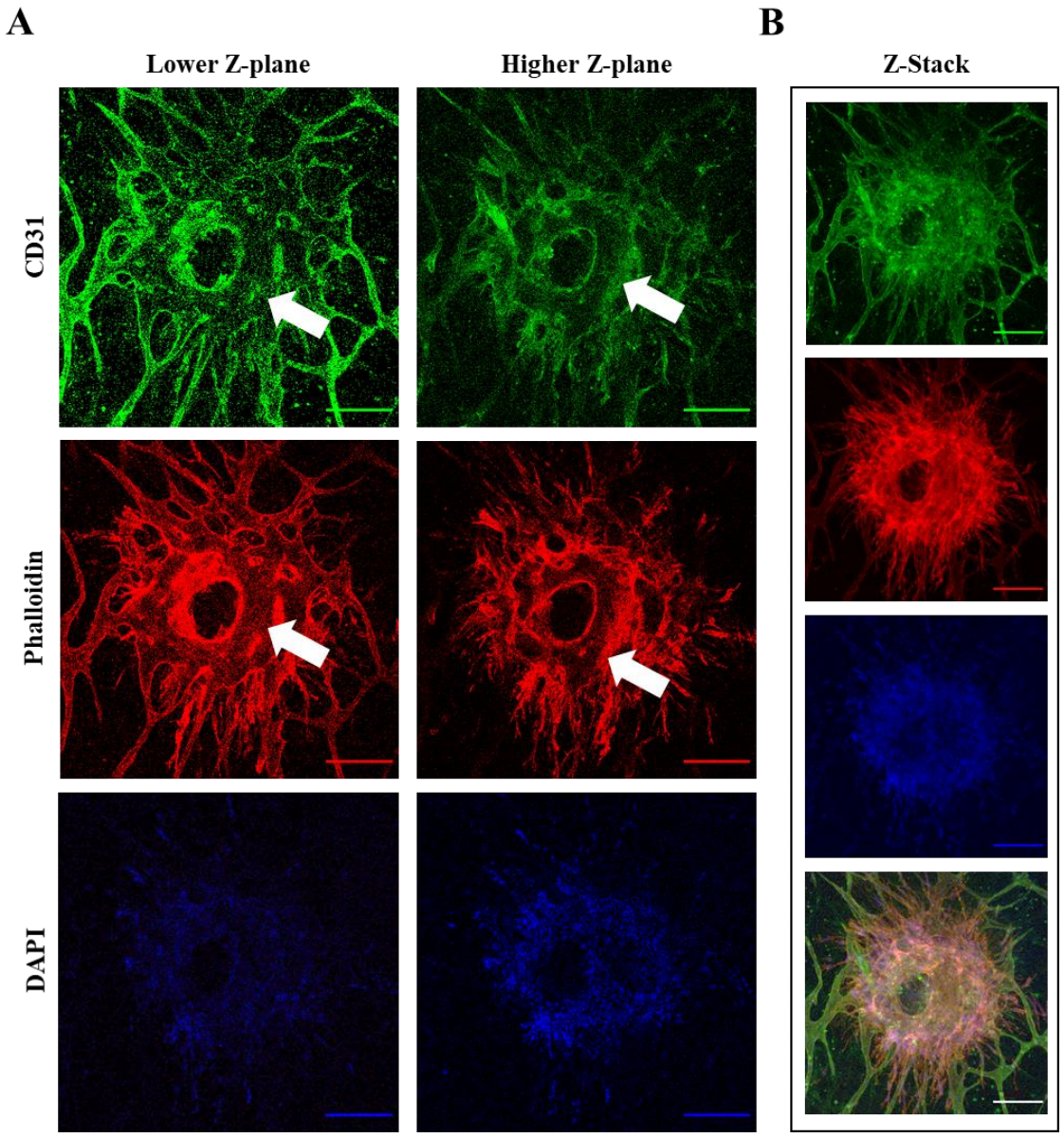

Figure 40. Spheroid vasculogenesis. An MCT spheroid can be observed, completely surrounded by microvasculature, with vessels being shown to permeate through the spheroid. **A)** Shows two separate Z-planes of the same MCT spheroid. Arrows in both the lower and higher plane highlights the CD31 stained vasculature infiltrating through the spheroid. **B)** Shows the complete vascularised MCT Z-stack. Red, phalloidin. Blue, DAPI. Green, CD31. Scale bar: 300 µm.

A method was next established for co-injecting MCT spheroids and HUVECs into three-channel devices. The technique for creating the MCT was identical to what has previously been reported in this thesis, with 8×10^6 HUVECs/mL seeded alongside the MCT. 8×10^6 HUVECs/mL was used in this experiment instead of 6×10^6 HUVECs/mL due to difficulties in isolating the MCTs. HUVECs were first re-suspended in a thrombin solution, before MCTs were isolated and mixed with 10 µL of the HUVEC-thrombin solution. Due to additional solution being added to the HUVEC-thrombin solution, the density of HUVECs was diluted and less vessel formation was observed (data not shown). To compensate for this, we used an initial higher concentration of HUVECs. Following re-suspension of the MCT in the HUVEC-thrombin solution, we mixed with fibrinogen and injected into the well of the central channel. Gels are then cured in a 37 °C incubator for 5 min before VEGF-supplemented EGM-2 was added to the lateral medium channels. Cultures were maintained for 10 days.

HUVECs undergo extensive vasculogenesis when cultured in the same channel as the MCT, see Figure 40. Analysis of the individual Z-planes of the confocal image revealed that the vasculature infiltrates throughout the MCT - suggesting this system may be suitable to introduce drugs into the MCT via the vasculature. In addition, vascularised MCTs appear to form hollow structures, with cells appearing to migrate away from the spheroid centre.

11.7. Functional perfusion of the vasculature through micro-tumours

Vessel perfusion was investigated following the establishment of the MCT injection method. This would establish whether the MCTs are vascularised and will allow the delivery of drugs and/or cells through the vasculature to the cancer spheroid. This was

investigated using a method further described in the Materials and Methods section (p. 60). Briefly, 70 kDa FITC-dextran is perfused through the vasculature, followed by qualitative analysis of intra- to extravascular leakage between T=0 and T=30 min.

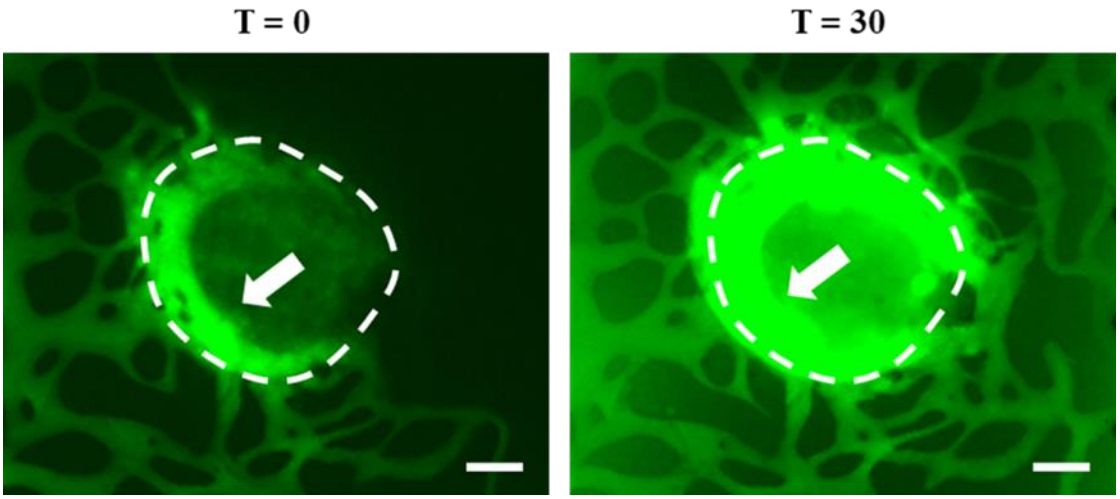

Figure 41. FITC-dextran perfusion through spheroids. 70kDa FITC-dextran was added to one of the medium channels of the device and allowed to perfuse through the network. The spheroid is outlined with a white dashed line, which was plotted according to initial background given by spheroid. White arrows indicate internal lumenised vessels embedded within the spheroid. The device was imaged for 30 min. Green, 70 kDa FITC-dextran. Scale bar: 100 µm.

Using FITC-dextran, we were able to visualise the perfusion of the vasculature through the MCT, similarly to what has previously been reported [216]. Interestingly, the spheroid appears not vascularised in the centre, rather it contains large lumenised structures at its periphery (see white arrows), this is similar to what is reported by Nashimoto *et al*. However, they also reported the formation of small lumenised vessels in the centre of the spheroid, which was not observed within this sample. However, similar structures are observed later in Figure 43, suggesting some issues with reproducibility. In addition, though FITC-dextran can be observed diffusing through the same X and Y plane as the spheroid, it does not ensure, in this experiment, that FITC-dextran is diffusing through the actual spheroid. As the spheroid may be found in a higher Z-plane than the underlying

vasculature. However, Figure 40 demonstrates that these spheroids can be vascularised throughout, implying we are observing FITC-dextran perfusion through the spheroid. Furthermore, the increased intensity of FITC-dextran within the spheroid at T=30 may be a result of vessel leakage within the spheroid, leading to dextran accumulation. These spheroids also have multiple layers of vasculature, as shown by Figure 40, this increased intensity could be dye perfusion in other Z-planes. Following the conclusion that these spheroid-on-a-chip models are perfusable, the next aim was to investigate the impact of the vasculature on drug delivery.

11.8. G33 response to carboplatin

Carboplatin is a second-generation platinum therapy and derivative of cisplatin which is commonly used in conjunction with paclitaxel as a first-line therapy in ovarian cancer [71]. The mechanism behind carboplatin's action is discussed further in the introduction (p. 23). Briefly, carboplatin acts by forming mono- and di-adducts with DNA, inhibiting cell replication and transcription, and inducing apoptosis [305]. Due to carboplatin's ubiquity as a chemotherapeutic in epithelial ovarian cancer therapy, we selected it to further investigate this system.

Prior to treating vascularised MCTs, we investigated carboplatin's IC50 with G33 cells cultured in 2D, 3D, and 3D spheroids. This was to ensure an appropriate carboplatin treatment was investigated. Rather than determining carboplatin's IC50 through directly measuring cell death, its impact on cell metabolism was instead measured using the CCK-8 assay (more information is provided in the Materials and Methods section, p. 58), which is a colorimetric assay commonly used to evaluate cell viabilities [306, 307]. To ensure these results are comparable with vascularised MCTs, 2×10^4 G33s per condition were

examined. Accordingly, 2×10^4 G33s per well (6 well plate) used to investigate 2D, 2×10^4 G33s per 40 µL fibrin gel to investigate 3D culture, and 2×10^4 G33 spheroids in 40 µL fibrin gel to investigate 3D spheroids. Samples were cultured for 24 h in EGM-2 supplemented with 50 ng/mL VEGF, before treatment with carboplatin with cell viability evaluated 24, 48 and 72 h post carboplatin treatment. Concentrations between 0-5000 µM were investigated according to data previously obtained by Dr Owen Heath (not currently published).

Carboplatin treatment consistently promoted a loss in cell viability, with the mean IC50 for each time-point and condition indicated in Figure 42. Our recorded IC50 values following 72 h culture were in range of the IC50 values of 32 commonly used ovarian cancer cell lines reported by Bicaku - between 27 - 247 µM [308]. Interestingly, across all time-points G33s cultured in 2D have a higher IC50 than cells cultured in 3D. This is unexpected as 3D culture is typically considered to promote a chemo-resistant phenotype and genotype in ovarian cancer [301, 309, 310]. Hypoxia plays an important role in chemo-resistance in ovarian cancer, and resistance to cisplatin and it's derivatives [295, 301, 311-313]. An interesting study by Selvendiran *et al* details how hypoxia significantly increases phosphorylation and activation of STAT3 in A2780 ovarian cancer cells. They went on to show that taxol and cisplatin are significantly less effective at eradicating A2780 cells in hypoxic conditions, however, this is reversed following the inhibition of STAT3 [313]. As stated in the introduction of this section, spheroids with diameters greater than 400-600 µm allow the development of a hypoxic core due to diffusion gradients [300]. The mean Feret diameter and minimum Feret diameter of spheroids examined in Figure 42 at day 0 was 529.0 and 424.8 µm, respectively (N=1, quadruplicate). These samples were therefore large enough to feature a hypoxic core (though this was not confirmed), as such, it was expected that carboplatin's IC50 would

be higher in 3D cultures compared with 2D. In addition, altered cell-cell and cell-matrix interactions in spheroid cultures compared with 2D culture has also been suggested to play a role in differing drug response, through changes in protein and RNA expression [295].

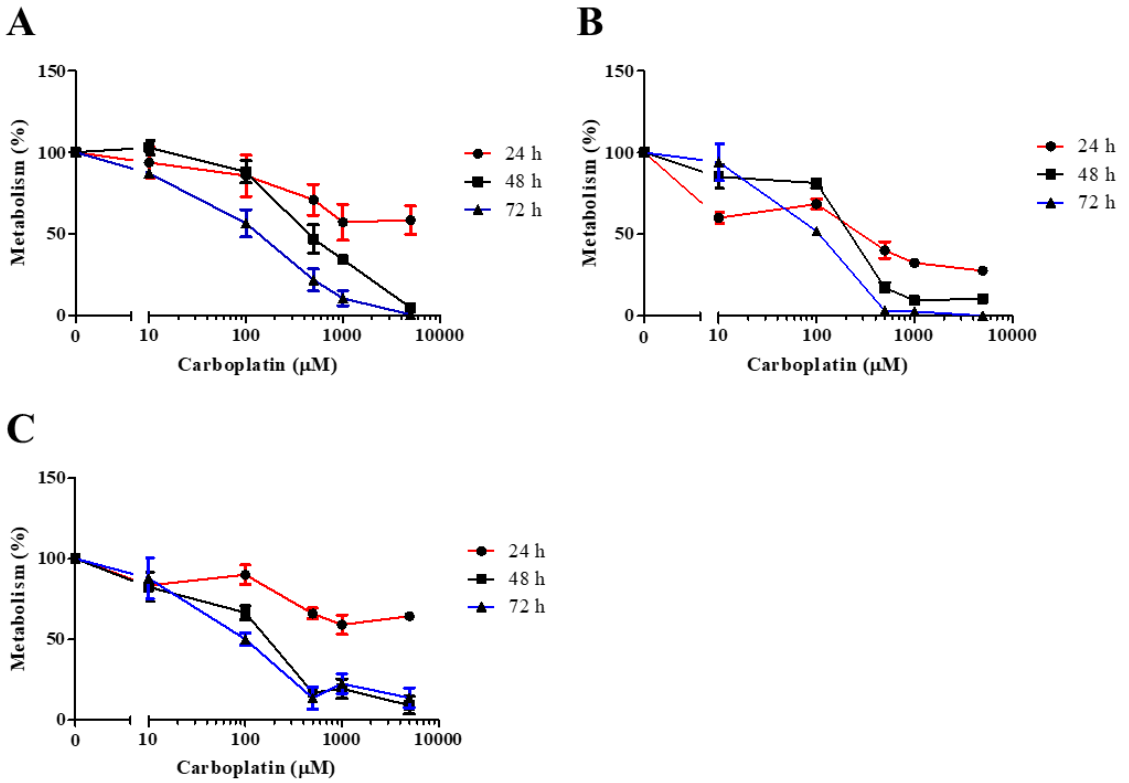

D

Carboplatin therapy, mean IC50 values (µM)			
Conditions	***Time-point (h)***		
	24	**48**	**72**
2D	228	525	141
3D	189	217	101
Spheroid	198	151	67

Figure 42. Impact of carboplatin treatment on G33 viability. Six different concentrations of carboplatin were investigated (0, 10, 100, 500, 1000 and 5000 µM) on 2×10^4 G33s in 2D **(A)**, dispersed in fibrin gel **(B)** and spheroid in fibrin gel **(C)**. **D)** Mean IC50 values (µM). CP = carboplatin. Statistics correspond >N3.

The CCK-8 assay uses WST-8 [2-(2-methoxy-4-nitrophenyl)-3-(4-nitrophenyl)-5-(2,4-disulfophenyl)-2H-tetrazolium, monosodium salt] which is reduced by cellular dehydrogenases to produce WST-8 formazan, an orange dye, to indicate cell metabolism and viability. When culturing G33s in 2D, the supernatant is easily collected and analysed, however, when culturing cells in fibrin, the WST-8 formazan dye stains the fibrin gel. This loss in WST-8 formazan may artificially reduce the recorded metabolic activity levels of cells cultured in fibrin. Indeed, when comparing the raw data, a 10-fold difference in the mean absorbance value, of WST-8 formazan, is observed when comparing G33 cells cultured in 2D vs spheroids (0.72 and 0.07, respectively), at day 1 in EGM-2. These experiments were not conducted in parallel, thus, statistical analysis is unsuitable. However, a clear reduction in WST-8 formazan is observed when culturing G33s in spheroids. This could be related to the observed staining of the fibrin gel, or reduction in G33 metabolism. WST-8 formazan production is dependent upon the activity of cellular dehydrogenases. As discussed, cells cultured within a spheroid have a spatial relationship with activity [300]. Thus, quiescent cells within the hypoxic region of the spheroid may, though not dead, not be active, and therefore not recorded by the CCK-8 assay. Further experiments would need to be conducted to confirm this with LIVE/DEAD^{TM} imaging or flow cytometry.

11.9. Vascularised micro-tumour response to carboplatin

Following the development of the spheroids-on-a-chip, and the experiments to study G33 response to carboplatin, the next stage was to combine these and assess the response of vascularised MCTs to carboplatin.

As shown in Figure 42, a concentration of approximately 150 µM carboplatin is required to elicit an IC50 response in G33 spheroids after 48 h. This concentration was used to treat vascularised MCTs after 8-days culture for 48 h (endpoint day 10). Vascularised MCTs were generated using the protocol described in section 11.6. In addition, the response of non-vascularised MCTs on-a-chip to carboplatin was also examined.

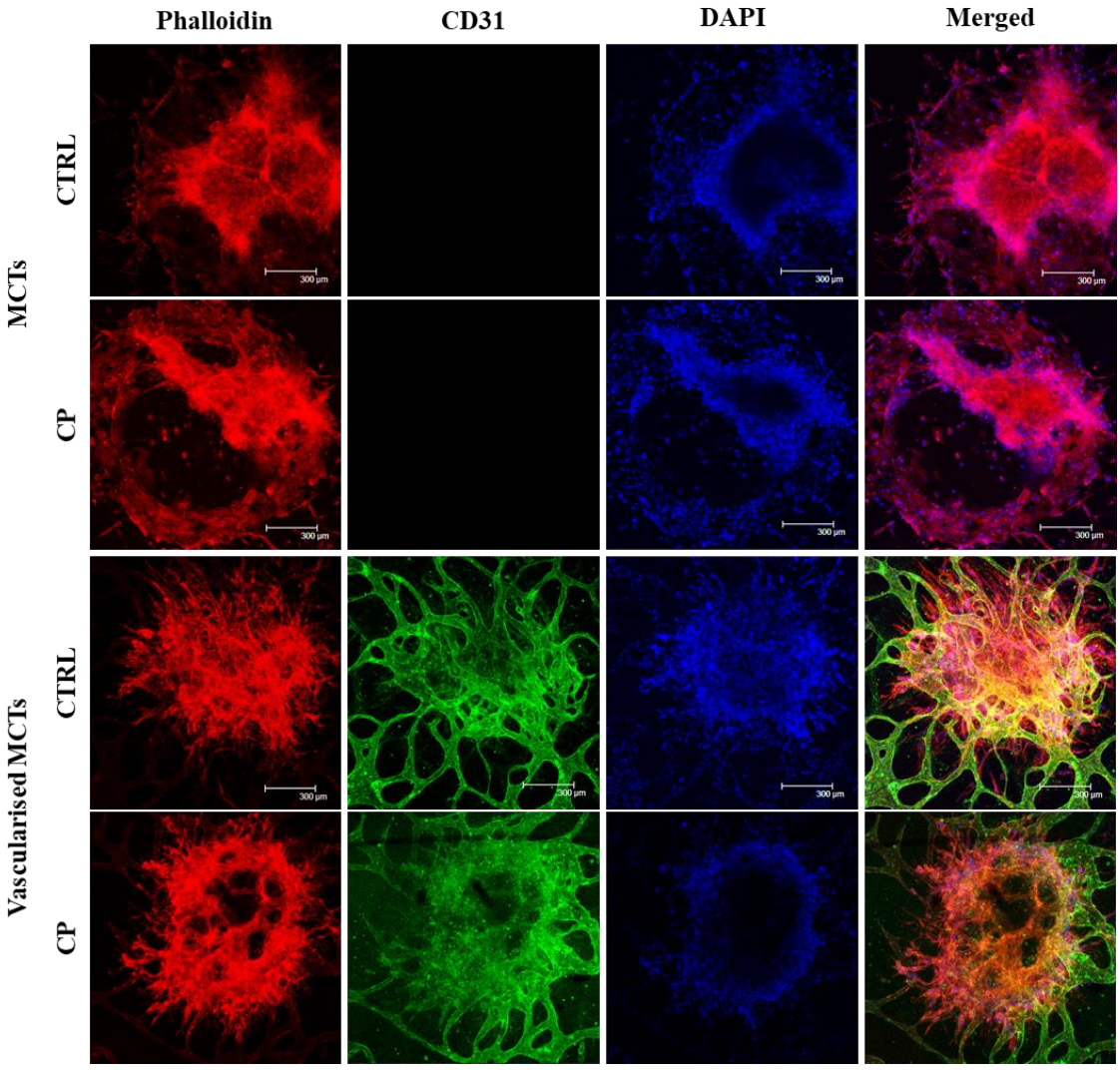

Figure 43. Response of micro-tumours to 150 µM carboplatin. The response of non-vascularised and vascularised MCTs to 150 µM carboplatin was examined. Carboplatin treatment was for the final 48 h. Total culture time 10 days. Representative images. Red, phalloidin. Green, CD31. Blue, DAPI. Scale bar: 300 µm. CP = carboplatin. Images represent N=1.

These preliminary experiments suggest that culturing MCT spheroids alongside HUVECs promotes a clear phenotypic change, when compared with MCT cultured separately. As shown in Figure 43, vascularised MCTs form a large spheroid body (area=0.95 mm^2), with many protrusions (circularity=0.039) (results represent N=1). Whereas, non-vascularised MCTs cover a smaller area (0.63 mm^2) and are also more circular (0.12). In addition, non-vascularised MCTs feature many G33 cells which have adhered to the underlying glass substrate and migrated from the main body. These 2D cells could be indicative that the MCT has significantly degraded the surrounding fibrin gel - perhaps suggesting that HUVECs are stabilising the fibrin ECM. Treating samples with 150 µM carboplatin had little impact on these parameters. Furthermore, non-vascularised MCTs display cell shrinking when cultured with 150 µM carboplatin, which is not observed in vascularised MCTs - these are recognised hallmarks of apoptosis [314]. This could suggest a protective effect from chemotherapy by HUVECs, perhaps as a result of the increased total cell mass involved in the vascularised models. In addition, 150 µM carboplatin treatment did not seem to have a significant impact on vascular coverage compared with VEGF control, with total tube lengths of 14.5 and 16.5 mm (N=1), respectively.

To more conclusively observe the response of MCTs to chemotherapy, the carboplatin concentration was increased from 150 to 300 µM. Similar to what is observed in Figure 43, vascularised MCTs form large bodies with many protrusions, whereas, non-vascularised MCTs form smaller bodies, with G33s adhering to the underlying glass substrate (Figure 44). Carboplatin treatment promoted significant vessel regression, leading to a loss in total tube length in vascularised MCTs, 12.3 ± 1.0 and 17.7 ± 1.3 mm, respectively. In addition, culturing MCTs alongside HUVECs appears to promote the formation of larger MCTs, with more protrusions. Indeed, analysis of area coverage

revealed vascularised MCTs formed significantly larger spheroids when compared with non-vascularised MCTs (0.85 ± 0.11 and 0.33 ± 0.05 mm^2, respectively) (see Figure 45). However, carboplatin had no significant impact on MCT area coverage. Furthermore, HUVECs promoted a phenotypic change in MCTs; as analysis of the MCT shape revealed vascularised MCTs to be significantly less circular than non-vascularised MCTs, 0.06 ± 0.01 and 0.22 ± 0.01, respectively. Carboplatin treatment also promoted a less circular phenotype in non-vascularised MCTs compared with control treated (0.16 ± 0.02).

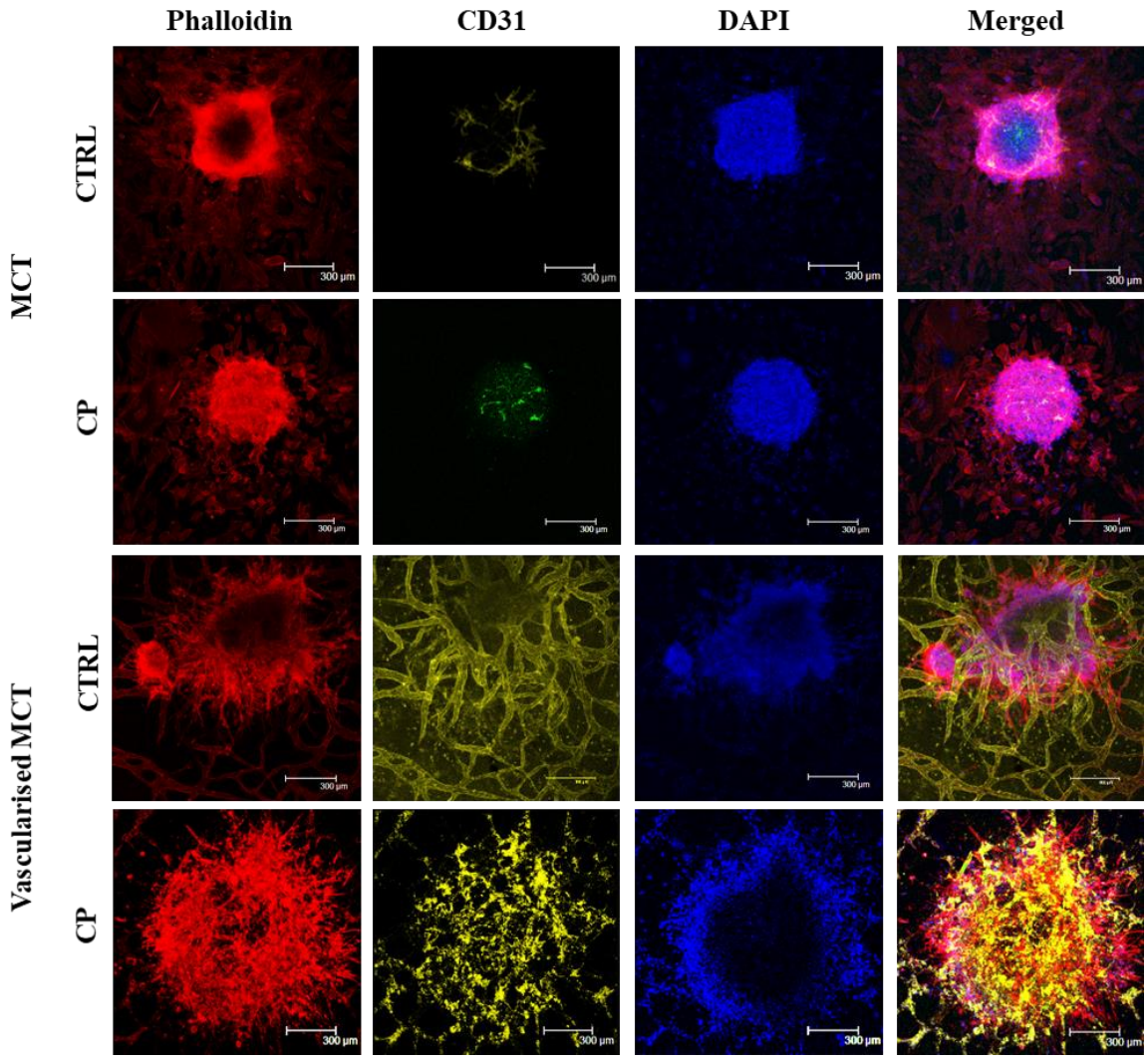

Figure 44. Images of MCTs response to 300 µM carboplatin. The response of non-vascularised and vascularised MCTs to 300 µM carboplatin was examined. Carboplatin treatment was for the final 48 h. Total culture time 10 days. Representative images. Red, phalloidin. Yellow and green, CD31. Blue, DAPI. Scale bar: 300 µm. CP = carboplatin. Images represent N=3.

Carboplatin treatment of non-vascularised MCTs promoted extensive G33 cell shrinkage (see Figure 46). The reduced circularity observed in non-vascularised MCTs following carboplatin treatment may be a result of this increased cell shrinkage and breakdown of the MCT. Extensive cellular shrinkage is not observed when MCTs are cultured alongside HUVECs. In addition, non-vascularised and vascularised MCTs display clear Ki67 staining, indicating cells are viable and continuing to proliferate following 10-days culture (Figure 46). However, following carboplatin treatment, this is completely ablated in non-vascularised MCTs and reduced in vascularised MCTs. These preliminary findings suggest that HUVECs are chemo-protective when cultured with G33 cells. However, further experiments need to confirm these observations.

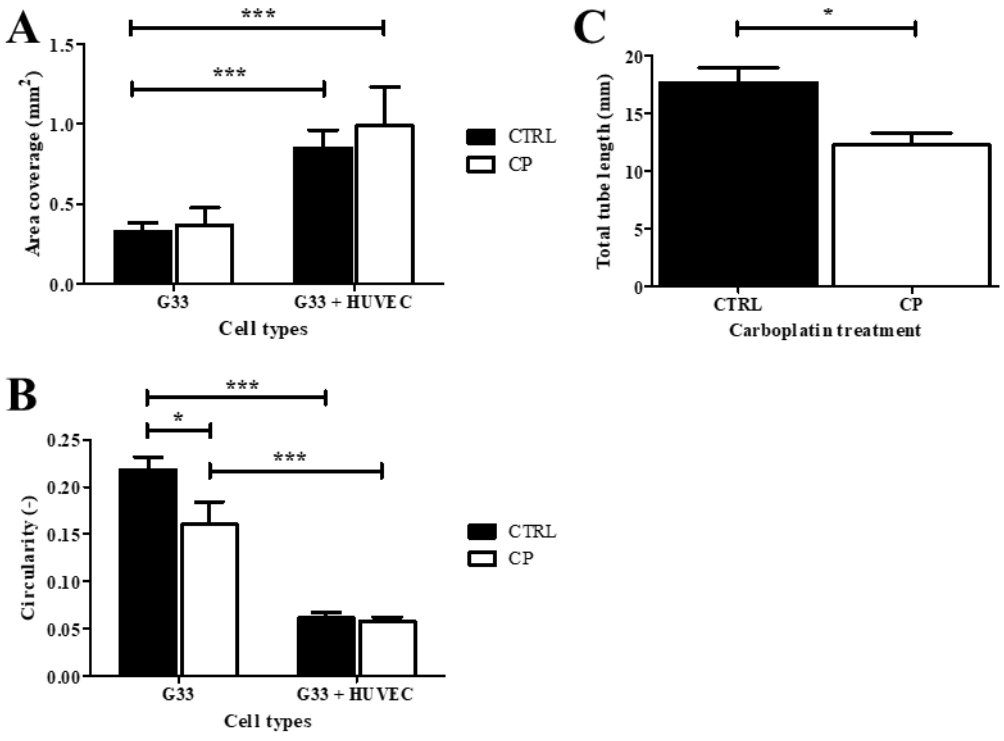

Figure 45. Micro-tumours response to 300 µM carboplatin. The response of non-vascularised and vascularised MCTs to 300 µM carboplatin. Carboplatin treatment was for the final 48 h. Total culture time 10 days. **A)** HUVECs significantly promoted the area coverage of MCTs, carboplatin had no impact. **B)** Vascularised MCTs were significantly less circular compared with non-vascularised, also carboplatin treatment reduced non-vascularised MCT circularity. **C)** Carboplatin treatment significantly reduced total tube length. Statistics correspond to N=3.

Vascularised MCTs enable paracrine and juxtacrine signalling between HUVECs and G33 HGSOC cells. Similar to what we report in Figure 33, culturing MCTs alongside HUVECs promotes the formation of larger spheroids, suggesting HUVECs are promoting G33 proliferation. This is comparable to what is reported by Hoarau-Véchot *et al*, who demonstrated that when ovarian cancer cells are directly co-cultured with endothelial cells they observe significantly enhanced proliferation [61]. This was further confirmed *in vivo*, with endothelial cells significantly increasing HGSOC tumour size. In addition, HGSOC cells were more chemo-resistant, to cisplatin and taxol treatment, when co-cultured with endothelials cells, compared with HGSOC mono-cultures. These responses were related to Jagged1-Notch3 interactions between endothelial-HGSOC cells, respectively. This axis led to the downstream activation of various signalling pathways, including the PI3K/Akt/mTOR signalling cascade, which is linked with proliferation and chemo-resistance [315]. Indeed, transfecting ovarian surface epithelium cells to over-express the Notch3 intracellular domain promoted carboplatin resistance, and knock-down of Notch3 in OVCAR3 cells increases sensitivity to carboplatin [316]. Notch3 signalling is mutated in 11% of all HGSOCs, with over-expression linked with poor prognosis [9, 316, 317]. This is in agreement with what is reported in this thesis; that when cultured alongside HUVECs, MCTs appear more chemo-resistant following treatment.

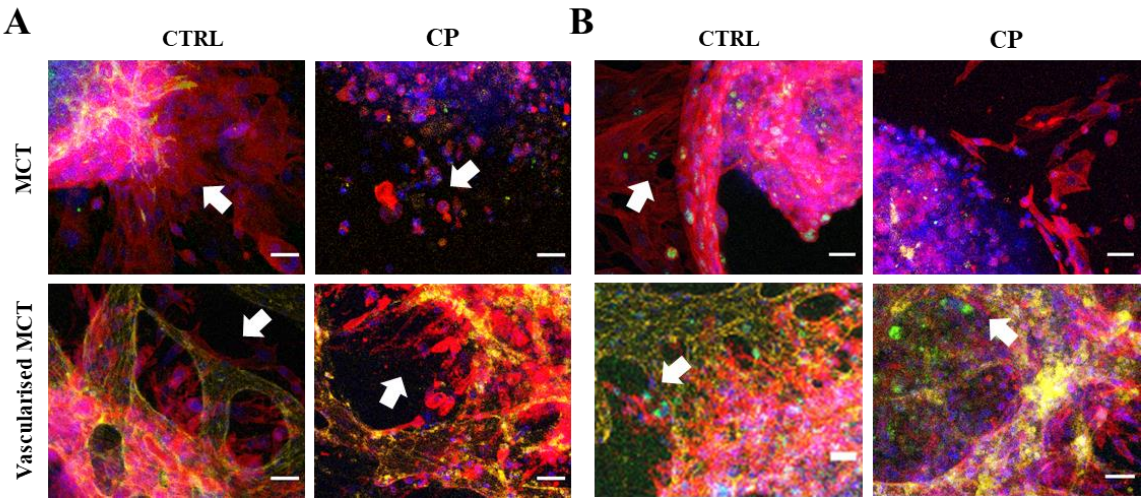

Figure 46. Cell shrinking and Ki67 staining in micro-tumours. Following 300 µM carboplatin treatment, vascularised MCTs appeared protected form chemotherapy. **A)** Extensive G33 cell shrinkage is observed in carboplatin treated non-vascularised MCTs. **B)** Carboplatin treatmed also ablates Ki67 expression in non-vascularised MCTs, whereas some expression is still observed when MCTs are vascularised. Representative images. Red, phalloidin. Green, Ki67. Blue, DAPI. Yellow, CD31. CP = carboplatin. Scale bar: 50 µm.

11.10. Summary

This chaper has focused on the development of a novel spheroid-on-a-chip model of HGSOC that is suitable for drug development studies. This system incorporated an MCT composed of a 4:1 ratio of G33 and HUVECs, with a vascular network which was developed in section 8 of this thesis. Using 70 kDa FITC-dextran and confocal imaging, we determined the MCT was both vascularised and perfusable, allowing the delivery of drugs through the vasculature into the MCT. The addition of HUVECs also promoted an increase in surface area of the MCTs, alluding to an increased proliferation and/or survival of HGSOC cells, which is similar to what is observed in section 10.5. In addition, HUVECs promote a phenotypic change in MCTs, as the spheroid becomes signficiantly less circular, again suggesting a phenotypic change to a more EMT phenotype. Following 300 µM carboplatin treatment, vascularised MCTs qualitatively appeared to undergo less cell shrinkage and also maintained expression of Ki67. This would imply that the vascular

network is chemo-protective in carboplatin treatment. However, these are preliminary results and further experiments are required to conclude these observations.

12. Conclusions and future directions

The aim of this thesis was to develop a novel high-grade serous ovarian cancer model using microfluidic and micropatterning techniques. This model would integrate a 'functional' vasculature with HGSOC cells and allow analysis of how these cells interact. An organ-on-a-chip approach was taken due to the advantages it offers over traditional *in vitro* models. This approach is more representative of disease, allows cell compartmentilization and control over cell-cell interactions, allows physical manipulation, and requires little material and cell numbers. It also offers advantages over *in vivo* models being cheaper, quicker with fewer ethical constraints, and the potential for live-imaging. We, and many other groups, believe that this gives organ-on-a-chip models a distinct ability to bridge the gap between traditional *in vitro* and *in vivo* models, and hopefully allows the better identification of lead compounds in drug development, and understanding of disease pathophysiology.

Due to the success of a number of organ-on-a-chip models there is a huge interest in this area, with the number of groups involved within this field continuing to grow [191]. However, one of the difficulties that organ-on-a-chip modeling faces is the successful uptake of these techniques by biology-based research groups, who have little expertise within the field of bioengineering. This is due to the general lack of published detailed protocols pertaining to the creation of these devices, and the lack of know-how within these groups. Within section 8 of this thesis we attempted to establish a general protocol for the development of a vasculature model on-a-chip. Following the method development to create PDMS microfluidic chips, we established a general 'recipe' to culture a functional HUVEC network, based upon the results of several groups, with the

details and concentrations shown in Table 4 [198-200, 205, 213, 222]. We next systematically progressed through these different ECM components (collagen and fibrin), growth factors (VEGF), solutions (thrombin and aprotinin), and cell densities before developing an established protocol which allows the formation of a stable and functional vasculature (see Table 4). The protocol also details how different factors impact the vasculature. Interestingly, a number of common fibrin gel constituents which are used in the literature, were superfluous within our system (type 1 collagen and aprotinin).

Following the establishment of the vasculature-on-a-chip system, we studied the interactions between HUVECs and a number of stromal cell types, namely NHLFs and pericytes. NHLFs were investigated due to their reported ability to promote a stable and mature vasculature without requiring further growth factor supplements [199, 222]. However, although NHLFs did promote vessel formation, there was no significant difference to when HUVECs were cultured separately with exogenous VEGF. Pericytes are important structural components in the vasculature, and the ablation of their interactions with endothelial cells is embryonic lethal, due to defects in the vasculature causing haemorrhaging and oedema [155, 166]. The addition of pericytes to our vascular model reduced vessel hyperplasia, promoted long-term total tube length, inhibited vascular permeability and promoted vessel stability during nutrient deprivation. The vascular networks developed also expressed important junction markers, including VE-cad, β-cat and ZO-1, implying a mature vessel network. Future work should focus on how pericytes are promoting these effects, and investigate the role of pericytes on endothelial proliferation, cell survival, and cellular hyperplasia. In addition, further analysis should investigate if pericytes alter vessel junction expression or localisation. In addition, pericytes play an important role in ovarian cancer progression, with a high pericyte score being highly correlated with poor prognosis in patients [67]. Indeed, co-injecting

pericytes and HGSOC cells in a mouse xenograft model promotes a more aggressive phenotype, and when co-cultured *in vitro*, pericytes promote HGSOC cell proliferation and invasion. Interestingly, the impact of pericyte was stated to be independent of the vasculature. Future experiments with pericytes could probe their interactions with HGSOC further.

Many studies have investigated the role of the vasculature in different types of cancer, however few *in vitro* models study HGSOC interactions with the vasculature, perhaps due to to HGSOC primarily relying upon a different mechanism of invasion and metastasis [198, 211, 214, 215, 318]. Using our vascular system we were able to demonstrate that G33 HGSOC cell promote HUVEC vessel formation. In addition, HUVECs increase the overall number of G33s through paracrine and/or juxtacrine signalling; this may be through promoting cell proliferation or enhanced cell survival. Furthemore, when cultured with HUVECs, G33s were signficantly more likely to form large cell clusters (5+ cell). Analysis of G33 clusters revealed that HUVECs promote the formation of larger clusters with reduced circularity, this may be indicative of an EMT phenotype. Further research needs to be conducted to confirm this, but these preliminary results may suggest that HUVECs, through angiocrine signalling, are promoting G33 cells to a more invasive phenotype.

When investigating and mimicing disease *in vitro*, culturing representative cells is important to ensure your results are characteristic of clinical observations. Therefore, when investigating the interactions between HGSOC and endothelial cells it is essential to use representative cell sources. Here we describe using G33 cells, which were isolated from omental metastases by the Balkwill lab and are known to be HGSOC cells. However, G33s are co-cultured with HUVECs, which are foetal, macrovascular cells. Future work should use a more representative endothelial cell source. Winiarski *et al*

proposed a method for isolating omental microvascular endothelial cells (HOMEC) from human biopsies [319]. HOMECs express a number of endothelial cell markers, including CD31 and CD105. In addition, HOMECs undergo tube formation when treated with VEGF. Indeed, Winiarski further demontrated that HOMECs undergo VEGF-independent vessel formation following the addition of ovarian cancer cell conditioned medium [320]. HOMECs are a more suitable cell source for future studies investigating HGSOC-endothelial cell interactions.

There has been a recent development in organ-on-a-chip models to incorporate spheroids or organoids into microfluidic devices. This has led to the development of systems including advanced brain and kidney organoids cultured within a microfluidic device, and NHLF and breast cancer spheroid-on-a-chip models [216, 304, 318, 321, 322]. This technique combines the advantages of two advanced *in vitro* models. This is demonstrated by Homan *et al* integrating flow into their system, which promoted kidney epithelium maturation and morphogenesis, compared with static culture [321]. In section 11, we combined endothelial vascular networks with G33 and HUVEC MCTs in a spheroid-on-a-chip device. Culturing MCTs alongside a vasculature promoted the formation of larger spheroids, demonstrated by their increased area. In addition, these MCTs displayed a different morphology, exhibiting a reduced circularity when compared with non-vascularised MCTs. These results may indicate HUVECs are promoting G33 survival, increasing their proliferation and also inducing an EMT phenotype - in agreement with what we report in section 10.5. Culturing vascularised spheroids also allows the delivery of chemotherapeutic agents into the MCT via the vasculature. Our preliminary results indicate that HUVECs may be chemo-protective when culturing alongside MCTs with 300 μM carboplatin - due to reduced cell shrinking and maintenance of Ki67 expression.

This study lays some light on the role of the endothelium in HGSOC. We demonstrate in two separate chip designs that HUVECs seem to promote the number of HGSOC cells and promote a phenotypic change to a more EMT phenotype. But we also raise some questions for the future. Do endothelial cells increase HGSOC cell proliferation? Do they promote HGSOC cell survival? Do they increase the expression of EMT markers? Do endothelial cells actually protect HGSOC cells from chemotherapy? As well as raising these questions, this thesis has also developed a model to answer them.

13. Bibliography

1. CancerResearchUK. https://www.cancerresearchuk.org/health-professional/cancer-statistics/statistics-by-cancer-type/ovarian-cancer#heading-Zero. 2016 [cited 2019 18/06/2019].
2. Auersperg, N., *The origin of ovarian cancers - hypotheses and controversies.* Frontiers in Bioscience, 2013. **5**(2): p. 709-719.
3. Bowtell, D.D., et al., *Rethinking ovarian cancer II: reducing mortality from high-grade serous ovarian cancer.* Nature Reviews. Cancer, 2015. **15**(11): p. 668-679.
4. Koshiyama, M., N. Matsumura, and I. Konishi, *Recent concepts of ovarian carcinogenesis: type I and type II.* BioMed Research International, 2014. **2014**: p. 934261-934261.
5. Mutch, D.G. and J. Prat, *2014 FIGO staging for ovarian, fallopian tube and peritoneal cancer.* Gynecologic Oncology, 2014. **133**(3): p. 401-404.
6. Shimizu, Y., et al., *Toward the development of a universal grading system for ovarian epithelial carcinoma: testing of a proposed system in a series of 461 patients with uniform treatment and follow-up.* Cancer, 1998. **82**(5): p. 893-901.
7. Malpica, A.D., Michael T. Lu, Karen. , *Grading ovarian serous carcinoma using a two-tier system.* American Journal of Surgical Pathology, 2004. **28**(4): p. 496-504.
8. Vang, R., M. Shih Ie, and R.J. Kurman, *Ovarian low-grade and high-grade serous carcinoma: pathogenesis, clinicopathologic and molecular biologic features, and diagnostic problems.* Advances in Anatomic Pathology, 2009. **16**(5): p. 267-82.
9. Cancer Genome Atlas Research, N., *Integrated genomic analyses of ovarian carcinoma.* Nature, 2011. **474**(7353): p. 609-15.
10. Freed-Pastor, W.A. and C. Prives, *Mutant p53: one name, many proteins.* Genes & Development, 2012. **26**(12): p. 1268-1286.
11. Zhang, Y., et al., *TP53 mutations in epithelial ovarian cancer.* Translational Cancer Research, 2016. **5**(6): p. 650-663.
12. Dittmer, D., et al., *Gain of function mutations in p53.* Nature Genetics, 1993. **4**(1): p. 42-6.
13. Di Agostino, S., et al., *Gain of function of mutant p53: The mutant p53/NF-Y protein complex reveals an aberrant transcriptional mechanism of cell cycle regulation.* Cancer Cell, 2006. **10**(3): p. 191-202.
14. Oren, M. and V. Rotter, *Mutant p53 gain-of-function in cancer.* Cold Spring Harbor Perspectives in Biology, 2010. **2**(2): p. 1107-1107.
15. Kuhn, E., et al., *TP53 mutations in serous tubal intraepithelial carcinoma and concurrent pelvic high-grade serous carcinoma--evidence supporting the clonal relationship of the two lesions.* The Journal of Pathology, 2012. **226**(3): p. 421-6.
16. Roy, R., J. Chun, and S.N. Powell, *BRCA1 and BRCA2: different roles in a common pathway of genome protection.* Nature reviews. Cancer, 2011. **12**(1): p. 68-78.
17. Powell, S.N. and L.A. Kachnic, *Roles of BRCA1 and BRCA2 in homologous recombination, DNA replication fidelity and the cellular response to ionizing radiation.* Oncogene, 2003. **22**(37): p. 5784-5791.
18. Venkitaraman, A.R., *Functions of BRCA1 and BRCA2 in the biological response to DNA damage.* Journal of Cell Science, 2001. **114**(20): p. 3591-3598.

19. Yun, M.H. and K. Hiom, *CtIP-BRCA1 modulates the choice of DNA double-strand-break repair pathway throughout the cell cycle.* Nature, 2009. **459**(7245): p. 460-3.
20. Moynahan, M.E., A.J. Pierce, and M. Jasin, *BRCA2 Is Required for Homology-Directed Repair of Chromosomal Breaks.* Molecular Cell, 2001. **7**(2): p. 263-272.
21. Cox, M.M., *Recombinational DNA repair in bacteria and the RecA protein.* Progress in Nucleic Acid Research and Molecular Biology, 1999. **63**: p. 311-66.
22. Song, H., et al., *Common variants in RB1 gene and risk of invasive ovarian cancer.* Cancer Research, 2006. **66**(20): p. 10220-6.
23. Hanahan, D. and R.A. Weinberg, *The Hallmarks of Cancer.* Cell, 2000. **100**(1): p. 57-70.
24. Weinberg, R.A., *The retinoblastoma protein and cell cycle control.* Cell, 1995. **81**(3): p. 323-330.
25. Hashiguchi, Y., et al., *Combined analysis of p53 and RB pathways in epithelial ovarian cancer.* Human Pathology, 2001. **32**(9): p. 988-96.
26. Hashiguchi, Y., et al., *Alteration of cell cycle regulators correlates with survival in epithelial ovarian cancer patients.* Human Pathology, 2004. **35**(2): p. 165-75.
27. Garsed, D.W., et al., *Homologous Recombination DNA Repair Pathway Disruption and Retinoblastoma Protein Loss Are Associated with Exceptional Survival in High-Grade Serous Ovarian Cancer.* Clinical Cancer Research, 2018. **24**(3): p. 569-580.
28. Kusume, T., et al., *The p16-Cyclin D1/CDK4-pRb Pathway and Clinical Outcome in Epithelial Ovarian Cancer.* Clinical Cancer Research, 1999. **5**(12): p. 4152-4157.
29. Talamo, T.S., et al., *Adenocarcinoma of the fallopian tube.* Virchows Archiv. A, Pathological Anatomy and Histology, 1982. **397**(3): p. 363-368.
30. Lee, Y., et al., *A candidate precursor to serous carcinoma that originates in the distal fallopian tube.* The Journal of Pathology, 2007. **211**(1): p. 26-35.
31. Xiang, L., et al., *Identification of candidate genes associated with tubal origin of high-grade serous ovarian cancer.* Oncol Letters, 2018. **15**(5): p. 7769-7775.
32. Perets, R., et al., *Transformation of the fallopian tube secretory epithelium leads to high-grade serous ovarian cancer in Brca;Tp53;Pten models.* Cancer Cell, 2013. **24**(6): p. 751-65.
33. Shay, J.W. and W.E. Wright, *Senescence and immortalization: role of telomeres and telomerase.* Carcinogenesis, 2005. **26**(5): p. 867-74.
34. Counter, C.M., et al., *Telomerase activity in human ovarian carcinoma.* Proceedings of the National Academy of Sciences of the United States of America, 1994. **91**(8): p. 2900-2904.
35. Kuhn, E., et al., *Shortened telomeres in serous tubal intraepithelial carcinoma: an early event in ovarian high-grade serous carcinogenesis.* The American Journal of Surgical Pathology, 2010. **34**(6): p. 829-36.
36. Kim, J., et al., *Cell Origins of High-Grade Serous Ovarian Cancer.* Cancers, 2018. **10**(11): p. 433.
37. Paget, S., *The distribution of secondary growths in cancer of the breast.* The Lancet, 1889. **133**(3421): p. 571-573.
38. Motohara, T., et al., *An evolving story of the metastatic voyage of ovarian cancer cells: cellular and molecular orchestration of the adipose-rich metastatic microenvironment.* Oncogene, 2019. **38**(16): p. 2885-2898.
39. Nieman, K.M., et al., *Adipocytes promote ovarian cancer metastasis and provide energy for rapid tumor growth.* Nature medicine, 2011. **17**(11): p. 1498-1503.

40. Lengyel, E., *Ovarian cancer development and metastasis.* The American journal of pathology, 2010. **177**(3): p. 1053-1064.
41. Huber, M.A., N. Kraut, and H. Beug, *Molecular requirements for epithelial–mesenchymal transition during tumor progression.* Current Opinion in Cell Biology, 2005. **17**(5): p. 548-558.
42. Symowicz, J., et al., *Engagement of collagen-binding integrins promotes matrix metalloproteinase-9-dependent E-cadherin ectodomain shedding in ovarian carcinoma cells.* Cancer Research, 2007. **67**(5): p. 2030-9.
43. Sood, A.K., et al., *Distant Metastases in Ovarian Cancer: Association with p53 Mutations.* Clinical Cancer Research, 1999. **5**(9): p. 2485-2490.
44. Cormio, G., et al., *Distant metastases in ovarian carcinoma.* International Journal of Gynecologic Cancer, 2003. **13**(2): p. 125-9.
45. Pradeep, S., et al., *Hematogenous metastasis of ovarian cancer: rethinking mode of spread.* Cancer Cell, 2014. **26**(1): p. 77-91.
46. Pearce, O.M.T., et al., *Deconstruction of a Metastatic Tumor Microenvironment Reveals a Common Matrix Response in Human Cancers.* Cancer Discovery, 2018. **8**(3): p. 304-319.
47. Balkwill, F.R., M. Capasso, and T. Hagemann, *The tumor microenvironment at a glance.* Journal of Cell Science, 2012. **125**(23): p. 5591-5596.
48. Dasari, S., Y. Fang, and A.K. Mitra, *Cancer Associated Fibroblasts: Naughty Neighbors That Drive Ovarian Cancer Progression.* Cancers, 2018. **10**(11): p. 406.
49. Mitra, A.K., et al., *MicroRNAs reprogram normal fibroblasts into cancer-associated fibroblasts in ovarian cancer.* Cancer Discovery, 2012. **2**(12): p. 1100-1108.
50. Gupta, V., F. Yull, and D. Khabele, *Bipolar Tumor-Associated Macrophages in Ovarian Cancer as Targets for Therapy.* Cancers, 2018. **10**(10): p. 366.
51. Carroll, M.J., et al., *M2 macrophages induce ovarian cancer cell proliferation via a heparin binding epidermal growth factor/matrix metalloproteinase 9 intercellular feedback loop.* Oncotarget, 2016. **7**(52): p. 86608-86620.
52. White, J.R., et al., *Genetic amplification of the transcriptional response to hypoxia as a novel means of identifying regulators of angiogenesis.* Genomics, 2004. **83**(1): p. 1-8.
53. Lan, C., et al., *Expression of M2-polarized macrophages is associated with poor prognosis for advanced epithelial ovarian cancer.* Technology in Cancer Research & Treatment, 2013. **12**(3): p. 259-67.
54. Ghoneum, A., et al., *Role of tumor microenvironment in ovarian cancer pathobiology.* Oncotarget, 2018. **9**(32): p. 22832-22849.
55. Mesiano, S., N. Ferrara, and R.B. Jaffe, *Role of Vascular Endothelial Growth Factor in Ovarian Cancer: Inhibition of Ascites Formation by Immunoneutralization.* The American Journal of Pathology, 1998. **153**(4): p. 1249-1256.
56. Nakanishi, Y., et al., *The expression of vascular endothelial growth factor and transforming growth factor-beta associates with angiogenesis in epithelial ovarian cancer.* International Journal of Gynecological Pathology, 1997. **16**(3): p. 256-62.
57. Leinster, D.A., et al., *The peritoneal tumour microenvironment of high-grade serous ovarian cancer.* The Journal of pathology, 2012. **227**(2): p. 136-145.

58. Kassim, S.K., et al., *Vascular endothelial growth factor and interleukin-8 are associated with poor prognosis in epithelial ovarian cancer patients.* Clinical Biochemistry, 2004. **37**(5): p. 363-9.
59. Masoumi Moghaddam, S., et al., *Significance of vascular endothelial growth factor in growth and peritoneal dissemination of ovarian cancer.* Cancer Metastasis Reviews, 2012. **31**(1-2): p. 143-162.
60. Folkman , J., *Tumor Angiogenesis: Therapeutic Implications.* New England Journal of Medicine, 1971. **285**(21): p. 1182-1186.
61. Hoarau-Véchot, J., et al., *Akt-activated endothelium promotes ovarian cancer proliferation through notch activation.* Journal of Translational Medicine, 2019. **17**(1): p. 194.
62. Nagy, J.A., et al., *Pathogenesis of Ascites Tumor Growth: Vascular Permeability Factor, Vascular Hyperpermeability, and Ascites Fluid Accumulation.* Cancer Research, 1995. **55**(2): p. 360-368.
63. Penet, M.F., et al., *Ascites Volumes and the Ovarian Cancer Microenvironment.* Frontiers in Oncology, 2018. **8**: p. 595.
64. Armulik, A., G. Genove, and C. Betsholtz, *Pericytes: developmental, physiological, and pathological perspectives, problems, and promises.* Developmental Cell, 2011. **21**(2): p. 193-215.
65. De Palma, M., D. Biziato, and T.V. Petrova, *Microenvironmental regulation of tumour angiogenesis.* Nature Reviews Cancer, 2017. **17**: p. 457.
66. Gopinathan, G., et al., *Interleukin-6 Stimulates Defective Angiogenesis.* Cancer Research, 2015. **75**(15): p. 3098-3107.
67. Sinha, D., et al., *Pericytes Promote Malignant Ovarian Cancer Progression in Mice and Predict Poor Prognosis in Serous Ovarian Cancer Patients.* Clinical Cancer Research, 2016. **22**(7): p. 1813-1824.
68. Gockley, A., et al., *Outcomes of Women With High-Grade and Low-Grade Advanced-Stage Serous Epithelial Ovarian Cancer.* Obstetrics and Gynecology, 2017. **129**(3): p. 439-447.
69. Aluloski, I., et al., *Survival of Advanced Stage High-Grade Serous Ovarian Cancer Patients in the Republic of Macedonia.* Macedonian Journal of Medical Sciences, 2017. **5**(7): p. 904-908.
70. Cortez, A.J., et al., *Advances in ovarian cancer therapy.* Cancer Chemotherapy and Pharmacology, 2018. **81**(1): p. 17-38.
71. Ozols, R.F., et al., *Phase III trial of carboplatin and paclitaxel compared with cisplatin and paclitaxel in patients with optimally resected stage III ovarian cancer: a Gynecologic Oncology Group study.* Journal of Clinical Oncology, 2003. **21**(17): p. 3194-200.
72. Sousa, G.F.d., S.R. Wlodarczyk, and G. Monteiro, *Carboplatin: molecular mechanisms of action associated with chemoresistance.* Brazilian Journal of Pharmaceutical Sciences, 2014. **50**: p. 693-701.
73. Dasari, S. and P.B. Tchounwou, *Cisplatin in cancer therapy: molecular mechanisms of action.* European Journal of Pharmacology, 2014. **740**: p. 364-78.
74. Rabik, C.A. and M.E. Dolan, *Molecular mechanisms of resistance and toxicity associated with platinating agents.* Cancer Treatment Reviews, 2007. **33**(1): p. 9-23.
75. Shi, L., et al., *Premature p34cdc2 activation required for apoptosis.* Science, 1994. **263**(5150): p. 1143-5.

76. Vaisman, A., et al., *Effect of DNA polymerases and high mobility group protein 1 on the carrier ligand specificity for translesion synthesis past platinum-DNA adducts.* Biochemistry, 1999. **38**(34): p. 11026-39.
77. Ho, G.Y., N. Woodward, and J.I. Coward, *Cisplatin versus carboplatin: comparative review of therapeutic management in solid malignancies.* Critical Reviews in Oncology/Hematology, 2016. **102**: p. 37-46.
78. Jangir, D.K. and R. Mehrotra, *Raman spectroscopic evaluation of DNA adducts of a platinum containing anticancer drug.* Spectrochimica Acta Part A: Molecular and Biomolecular Spectroscopy, 2014. **130**: p. 386-9.
79. Hah, S.S., et al., *Kinetics of carboplatin-DNA binding in genomic DNA and bladder cancer cells as determined by accelerator mass spectrometry.* Chemical Research in Toxicology, 2006. **19**(5): p. 622-6.
80. Kuchenbaecker, K.B., et al., *Risks of Breast, Ovarian, and Contralateral Breast Cancer for BRCA1 and BRCA2 Mutation CarriersRisks of Breast, Ovarian, and Contralateral Breast Cancer Among BRCA Mutation CarriersRisks of Breast, Ovarian, and Contralateral Breast Cancer Among BRCA Mutation Carriers.* JAMA, 2017. **317**(23): p. 2402-2416.
81. Kotsopoulos, J., et al., *Factors influencing ovulation and the risk of ovarian cancer in BRCA1 and BRCA2 mutation carriers.* International Journal of Cancer, 2015. **137**(5): p. 1136-46.
82. Karst, A.M., K. Levanon, and R. Drapkin, *Modeling high-grade serous ovarian carcinogenesis from the fallopian tube.* Proceedings of the National Academy of Sciences, 2011. **108**(18): p. 7547-7552.
83. Jacobs, I.J., et al., *Ovarian cancer screening and mortality in the UK Collaborative Trial of Ovarian Cancer Screening (UKCTOCS): a randomised controlled trial.* The Lancet, 2016. **387**(10022): p. 945-956.
84. Oun, R., Y.E. Moussa, and N.J. Wheate, *The side effects of platinum-based chemotherapy drugs: a review for chemists.* Dalton Transactions, 2018. **47**(19): p. 6645-6653.
85. Dziadkowiec, K.N., et al., *PARP inhibitors: review of mechanisms of action and BRCA1/2 mutation targeting.* Menopause Review, 2016. **15**(4): p. 215-219.
86. Heale, J.T., et al., *Condensin I interacts with the PARP-1-XRCC1 complex and functions in DNA single-strand break repair.* Molecular Cell, 2006. **21**(6): p. 837-48.
87. Helleday, T., *The underlying mechanism for the PARP and BRCA synthetic lethality: clearing up the misunderstandings.* Molecular Oncology, 2011. **5**(4): p. 387-93.
88. Moore, K., et al., *Maintenance Olaparib in Patients with Newly Diagnosed Advanced Ovarian Cancer.* New England Journal of Medicine, 2018. **379**(26): p. 2495-2505.
89. He, L., Q. Wang, and X. Zhao, *Microvessel density as a prognostic factor in ovarian cancer: a systematic review and meta-analysis.* Asian Pacific Journal of Cancer Prevention, 2015. **16**(3): p. 869-74.
90. Ferrara, N., K.J. Hillan, and W. Novotny, *Bevacizumab (Avastin), a humanized anti-VEGF monoclonal antibody for cancer therapy.* Biochemical and Biophysical Research Communications, 2005. **333**(2): p. 328-335.
91. Perren, T.J., et al., *A Phase 3 Trial of Bevacizumab in Ovarian Cancer.* New England Journal of Medicine, 2011. **365**(26): p. 2484-2496.

92. Burger , R.A., et al., *Incorporation of Bevacizumab in the Primary Treatment of Ovarian Cancer.* New England Journal of Medicine, 2011. **365**(26): p. 2473-2483.
93. Oza, A.M., et al., *Standard chemotherapy with or without bevacizumab for women with newly diagnosed ovarian cancer (ICON7): overall survival results of a phase 3 randomised trial.* The Lancet. Oncology, 2015. **16**(8): p. 928-936.
94. Kubis, N. and B.I. Levy, *Vasculogenesis and angiogenesis: molecular and cellular controls. Part 1: growth factors.* Journal of Peritherapeutic Neuroradiology, Surgical Procedures and Related Neurosciences, 2003. **9**(3): p. 227-237.
95. Patel-Hett, S. and P.A. D'Amore, *Signal transduction in vasculogenesis and developmental angiogenesis.* The International Journal of Developmental Biology, 2011. **55**(4-5): p. 353-363.
96. Reale, A., et al., *Functional and Biological Role of Endothelial Precursor Cells in Tumour Progression: A New Potential Therapeutic Target in Haematological Malignancies.* Stem Cells International, 2016. **2016**: p. 7954580-7954580.
97. Tahergorabi, Z. and M. Khazaei, *A review on angiogenesis and its assays.* Iranian Journal of Basic Medical Sciences, 2012. **15**(6): p. 1110-1126.
98. Ferrara, N., *Vascular Endothelial Growth Factor: Basic Science and Clinical Progress.* Endocrine Reviews, 2004. **25**(4): p. 581-611.
99. Shibuya, M., *Vascular Endothelial Growth Factor (VEGF) and Its Receptor (VEGFR) Signaling in Angiogenesis: A Crucial Target for Anti- and Pro-Angiogenic Therapies.* Genes & Cancer, 2011. **2**(12): p. 1097-1105.
100. Soker, S., et al., *Inhibition of vascular endothelial growth factor (VEGF)-induced endothelial cell proliferation by a peptide corresponding to the exon 7-encoded domain of VEGF165.* The Journal of Biological Chemistry, 1997. **272**(50): p. 31582-8.
101. Simons, M., E. Gordon, and L. Claesson-Welsh, *Mechanisms and regulation of endothelial VEGF receptor signalling.* Nature Reviews Molecular Cell Biology, 2016. **17**: p. 611.
102. Dvorak, H.F., *Vascular Permeability Factor/Vascular Endothelial Growth Factor: A Critical Cytokine in Tumor Angiogenesis and a Potential Target for Diagnosis and Therapy.* Journal of Clinical Oncology, 2002. **20**(21): p. 4368-4380.
103. Wiesmann, C., et al., *Crystal structure at 1.7 A resolution of VEGF in complex with domain 2 of the Flt-1 receptor.* Cell, 1997. **91**(5): p. 695-704.
104. Ferrara, N., H.-P. Gerber, and J. LeCouter, *The biology of VEGF and its receptors.* Nature Medicine, 2003. **9**(6): p. 669-676.
105. Gerber, H.P., et al., *Vascular endothelial growth factor regulates endothelial cell survival through the phosphatidylinositol 3'-kinase/Akt signal transduction pathway. Requirement for Flk-1/KDR activation.* The Journal of Biological Chemistry, 1998. **273**(46): p. 30336-30343.
106. Takahashi, T., H. Ueno, and M. Shibuya, *VEGF activates protein kinase C-dependent, but Ras-independent Raf-MEK-MAP kinase pathway for DNA synthesis in primary endothelial cells.* Oncogene, 1999. **18**(13): p. 2221-2230.
107. Drake, C.J., *Embryonic and adult vasculogenesis.* Birth Defects Research Part C: Embryo Today: Reviews, 2003. **69**(1): p. 73-82.
108. Liang, D., et al., *The role of vascular endothelial growth factor (VEGF) in vasculogenesis, angiogenesis, and hematopoiesis in zebrafish development.* Mechanisms of Development, 2001. **108**(1): p. 29-43.

109. Shalaby, F., et al., *Failure of blood-island formation and vasculogenesis in Flk-1-deficient mice.* Nature, 1995. **376**(6535): p. 62-6.
110. Drake, C.J. and C.D. Little, *Exogenous vascular endothelial growth factor induces malformed and hyperfused vessels during embryonic neovascularization.* Proceedings of the National Academy of Sciences of the United States of America, 1995. **92**(17): p. 7657-61.
111. Krah, K., et al., *Induction of vasculogenesis in quail blastodisc-derived embryoid bodies.* Developmental Biology, 1994. **164**(1): p. 123-32.
112. Shi, Q., et al., *Proof of fallout endothelialization of impervious Dacron grafts in the aorta and inferior vena cava of the dog.* Journal of Vascular Surgery, 1994. **20**(4): p. 546-557.
113. Asahara, T., et al., *Bone marrow origin of endothelial progenitor cells responsible for postnatal vasculogenesis in physiological and pathological neovascularization.* Circulation Research, 1999. **85**(3): p. 221-8.
114. Conway, E.M., D. Collen, and P. Carmeliet, *Molecular mechanisms of blood vessel growth.* Cardiovascular Research, 2001. **49**(3): p. 507-521.
115. Burri, P.H., R. Hlushchuk, and V. Djonov, *Intussusceptive angiogenesis: Its emergence, its characteristics, and its significance.* Developmental Dynamics, 2004. **231**(3): p. 474-488.
116. Kalluri, R., *Basement membranes: structure, assembly and role in tumour angiogenesis.* Nature Reviews Cancer, 2003. **3**(6): p. 422-433.
117. Egeblad, M. and Z. Werb, *New functions for the matrix metalloproteinases in cancer progression.* Nature Reviews Cancer, 2002. **2**(3): p. 161-174.
118. Form, D.M., B.M. Pratt, and J.A. Madri, *Endothelial cell proliferation during angiogenesis. In vitro modulation by basement membrane components.* Laboratory Investigation, 1986. **55**(5): p. 521-30.
119. Gerhardt, H., *VEGF and endothelial guidance in angiogenic sprouting.* Organogenesis, 2008. **4**(4): p. 241-246.
120. Blanco, R. and H. Gerhardt, *VEGF and Notch in tip and stalk cell selection.* Cold Spring Harbor Perspectives in Medicine. **3**(1): p. 6569-6569.
121. Suchting, S., et al., *The Notch ligand Delta-like 4 negatively regulates endothelial tip cell formation and vessel branching.* Proceedings of the National Academy of Sciences of the United States of America, 2007. **104**(9): p. 3225-3230.
122. Gerhardt, H., et al., *VEGF guides angiogenic sprouting utilizing endothelial tip cell filopodia.* The Journal of Cell Biology, 2003. **161**(6): p. 1163-77.
123. Hellström, M., et al., *Dll4 signalling through Notch1 regulates formation of tip cells during angiogenesis.* Nature, 2007. **445**: p. 776.
124. Funahashi, Y., et al., *Notch regulates the angiogenic response via induction of VEGFR-1.* Journal of Angiogenesis Research, 2010. **2**(1): p. 3-3.
125. Williams, C.K., et al., *Up-regulation of the Notch ligand Delta-like 4 inhibits VEGF-induced endothelial cell function.* Blood, 2006. **107**(3): p. 931-939.
126. Jakobsson, L., et al., *Endothelial cells dynamically compete for the tip cell position during angiogenic sprouting.* Nature Cell Biology, 2010. **12**(10): p. 943-53.
127. Lamalice, L., F. Le Boeuf, and J. Huot, *Endothelial cell migration during angiogenesis.* Circulation Research, 2007. **100**(6): p. 782-94.
128. Norton, K.A. and A.S. Popel, *Effects of endothelial cell proliferation and migration rates in a computational model of sprouting angiogenesis.* Scientific Reports, 2016. **6**: p. 36992.

129. Sainson, R.C., et al., *Cell-autonomous notch signaling regulates endothelial cell branching and proliferation during vascular tubulogenesis.* The FASEB Journal, 2005. **19**(8): p. 1027-9.
130. Leslie, J.D., et al., *Endothelial signalling by the Notch ligand Delta-like 4 restricts angiogenesis.* Development, 2007. **134**(5): p. 839-44.
131. Harrington, L.S., et al., *Regulation of multiple angiogenic pathways by Dll4 and Notch in human umbilical vein endothelial cells.* Microvascular Research, 2008. **75**(2): p. 144-154.
132. Krebs, L.T., et al., *The Nrarp Gene Encodes an Ankyrin-Repeat Protein That Is Transcriptionally Regulated by the Notch Signaling Pathway.* Developmental Biology, 2001. **238**(1): p. 110-119.
133. Phng, L.K. and H. Gerhardt, *Angiogenesis: A Team Effort Coordinated by Notch.* Developmental Cell, 2009. **16**(2): p. 196-208.
134. Lamar, E., et al., *Nrarp is a novel intracellular component of the Notch signaling pathway.* Genes & Development, 2001. **15**(15): p. 1885-1899.
135. Phng, L.-K., et al., *Nrarp Coordinates Endothelial Notch and Wnt Signaling to Control Vessel Density in Angiogenesis.* Developmental Cell, 2009. **16**(1): p. 70-82.
136. Ishitani, T., et al., *Nrarp functions to modulate neural-crest-cell differentiation by regulating LEF1 protein stability.* Nature Cell Biology, 2005. **7**(11): p. 1106-1112.
137. Shtutman, M., et al., *The cyclin D1 gene is a target of the beta-catenin/LEF-1 pathway.* Proceedings of the National Academy of Sciences of the United States of America, 1999. **96**(10): p. 5522-5527.
138. Masckauchán, T.N.H., et al., *Wnt5a signaling induces proliferation and survival of endothelial cells in vitro and expression of MMP-1 and Tie-2.* Molecular Biology of the Cell, 2006. **17**(12): p. 5163-5172.
139. Xu, K. and O. Cleaver, *Tubulogenesis during blood vessel formation.* Seminars in Cell & Developmental Biology, 2011. **22**(9): p. 993-1004.
140. Davis, G.E., S.M. Black, and K.J. Bayless, *Capillary morphogenesis during human endothelial cell invasion of three-dimensional collagen matrices.* In Vitro Cellular & Developmental Biology – Animal, 2000. **36**(8): p. 513-519.
141. Zovein, A.C., et al., *Beta1 integrin establishes endothelial cell polarity and arteriolar lumen formation via a Par3-dependent mechanism.* Developmental Cell, 2010. **18**(1): p. 39-51.
142. Fagiani, E. and G. Christofori, *Angiopoietins in angiogenesis.* Cancer Letters, 2013. **328**(1): p. 18-26.
143. Puri, M.C., et al., *The receptor tyrosine kinase TIE is required for integrity and survival of vascular endothelial cells.* The EMBO journal, 1995. **14**(23): p. 5884-5891.
144. Gamble, J.R., et al., *Angiopoietin-1 is an antipermeability and anti-inflammatory agent in vitro and targets cell junctions.* Circulation Research, 2000. **87**(7): p. 603-7.
145. Saharinen, P., et al., *Angiopoietins assemble distinct Tie2 signalling complexes in endothelial cell–cell and cell–matrix contacts.* Nature Cell Biology, 2008. **10**: p. 527.
146. Fukuhara, S., et al., *Differential function of Tie2 at cell–cell contacts and cell–substratum contacts regulated by angiopoietin-1.* Nature Cell Biology, 2008. **10**: p. 513.

147. Hawighorst, T., et al., *Activation of the tie2 receptor by angiopoietin-1 enhances tumor vessel maturation and impairs squamous cell carcinoma growth.* The American Journal of Pathology, 2002. **160**(4): p. 1381-1392.
148. Jones, N., et al., *Identification of Tek/Tie2 binding partners. Binding to a multifunctional docking site mediates cell survival and migration.* The Journal of Biological Chemistry, 1999. **274**(43): p. 30896-905.
149. Tadros, A., et al., *ABIN-2 protects endothelial cells from death and has a role in the antiapoptotic effect of angiopoietin-1.* Blood, 2003. **102**(13): p. 4407-4409.
150. Machein, M.R., et al., *Angiopoietin-1 promotes tumor angiogenesis in a rat glioma model.* The American Journal of Pathology, 2004. **165**(5): p. 1557-70.
151. Holash, J., S.J. Wiegand, and G.D. Yancopoulos, *New model of tumor angiogenesis: dynamic balance between vessel regression and growth mediated by angiopoietins and VEGF.* Oncogene, 1999. **18**(38): p. 5356-5362.
152. Uemura, A., et al., *Recombinant angiopoietin-1 restores higher-order architecture of growing blood vessels in mice in the absence of mural cells.* The Journal of Clinical Investigation, 2002. **110**(11): p. 1619-1628.
153. Ferland-McCollough, D., et al., *Pericytes, an overlooked player in vascular pathobiology.* Pharmacology & Therapeutics, 2017. **171**: p. 30-42.
154. Darland, D.C., et al., *Pericyte production of cell-associated VEGF is differentiation-dependent and is associated with endothelial survival.* Developmental Biology, 2003. **264**(1): p. 275-88.
155. Lindahl, P., et al., *Pericyte Loss and Microaneurysm Formation in PDGF-B-Deficient Mice.* Science, 1997. **277**(5323): p. 242-245.
156. Kim, J., et al., *Engineering of a Biomimetic Pericyte-Covered 3D Microvascular Network.* PLoS One, 2015. **10**(7): p. 133880.
157. Mathiisen, T.M., et al., *The perivascular astroglial sheath provides a complete covering of the brain microvessels: an electron microscopic 3D reconstruction.* Glia, 2010. **58**(9): p. 1094-103.
158. Kyoko, Y., et al., *Construction of Continuous Capillary Networks Stabilized by Pericyte-like Perivascular Cells.* Tissue Engineering Part A, 2019. **25**(5-6): p. 499-510.
159. Sobrino, A., et al., *3D microtumors in vitro supported by perfused vascular networks.* Scientific Reports, 2016. **6**: p. 31589.
160. Gerhardt, H. and C. Betsholtz, *Endothelial-pericyte interactions in angiogenesis.* Cell and Tissue Research, 2003. **314**: p. 15-23.
161. Cushing, M.C., et al., *Material-based regulation of the myofibroblast phenotype.* Biomaterials, 2007. **28**(23): p. 3378-87.
162. Tallquist, M.D., et al., *Retention of PDGFR-beta function in mice in the absence of phosphatidylinositol 3'-kinase and phospholipase Cgamma signaling pathways.* Genes & Development, 2000. **14**(24): p. 3179-3190.
163. Yu, J., T.F. Deuel, and H.-R.C. Kim, *Platelet-derived Growth Factor (PDGF) Receptor-α Activates c-Jun NH2-terminal Kinase-1 and Antagonizes PDGF Receptor-β-induced Phenotypic Transformation.* Journal of Biological Chemistry, 2000. **275**(25): p. 19076-19082.
164. Armulik, A., A. Abramsson, and C. Betsholtz, *Endothelial/Pericyte Interactions.* Circulation Research, 2005. **97**(6): p. 512-523.
165. Hellstrom, M., et al., *Role of PDGF-B and PDGFR-beta in recruitment of vascular smooth muscle cells and pericytes during embryonic blood vessel formation in the mouse.* Development, 1999. **126**(14): p. 3047-55.

166. Hellström, M., et al., *Lack of pericytes leads to endothelial hyperplasia and abnormal vascular morphogenesis.* The Journal of Cell Biology, 2001. **153**(3): p. 543-553.
167. Luissint, A.-C., et al., *Tight junctions at the blood brain barrier: physiological architecture and disease-associated dysregulation.* Fluids and Barriers of the CNS, 2012. **9**(1): p. 23-23.
168. Bauer, H.-C., et al., *"You Shall Not Pass"-tight junctions of the blood brain barrier.* Frontiers in Neuroscience, 2014. **8**: p. 392-392.
169. Günzel, D. and A.S.L. Yu, *Claudins and the modulation of tight junction permeability.* Physiological Reviews, 2013. **93**(2): p. 525-569.
170. Van Itallie, C.M., et al., *ZO-1 stabilizes the tight junction solute barrier through coupling to the perijunctional cytoskeleton.* Molecular Biology of the Cell, 2009. **20**(17): p. 3930-3940.
171. McNeil, E., C.T. Capaldo, and I.G. Macara, *Zonula occludens-1 function in the assembly of tight junctions in Madin-Darby canine kidney epithelial cells.* Molecular Biology of the Cell, 2006. **17**(4): p. 1922-1932.
172. Tornavaca, O., et al., *ZO-1 controls endothelial adherens junctions, cell-cell tension, angiogenesis, and barrier formation.* The Journal of Cell Biology, 2015. **208**(6): p. 821-38.
173. Katsuno, T., et al., *Deficiency of zonula occludens-1 causes embryonic lethal phenotype associated with defected yolk sac angiogenesis and apoptosis of embryonic cells.* Molecular Biology of the Cell, 2008. **19**(6): p. 2465-2475.
174. Hartsock, A. and W.J. Nelson, *Adherens and tight junctions: Structure, function and connections to the actin cytoskeleton.* Biochimica et Biophysica Acta (BBA) - Biomembranes, 2008. **1778**(3): p. 660-669.
175. Dejana, E., F. Orsenigo, and M.G. Lampugnani, *The role of adherens junctions and VE-cadherin in the control of vascular permeability.* Journal of Cell Science, 2008. **121**(Pt 13): p. 2115-22.
176. Carmeliet, P., et al., *Targeted Deficiency or Cytosolic Truncation of the VE-cadherin Gene in Mice Impairs VEGF-Mediated Endothelial Survival and Angiogenesis.* Cell, 1999. **98**(2): p. 147-157.
177. Corada, M., et al., *Vascular endothelial-cadherin is an important determinant of microvascular integrity in vivo.* Proceedings of the National Academy of Sciences of the United States of America, 1999. **96**(17): p. 9815-9820.
178. Sale, S. and S. Orsulic, *Models of ovarian cancer metastasis: Murine models.* Drug Discovery Today Disease Models, 2006. **3**(2): p. 149-154.
179. Xu, Y., et al., *Characterization of Human Ovarian Carcinomas in a SCID Mouse Model.* Gynecologic Oncology, 1999. **72**(2): p. 161-170.
180. Elkas, J.C., et al., *A Human Ovarian Carcinoma Murine Xenograft Model Useful for Preclinical Trials.* Gynecologic Oncology, 2002. **87**(2): p. 200-206.
181. Domcke, S., et al., *Evaluating cell lines as tumour models by comparison of genomic profiles.* Nature Communications, 2013. **4**: p. 2126.
182. Jacob, F., et al., *Reliable in vitro studies require appropriate ovarian cancer cell lines.* Journal of Ovarian Research, 2014. **7**: p. 60-60.
183. Wenger, S.L., et al., *Comparison of established cell lines at different passages by karyotype and comparative genomic hybridization.* Bioscience Reports, 2004. **24**(6): p. 631-9.
184. Schmeichel, K.L. and M.J. Bissell, *Modeling tissue-specific signaling and organ function in three dimensions.* Journal of Cell Science, 2003. **116**(12): p. 2377-2388.

185. Gandhi, J.K., et al., *Enhanced Viability of Endothelial Colony Forming Cells in Fibrin Microbeads for Sensor Vascularization.* Sensors 2015. **15**(9): p. 23886-23902.
186. Duong, H., B. Wu, and B. Tawil, *Modulation of 3D fibrin matrix stiffness by intrinsic fibrinogen-thrombin compositions and by extrinsic cellular activity.* Tissue engineering. Part A, 2009. **15**(7): p. 1865-1876.
187. Loessner, D., et al., *Bioengineered 3D platform to explore cell-ECM interactions and drug resistance of epithelial ovarian cancer cells.* Biomaterials, 2010. **31**(32): p. 8494-8506.
188. Yamada, K.M. and E. Cukierman, *Modeling tissue morphogenesis and cancer in 3D.* Cell, 2007. **130**(4): p. 601-610.
189. Cukierman, E., R. Pankov, and K.M. Yamada, *Cell interactions with three-dimensional matrices.* Current Opinion in Cell Biology, 2002. **14**(5): p. 633-640.
190. Lawrenson, K., et al., *In vitro three-dimensional modeling of fallopian tube secretory epithelial cells.* BMC Cell Biology, 2013. **14**(43).
191. Huh, D., B.D. Matthews, and A. Mammoto, *Reconstituting Organ-Level Lung Functions on a Chip.* Science 2010. **328**(25): p. 1662-1668.
192. Huh, D., et al., *A Human Disease Model of Drug Toxicity–Induced Pulmonary Oedema in a Lung-on-a-Chip Microdevice.* Science Translational Medicine 2012. **4**(159).
193. Peyrin, J.-M., et al., *Axon diodes for the reconstruction of oriented neuronal networks in microfluidic chambers.* Lab on a Chip, 2011. **11**(21).
194. Lee, J., et al., *Fabrication and characterization of microfluidic liver-on-a-chip using microsomal enzymes.* Enzyme and Microbial Technology, 2013. **53**(3): p. 159-164.
195. Wilmer, M.J., et al., *Kidney-on-a-Chip Technology for Drug-Induced Nephrotoxicity Screening.* Trends in Biotechnology. **34**(2): p. 156-170.
196. Kim, H.J., et al., *Human gut-on-a-chip inhabited by microbial flora that experiences intestinal peristalsis-like motions and flow.* Lab on a Chip, 2012. **12**(12): p. 2165-74.
197. Torisawa, Y.S., et al., *Bone marrow-on-a-chip replicates hematopoietic niche physiology in vitro.* Nature Methods, 2014. **11**(6): p. 663-669.
198. Jeon, J.S., et al., *Human 3D vascularized organotypic microfluidic assays to study breast cancer cell extravasation.* Proceedings of the National Academy of Sciences, 2015. **112**(1): p. 214-219.
199. Kim, S., et al., *Engineering of functional, perfusable 3D microvascular networks on a chip.* Lab on a Chip, 2013. **13**(8): p. 1489-1500.
200. Shin, Y., et al., *Microfluidic assay for simultaneous culture of multiple cell types on surfaces or within hydrogels.* Nature protocols, 2012. **7**(7): p. 1247-1259.
201. Sudo, R., et al., *Transport-mediated angiogenesis in 3D epithelial coculture.* The FASEB Journal 2009. **23**(7): p. 2155-2164.
202. Chung, S., et al., *Cell migration into scaffolds under co-culture conditions in a microfluidic platform.* Lab on a Chip, 2009. **9**(2): p. 269-75.
203. Avorn, J., *The $2.6 Billion Pill — Methodologic and Policy Considerations.* New England Journal of Medicine, 2015. **372**(20): p. 1877-1879.
204. Aref, A.R., et al., *Screening therapeutic EMT blocking agents in a three-dimensional microenvironment.* Integrative Biology, 2013. **5**(2): p. 381-389.
205. Moya, M.L., et al., *In vitro perfused human capillary networks.* Tissue Engineering. Part C, Methods, 2013. **19**(9): p. 730-737.

206. Weigert, R., N. Porat-Shliom, and P. Amornphimoltham, *Imaging cell biology in live animals: Ready for prime time.* The Journal of Cell Biology, 2013. **201**(7): p. 969-979.
207. Lee, S., M. Chung, and N. Li Jeon, *3D brain angiogenesis model to reconstitute maturation of functional human blood-brain barrier in vitro.* BioRxiv, 2018: p. 471334.
208. Kilic, O., et al., *Brain-on-a-chip model enables analysis of human neuronal differentiation and chemotaxis.* Lab on a Chip, 2016. **16**(21): p. 4152-4162.
209. Berthier, E., E.W. Young, and D. Beebe, *Engineers are from PDMS-land, Biologists are from Polystyrenia.* Lab on a Chip, 2012. **12**(7): p. 1224-1237.
210. Choucha Snouber, L., et al., *Metabolomics-on-a-chip of hepatotoxicity induced by anticancer drug flutamide and Its active metabolite hydroxyflutamide using HepG2/C3a microfluidic biochips.* Toxicological Sciences, 2013. **132**(1): p. 8-20.
211. Bersini, S., et al., *A microfluidic 3D in vitro model for specificity of breast cancer metastasis to bone.* Biomaterials, 2014. **35**(8): p. 2454-2461.
212. Jones, T.R., et al., *CellProfiler Analyst: data exploration and analysis software for complex image-based screens.* BMC Bioinformatics, 2008. **9**(1): p. 482.
213. Jeon, J.S., et al., *Generation of 3D functional microvascular networks with human mesenchymal stem cells in microfluidic systems.* Integrative Biology, 2014. **6**(5): p. 555-563.
214. Nagaraju, S., et al., *Microfluidic Tumor–Vascular Model to Study Breast Cancer Cell Invasion and Intravasation.* Advanced Healthcare Materials, 2018. **7**(9): p. 1701257.
215. Oh, S., et al., *"Open-top" microfluidic device for in vitro three-dimensional capillary beds.* Lab on a Chip, 2017. **17**(20): p. 3405-3414.
216. Nashimoto, Y., et al., *Integrating perfusable vascular networks with a three-dimensional tissue in a microfluidic device.* Integrative Biology, 2017. **9**(6): p. 506-518.
217. Astrof, S. and R.O. Hynes, *Fibronectins in vascular morphogenesis.* Angiogenesis, 2009. **12**(2): p. 165-175.
218. Bodas, D. and C. Khan-Malek, *Hydrophilization and hydrophobic recovery of PDMS by oxygen plasma and chemical treatment—An SEM investigation.* Sensors and Actuators B: Chemical, 2007. **123**(1): p. 368-373.
219. Eddington, D.T., J.P. Puccinelli, and D.J. Beebe, *Thermal aging and reduced hydrophobic recovery of polydimethylsiloxane.* Sensors and Actuators B: Chemical, 2006. **114**(1): p. 170-172.
220. Owen, M.J. and P.J. Smith, *Plasma treatment of polydimethylsiloxane.* Journal of Adhesion Science and Technology, 1994. **8**(10): p. 1063-1075.
221. Kaneda, S., et al., *Modification of the Glass Surface Property in PDMS-Glass Hybrid Microfluidic Devices.* Analytical Sciences, 2012. **28**(1): p. 39-44.
222. Whisler, J.A., M.B. Chen, and R.D. Kamm, *Control of perfusable microvascular network morphology using a multiculture microfluidic system.* Tissue Engineering Part C Methods, 2014. **20**(7): p. 543-552.
223. Nakatsu, M.N., et al., *VEGF(121) and VEGF(165) regulate blood vessel diameter through vascular endothelial growth factor receptor 2 in an in vitro angiogenesis model.* Laboratory Investigation, 2003. **83**(12): p. 1873-1885.
224. Murohara, T., et al., *Vascular Endothelial Growth Factor/Vascular Permeability Factor Enhances Vascular Permeability Via Nitric Oxide and Prostacyclin.* Circulation, 1998. **97**(1): p. 99-107.

225. Marin, V., et al., *Endothelial cell culture: protocol to obtain and cultivate human umbilical endothelial cells.* Journal of Immunological Methods, 2001. **254**(1-2): p. 183-190.
226. Cao, Y., et al., *The use of human umbilical vein endothelial cells (HUVECs) as an in vitro model to assess the toxicity of nanoparticles to endothelium: a review.* Journal of Applied Toxicology, 2017. **37**(12): p. 1359-1369.
227. Marcu, R., et al., *Human Organ-Specific Endothelial Cell Heterogeneity.* iScience, 2018. **4**: p. 20-35.
228. Aird, W.C., *Endothelial cell heterogeneity.* Cold Spring Harbor Perspectives in Medicine, 2012. **2**(1): p. 6429.
229. Katt, M.E., et al., *Functional brain-specific microvessels from iPSC-derived human brain microvascular endothelial cells: the role of matrix composition on monolayer formation.* Fluids and Barriers of the CNS, 2018. **15**(1): p. 7.
230. Lacorre, D.-A., et al., *Plasticity of endothelial cells: rapid dedifferentiation of freshly isolated high endothelial venule endothelial cells outside the lymphoid tissue microenvironment.* Blood, 2004. **103**(11): p. 4164-4172.
231. Chen, M.B., et al., *Mechanisms of tumor cell extravasation in an in vitro microvascular network platform.* Integrative Biology, 2013. **5**(10): p. 1262-1271.
232. Schneeweiss, S., et al., *Aprotinin during Coronary-Artery Bypass Grafting and Risk of Death.* New England Journal of Medicine, 2008. **358**(8): p. 771-783.
233. Chapin, J.C. and K.A. Hajjar, *Fibrinolysis and the control of blood coagulation.* Blood Rev, 2015. **29**(1): p. 17-24.
234. Mazar, A.P., J. Henkin, and R.H. Goldfarb, *The urokinase plasminogen activator system in cancer: Implications for tumor angiogenesis and metastasis.* Angiogenesis, 1999. **3**(1): p. 15.
235. Kang, H.M., et al., *The kinetics of plasmin inhibition by aprotinin in vivo.* Thrombosis Research, 2005. **115**(4): p. 327-340.
236. Longstaff, C., *Studies on the mechanisms of action of aprotinin and tranexamic acid as plasmin inhibitors and antifibrinolytic agents.* Blood Coagulation & Fibrinolysis, 1994. **5**(4): p. 537-542.
237. Chen, Z., et al., *In vitro angiogenesis by human umbilical vein endothelial cells (HUVEC) induced by three-dimensional co-culture with glioblastoma cells.* Journal of Neuro-Oncology, 2009. **92**(2): p. 121-128.
238. Weisel, J.W. and R.I. Litvinov, *Fibrin Formation, Structure and Properties.* Sub-cellular Biochemistry, 2017. **82**: p. 405-456.
239. Griffith, C.K., et al., *Diffusion limits of an in vitro thick prevascularized tissue.* Journal of Tissue Engineering, 2005. **11**(1-2): p. 257-266.
240. Morin, K.T. and R.T. Tranquillo, *In vitro models of angiogenesis and vasculogenesis in fibrin gel.* Experimental Cell Research, 2013. **319**(16): p. 2409-2417.
241. Newman, A.C., et al., *The requirement for fibroblasts in angiogenesis: fibroblast-derived matrix proteins are essential for endothelial cell lumen formation.* Molecular Biology of the Cell, 2011. **22**(20): p. 3791-3800.
242. Blombäck, B. and M. Okada, *Fibrin gel structure and clotting time.* Thrombosis Research, 1982. **25**(1): p. 51-70.
243. Ghajar, C.M., et al., *The effect of matrix density on the regulation of 3-D capillary morphogenesis.* Biophysical Journal, 2008. **94**(5): p. 1930-1941.
244. Chen, M.B., et al., *On-chip human microvasculature assay for visualization and quantification of tumor cell extravasation dynamics.* Nature Protocols, 2017. **12**(5): p. 865-880.

245. Lee, H., et al., *A bioengineered array of 3D microvessels for vascular permeability assay.* Microvascular Research, 2014. **91**: p. 90-98.
246. Fukumura, D., et al., *Tumor induction of VEGF promoter activity in stromal cells.* Cell, 1998. **94**(6): p. 715-725.
247. Paunescu, V., et al., *Tumour-associated fibroblasts and mesenchymal stem cells: more similarities than differences.* Journal of Cellular and Molecular Medicine, 2011. **15**(3): p. 635-646.
248. Antoniades, H.N., et al., *Injury induces in vivo expression of platelet-derived growth factor (PDGF) and PDGF receptor mRNAs in skin epithelial cells and PDGF mRNA in connective tissue fibroblasts.* Proceedings of the National Academy of Sciences of the United States of America, 1991. **88**(2): p. 565-569.
249. Tracy, L.E., R.A. Minasian, and E.J. Caterson, *Extracellular Matrix and Dermal Fibroblast Function in the Healing Wound.* Advances in wound care, 2016. **5**(3): p. 119-136.
250. Lee, Y., et al., *Microfluidics within a well: an injection-molded plastic array 3D culture platform.* Lab on a Chip, 2018. **18**(16): p. 2433-2440.
251. Zimmerman, K.W., *Der feinere Bau der Blutcapillaren.* Zeitschrift für Anatomie Und Entwicklungsgeschichte, 1923. **68**(1): p. 29-109.
252. Harrell, C.R., et al., *Molecular mechanisms underlying therapeutic potential of pericytes.* Journal of Biomedical Science, 2018. **25**(1): p. 21.
253. Courtoy, P.J. and J. Boyles, *Fibronectin in the microvasculature: localization in the pericyte-endothelial interstitium.* Journal of Ultrastructure Research, 1983. **83**(3): p. 258-273.
254. Bergers, G. and S. Song, *The role of pericytes in blood-vessel formation and maintenance.* Neuro-oncology, 2005. **7**(4): p. 452-464.
255. Larson, D.M., M.P. Carson, and C.C. Haudenschild, *Junctional transfer of small molecules in cultured bovine brain microvascular endothelial cells and pericytes.* Microvascular Research, 1987. **34**(2): p. 184-199.
256. Fujimoto, K., *Pericyte-endothelial gap junctions in developing rat cerebral capillaries: A fine structural study*. The Anatomical Record, 1995. **242**(4): p. 562-565.
257. Caruso, R.A., et al., *Ultrastructural Descriptions of Pericyte/endothelium Peg-socket Interdigitations in the Microvasculature of Human Gastric Carcinomas.* Anticancer Research, 2009. **29**(1): p. 449-453.
258. Wakui, S., *Epidermal growth factor receptor at endothelial cell and pericyte interdigitation in human granulation tissue.* Microvascular Research, 1992. **44**(3): p. 255-262.
259. Gerhardt, H., H. Wolburg, and C. Redies, *N-cadherin mediates pericytic-endothelial interaction during brain angiogenesis in the chicken.* Developmental Dynamics, 2000. **218**(3): p. 472-479.
260. Jablonka-Shariff, A., et al., *Evidence for a Role of Capillary Pericytes in Vascular Growth of the Developing Ovine Corpus Luteum1*. Biology of Reproduction, 2001. **65**(3): p. 879-889.
261. Fraser, H.M. and C. Wulff, *Angiogenesis in the corpus luteum.* Reproductive Biology and Endocrinology 2003. **1**: p. 88-88.
262. Sakagami, K., T. Kodama, and D.G. Puro, *PDGF-induced coupling of function with metabolism in microvascular pericytes of the retina.* Investigative Ophthalmology & Visual Science, 2001. **42**(8): p. 1939-1944.
263. Rucker, H.K., H.J. Wynder, and W.E. Thomas, *Cellular mechanisms of CNS pericytes.* Brain Research Bulletin, 2000. **51**(5): p. 363-369.

264. Sweeney, M. and G. Foldes, *It Takes Two: Endothelial-Perivascular Cell Cross-Talk in Vascular Development and Disease.* Frontiers in Cardiovascular Medicine, 2018. **5**: p. 154.
265. Yamamoto, K., et al., *The Stabilization Effect of Mesenchymal Stem Cells on the Formation of Microvascular Networks in a Microfluidic Device.* Journal of Biomechanical Science and Engineering, 2013. **8**(2): p. 114-128.
266. Orlidge, A. and P.A. D'Amore, *Inhibition of capillary endothelial cell growth by pericytes and smooth muscle cells.* The Journal of Cell Biology, 1987. **105**(3): p. 1455-1462.
267. Hirschi, K.K., et al., *Endothelial cells modulate the proliferation of mural cell precursors via platelet-derived growth factor-BB and heterotypic cell contact.* Circulation Research, 1999. **84**(3): p. 298-305.
268. Nakagawa, S., et al., *A new blood–brain barrier model using primary rat brain endothelial cells, pericytes and astrocytes.* Neurochemistry International, 2009. **54**(3): p. 253-263.
269. Braun, A., et al., *Paucity of Pericytes in Germinal Matrix Vasculature of Premature Infants.* The Journal of Neuroscience, 2007. **27**(44): p. 12012-12024.
270. Daneman, R., et al., *Pericytes are required for blood-brain barrier integrity during embryogenesis.* Nature, 2010. **468**(7323): p. 562-566.
271. Alcendor, D.J., *Human Vascular Pericytes and Cytomegalovirus Pathobiology.* International Journal of Molecular Sciences, 2019. **20**(6): p. 1456.
272. Franco, M., et al., *Pericytes promote endothelial cell survival through induction of autocrine VEGF-A signaling and Bcl-w expression.* Blood, 2011. **118**(10): p. 2906-2917.
273. Papapetropoulos, A., et al., *Direct actions of angiopoietin-1 on human endothelium: evidence for network stabilization, cell survival, and interaction with other angiogenic growth factors.* Laboratory Investigation, 1999. **79**(2): p. 213-23.
274. Benjamin, L.E., et al., *Selective ablation of immature blood vessels in established human tumors follows vascular endothelial growth factor withdrawal.* The Journal of Clinical Investigation, 1999. **103**(2): p. 159-165.
275. Nör, J.E., et al., *Vascular Endothelial Growth Factor (VEGF)-Mediated Angiogenesis Is Associated with Enhanced Endothelial Cell Survival and Induction of Bcl-2 Expression.* The American Journal of Pathology, 1999. **154**(2): p. 375-384.
276. Harfouche, R., et al., *Mechanisms Which Mediate the Antiapoptotic Effects of Angiopoietin-1 on Endothelial Cells.* Microvascular Research, 2002. **64**(1): p. 135-147.
277. Kwak, H.J., et al., *Angiopoietin-1 is an apoptosis survival factor for endothelial cells.* FEBS Letters, 1999. **448**(2-3): p. 249-253.
278. Ramsauer, M., D. Krause, and R. Dermietzel, *Angiogenesis of the blood–brain barrier in vitro and the function of cerebral pericytes.* The FASEB Journal, 2002. **16**(10): p. 1274-1276.
279. Nishida, N., et al., *Vascular endothelial growth factor C and vascular endothelial growth factor receptor 2 are related closely to the prognosis of patients with ovarian carcinoma.* Cancer, 2004. **101**(6): p. 1364-1374.
280. Spannuth, W.A., et al., *Functional significance of VEGFR-2 on ovarian cancer cells.* International Journal of Cancer, 2009. **124**(5): p. 1045-1053.
281. Bensaïd, W., et al., *A biodegradable fibrin scaffold for mesenchymal stem cell transplantation.* Biomaterials, 2003. **24**(14): p. 2497-2502.

282. Wan, X., et al., *Morphological analysis of human umbilical vein endothelial cells co-cultured with ovarian cancer cells in 3D: An oncogenic angiogenesis assay.* PLOS ONE, 2017. **12**(7): p. 180296.
283. Li, Y., M. Xiao, and F. Guo, *The role of Sox6 and Netrin-1 in ovarian cancer cell growth, invasiveness, and angiogenesis.* Tumour Biology, 2017. **39**(5): p. 1010428317705508.
284. Al Thawadi, H., et al., *VE-cadherin cleavage by ovarian cancer microparticles induces β-catenin phosphorylation in endothelial cells.* Oncotarget, 2016. **7**(5): p. 5289-5305.
285. Kaneko, T., et al., *Bcl-2 Orchestrates a Cross-talk between Endothelial and Tumor Cells that Promotes Tumor Growth.* Cancer Research, 2007. **67**(20): p. 9685-9693.
286. Watson, E.C., et al., *Apoptosis regulates endothelial cell number and capillary vessel diameter but not vessel regression during retinal angiogenesis.* Development, 2016. **143**(16): p. 2973-2982.
287. Lee, E., N.B. Pandey, and A.S. Popel, *Lymphatic endothelial cells support tumor growth in breast cancer.* Scientific Reports, 2014. **4**: p. 5853.
288. Warner, K.A., et al., *Endothelial cells enhance tumor cell invasion through a crosstalk mediated by CXC chemokine signaling.* Neoplasia 2008. **10**(2): p. 131-139.
289. Karl, E., et al., *Bcl-2 acts in a proangiogenic signaling pathway through nuclear factor-kappaB and CXC chemokines.* Cancer Research, 2005. **65**(12): p. 5063-9.
290. Moreno-Bueno, G., et al., *The morphological and molecular features of the epithelial-to-mesenchymal transition.* Nature Protocols, 2009. **4**: p. 1591.
291. Moreno-Bueno, G., et al., *Genetic Profiling of Epithelial Cells Expressing E-Cadherin Repressors Reveals a Distinct Role for Snail, Slug, and E47 Factors in Epithelial-Mesenchymal Transition.* Cancer Research, 2006. **66**(19): p. 9543-9556.
292. Cano, A., et al., *The transcription factor Snail controls epithelial–mesenchymal transitions by repressing E-cadherin expression.* Nature Cell Biology, 2000. **2**(2): p. 76-83.
293. Rosso, M., et al., *E-cadherin: A determinant molecule associated with ovarian cancer progression, dissemination and aggressiveness.* PloS one, 2017. **12**(9): p. e0184439-e0184439.
294. Pakuła, M., et al., *The Epithelial-Mesenchymal Transition Initiated by Malignant Ascites Underlies the Transmesothelial Invasion of Ovarian Cancer Cells.* International Journal of Molecular Sciences, 2019. **20**(1): p. 137.
295. Mehta, G., et al., *Opportunities and challenges for use of tumor spheroids as models to test drug delivery and efficacy.* Journal of Controlled Release, 2012. **164**(2): p. 192-204.
296. Brown, J.M. and W.R. Wilson, *Exploiting tumour hypoxia in cancer treatment.* Nature Reviews Cancer, 2004. **4**(6): p. 437-447.
297. Zhang, K., et al., *Investigation of hypoxia networks in ovarian cancer via bioinformatics analysis.* Journal of Ovarian Research, 2018. **11**(1): p. 16.
298. Ai, Z., et al., *Overcoming cisplatin resistance of ovarian cancer cells by targeting HIF-1-regulated cancer metabolism.* Cancer Letters, 2016. **373**(1): p. 36-44.
299. Katt, M.E., et al., *In Vitro Tumor Models: Advantages, Disadvantages, Variables, and Selecting the Right Platform.* Frontiers in Bioengineering and Biotechnology, 2016. **4**: p. 12.

300. Hirschhaeuser, F., et al., *Multicellular tumor spheroids: An underestimated tool is catching up again.* Journal of Biotechnology, 2010. **148**(1): p. 3-15.
301. Shield, K., et al., *Multicellular spheroids in ovarian cancer metastases: Biology and pathology.* Gynecologic Oncology, 2009. **113**(1): p. 143-148.
302. Ivascu, A. and M. Kubbies, *Rapid generation of single-tumor spheroids for high-throughput cell function and toxicity analysis.* J Biomol Screen, 2006. **11**(8): p. 922-32.
303. Foty, R., *A simple hanging drop cell culture protocol for generation of 3D spheroids.* Journal of Visualized Experiments 2011(51): p. 2720.
304. Osaki, T., V. Sivathanu, and R.D. Kamm, *Engineered 3D vascular and neuronal networks in a microfluidic platform.* Scientific Reports, 2018. **8**(1): p. 5168.
305. Brabec, V. and J. Kasparkova, *Modifications of DNA by platinum complexes: Relation to resistance of tumors to platinum antitumor drugs.* Drug Resistance Updates, 2005. **8**(3): p. 131-146.
306. Johansen, M.E., C.A. Reilly, and G.S. Yost, *TRPV1 Antagonists Elevate Cell Surface Populations of Receptor Protein and Exacerbate TRPV1-Mediated Toxicities in Human Lung Epithelial Cells.* Toxicological Sciences, 2005. **89**(1): p. 278-286.
307. Tessier, J., et al., *Contributions of Histamine, Prostanoids, and Neurokinins to Edema Elicited by Edema Toxin from Bacillus anthracis.* Infection and Immunity, 2007. **75**(4): p. 1895-1903.
308. Bicaku, E., et al., *In vitro analysis of ovarian cancer response to cisplatin, carboplatin, and paclitaxel identifies common pathways that are also associated with overall patient survival.* British Journal of Cancer, 2012. **106**(12): p. 1967-1975.
309. Makhija, S., et al., *Taxol-induced Bcl-2 phosphorylation in ovarian cancer cell monolayer and spheroids.* International Journal of Oncology, 1999. **14**(3): p. 515-536.
310. L'Espérance, S., et al., *Global gene expression analysis of early response to chemotherapy treatment in ovarian cancer spheroids.* BMC Genomics, 2008. **9**: p. 99.
311. Olive, P.L. and R.E. Durand, *Detection of hypoxic cells in a murine tumor with the use of the comet assay.* Journal of the National Cancer Institute, 1992. **84**(9): p. 707-11.
312. Deben, C., et al., *Hypoxia-Induced Cisplatin Resistance in Non-Small Cell Lung Cancer Cells Is Mediated by HIF-1α and Mutant p53 and Can Be Overcome by Induction of Oxidative Stress.* Cancers, 2018. **10**(4): p. 126.
313. Selvendiran, K., et al., *Hypoxia induces chemoresistance in ovarian cancer cells by activation of signal transducer and activator of transcription 3.* International Journal of Cancer, 2009. **125**(9): p. 2198-2204.
314. Elmore, S., *Apoptosis: a review of programmed cell death.* Toxicologic Pathology, 2007. **35**(4): p. 495-516.
315. Khan, K.H., et al., *Targeting the PI3K-AKT-mTOR signaling network in cancer.* Chinese Journal of Cancer, 2013. **32**(5): p. 253-265.
316. Park, J.T., et al., *Notch3 overexpression is related to the recurrence of ovarian cancer and confers resistance to carboplatin.* The American Journal of Pathology, 2010. **177**(3): p. 1087-1094.
317. Jung, S.G., et al., *Prognostic significance of Notch 3 gene expression in ovarian serous carcinoma.* Cancer Science, 2010. **101**(9): p. 1977-1983.

318. Benton, G., et al., *In Vitro Microtumors Provide a Physiologically Predictive Tool for Breast Cancer Therapeutic Screening.* PLOS ONE, 2015. **10**(4): p. e0123312.
319. Winiarski, B.K., et al., *An Improved and Reliable Method for Isolation of Microvascular Endothelial Cells from Human Omentum.* Microcirculation, 2011. **18**(8): p. 635-645.
320. Winiarski, B.K., et al., *Epithelial Ovarian Cancer-Induced Angiogenic Phenotype of Human Omental Microvascular Endothelial Cells May Occur Independently of VEGF Signaling.* Translational Oncology, 2013. **6**(6): p. 703-723.
321. Homan, K.A., et al., *Flow-enhanced vascularization and maturation of kidney organoids in vitro.* Nature Methods, 2019. **16**(3): p. 255-262.
322. Park, J., et al., *Three-dimensional brain-on-a-chip with an interstitial level of flow and its application as an in vitro model of Alzheimer's disease.* Lab on a Chip, 2015. **15**(1): p. 141-150.